SILVER VANADATE AND GRAPHITIC CARBON NITRIDE COMPOSITE FOR THE REMOVAL OF OXYTETRACYCLINE

LIM KWEE CHEIN

UNIVERSITI TUNKU ABDUL RAHMAN

SILVER VANADATE AND GRAPHITIC CARBON NITRIDE COMPOSITE FOR THE REMOVAL OF OXYTETRACYCLINE

Lim Kwee Chein

A project report submitted in partial fulfilment of the requirements for the award of Bachelor of Chemical Engineering with Honours

Lee Kong Chian Faculty of Engineering and Science
Universiti Tunku Abdul Rahman

May 2023

DECLARATION

I hereby declare that this project report is based on my original work except for citations and quotations which have been duly acknowledged. I also declare that it has not been previously and concurrently submitted for any other degree or award at UTAR or other institutions.

Signature : KweeChein

Name : Lim Kwee Chein

ID No. : 1801551

Date : 20/5/2023

APPROVAL FOR SUBMISSION

I certify that this project report entitled **"SILVER VANADATE AND GRAPHITIC CARBON NITRIDE COMPOSITE FOR THE REMOVAL OF OXYTETRACYCLINE"** was prepared by **Lim Kwee Chein** has met the required standard for submission in partial fulfilment of the requirements for the award of Bachelor of (Honours) Engineering with Honours at Universiti Tunku Abdul Rahman.

Approved by,

Signature : 

Supervisor : Dr. Sim Lan Ching

Date : 20/5/2023

Signature :

Co-Supervisor :

Date :

The copyright of this report belongs to the author under the terms of the copyright Act 1987 as qualified by Intellectual Property Policy of Universiti Tunku Abdul Rahman. Due acknowledgement shall always be made of the use of any material contained in, or derived from, this report.

© 2023, Lim Kwee Chein. All right reserved.

ACKNOWLEDGEMENTS

I would like to thank everyone who had contributed to the successful completion of this project. I would like to express my gratitude to my research supervisor, Dr. Sim Lan Ching for her invaluable advice, guidance and her enormous patience throughout the development of the research. Moreover, I would like to thank to all the laboratory staffs who provided me the permission to use the laboratory apparatus and equipment needed during the laboratory works of the research.

In addition, I would also like to express my gratitude to my loving parents and friends who had helped and given me encouragement during the entire research process.

ABSTRACT

Nowadays, our environment has been polluted due to the extensive use of antibiotics. Conventional technologies are ineffective in antibiotic removal and high operational costs are required. Photocatalysis received major attention due to its ease of operation and low cost. Thus, this research will solely investigate the performance of the photocatalyst, silver vanadate and graphitic carbon nitride (AgVA/g-C_3N_4) composite for the removal of oxytetracycline (OTC) under visible light irradiation. Various AgVA/g-C_3N_4 composite photocatalysts with different weight percentages of 10 wt%, 30 wt%, and 50 wt% of AgVA were synthesized using wet chemical methods and the prepared samples were named as A10, A30, and A50. The physicochemical properties of the synthesized photocatalysts were characterized by Brunauer-Emmett-Teller surface area (BET), Fourier-transform infrared spectroscopy (FTIR), scanning electron microscopy (SEM), X-ray diffraction (XRD), and energy dispersive X-ray (EDX). Based on SEM analysis, the synthesized pure g-C_3N_4 exhibited a two-dimensional structure with typical irregular porosity whereas pure AgVA had a rod-like shape. In XRD analysis, the diffraction peaks of both g-C_3N_4 and AgVA could be observed in the synthesized photocatalysts, indicating that AgVA had successfully been coupled into g-C_3N_4. Based on FTIR analysis, the stretching vibration of V-O was found in pure AgVA and all the composites. Besides, N-H, O-H, C=N, C-N(-C)-C, and C-NH-C stretching vibrations were observed in the FTIR spectra of pure g-C_3N_4 and all the composites. Moreover, EDX analysis reports showed that the elements which existed in both g-C_3N_4 and AgVA, including C, N, Ag, V, and O were found in all the composites. Through BET analysis, A10 was found to have a large BET surface, small particle size and large pore volume as compared to pure g-C_3N_4. Based on the result obtained from the OTC photodegradation test, the highest photocatalytic effect and rate were found with A10 among all the synthesized photocatalysts and its degradation efficiency to degrade 100 ppm of OTC was found to be 56.52 %. The scavenging test showed that the active species which contributed to most of the photocatalytic activity of A10 in OTC photodegradation were arranged in the order of $^{\bullet}O_2^-$ followed by h^+, e^-, and $^{\bullet}OH$.

TABLE OF CONTENTS

LIST OF TABLES

LIST OF FIGURES

LIST OF SYMBOLS / ABBREVIATIONS

$^{\bullet}O_2^-$	Superoxide radical
$^{\bullet}OH$	Hydroxyl radical
$AgNO_3$	Silver nitrate
AgVA	Silver vanadate
AgVA/g-C_3N_4	Silver vanadate and graphitic carbon nitride composite
AOPs	Advanced oxidation processes
BET	Brunauer-Emmett-Teller
BiOX	Bismuth oxyhalide
$BiVO_4$	Bismuth vanadate
$C_{10}H_{16}N_2Na_2O_8^{+2}$	Ethylenediaminetetraacetic acid disodium salt
$C_{22}H_{24}N_2O_9$•HCl	Oxytetracycline hydrochloride
C_2H_6OS	Dimethyl sulfoxide
C_3H_8O	Isopropanol
$C_6H_4O_2$	Benzoquinone
CB	Conduction band
CdS	Cadmium sulfide
CH_4N_2O	Urea powder
CO_2	Carbon dioxide
Cu	Copper
CuVA	Copper vanadate
e^-	Electrons
EDX	Energy dispersive X-ray
E_g	Band gap energy
Fe_2O_3	Ferric oxide
FTIR	Fourier-transform infrared spectroscopy
g-C_3N_4	Graphitic carbon nitride
h^+	Holes
H_2	Hydrogen
H_2O	Water
HCl	Hydrochloric acid
hv	Photon energy

MB	Methylene blue
MgO	Magnesium oxide
MO	Methyl orange
NaOH	Sodium hydroxide
NH_4OH	Ammonium hydroxide
NH_4VO_3	Ammonium metavanadate
O_2	Oxygen
OH^-	Hydroxyl ion
OTC	Oxytetracycline
pH	Potential of Hydrogen
RhB	Rhodamine B
SEM	Scanning electron microscopy
TC	Tetracycline
TCs	Tetracyclines
TiO_2	Titanium dioxide
UV light	Ultraviolet light
V	Vanadium
VB	Valence band
WO_3	Tungsten oxide
WWTPs	Wastewater treatment plants
XRD	X-ray diffraction
ZnO	Zinc oxide
α-$AgVO_3$	Alpha-Silver Vanadate
β-$AgVO_3$	Beta-Silver Vanadate

LIST OF APPENDICES

CHAPTER 1

INTRODUCTION

1.1 Background

Water is important for all living organisms such as plants, humans and animals to survive and it has covered 71% of the earth surface (Water Science School, 2019). However, the development of science and technology has caused a great negative impact to the environment such as water pollution. According to the global report, 80% of the wastewater is disposed directly from the industries into the ecosystem without any treatment (The World Bank, 2020). This has caused a great environmental issue as many of the water sources such as rivers, lakes, ponds have been polluted. One of the pollutants that contribute to water pollution is antibiotics (a chemical compound utilized to kill the bacteria).

Danner, et al. (2019) reported that some of the countries have suffered antibiotic pollution in their fresh water. For example, up to 15 μg/L of the antibiotic concentration has been measured in the fresh water of the Americas. Besides, higher antibiotic content with a concentration over 450 μg/L has been detected in Asian-pacific countries. These concentrations might not bring any negative impact to humans but could harm the non-target freshwater organisms. In addition, the presence of antibiotic in the environment with a low concentration could accumulate in the human population through a long period of exposure to the food or drinking water which resulted in the unknown health issue to the human being (Kraemer, et al., 2019).

In other words, our environment has now been polluted by antibiotics due to extensive use of antibiotics. This could be proved by the fact that tap water, sediment, groundwater, sludge, surface water, aquatic animals and plants have been reported to be contaminated by antibiotic pollutants (Gothwal and Shashidhar, 2015). Antibiotic pollution which results in the spreading of antibiotic resistance in the environment has become a global threat as numerous effects, especially risk for global public health in future might be raised (WHO, 2014). Based on the statistics, antibiotics consumed in animal

husbandry showed higher results when compared to human medicine (Polianciuc, et al., 2020). Furthermore, about two-thirds of the antibiotic synthesis is utilized on animals. The animal would secrete them into slurry pits or onto the land which could run off into the sources of water such as groundwater, lakes and rivers. Other main sources of antibiotic pollutants in the environment might come from the waste disposed from the pharmaceuticals industry and antibiotic waste produced from fish farms (King, 2018). Figure 1.1 shows the possible routes for antibiotics to enter the environment.

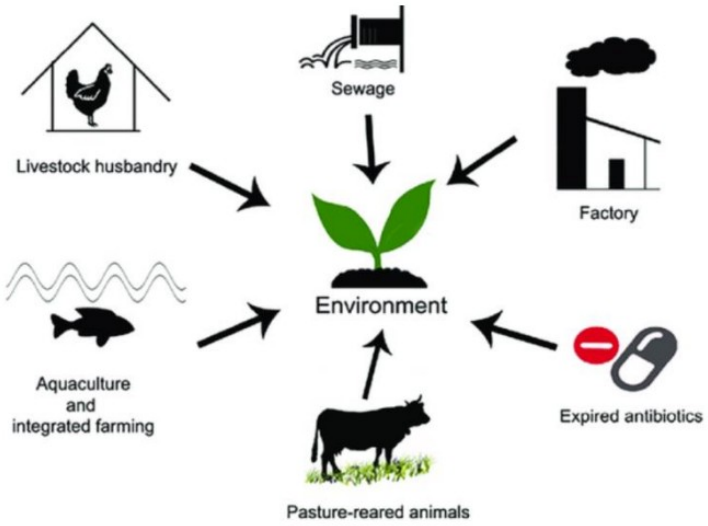

Figure 1.1: Possible Routes for Antibiotics to Enter the Environment (Quaik, et al., 2020).

Wastewater treatment techniques that apply for the elimination of these antibiotic residues from the environment have played an important role in protecting ecosystems and humans from the toxic or harmful contaminants found in wastewater (Masterflex, 2021). This technology not only to limit the contribution of water pollution by the antibiotic residues in the environment but also to ensure the sustainability of the water source. Le Page, et al. (2018) suggested a limit of 100 ng/L antibiotic discharge in order to protect the ecosystem function and limit the risk for the development of antibiotic resistance. Several techniques including membrane filtration, advanced oxidation processes (AOPs), adsorption, flocculation and coagulation, and

reverse osmosis (Figure 1.2) are introduced to treat the wastewater by eliminating the antibiotic pollutants from water.

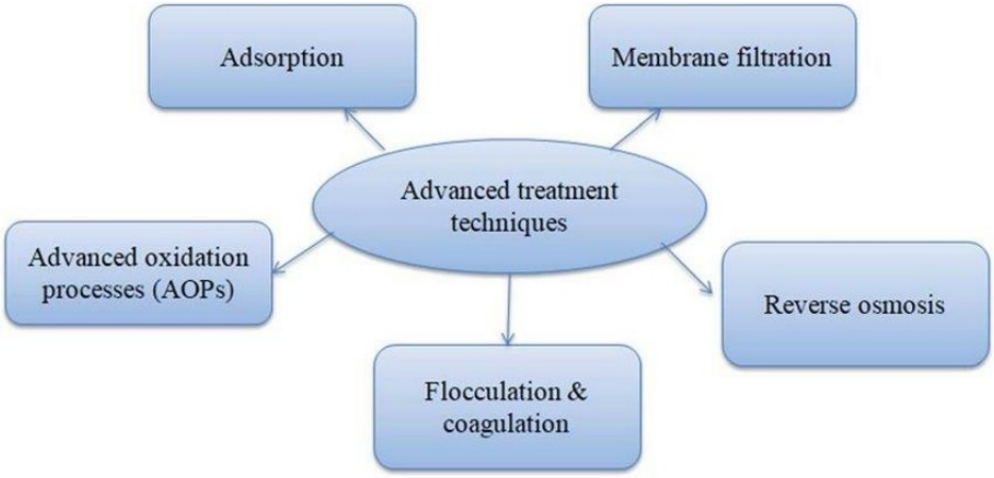

Figure 1.2: Treatment Methods Suggested for the Removal of Antibiotic Contaminants (Gopal, et al., 2020).

1.2 Photocatalysis

Advanced oxidation processes (AOPs) are considered as an effective and useful technique for the treatment of organic wastewater as well as antibiotic contaminated water (Wang, et al., 2012). Sonawane, et al. (2018) reported that a highly reactive species like hydroxyl radical ($^{\bullet}OH$) was generated during AOPs so that the organic pollutant could be oxidized into non-toxic components such as carbon dioxide and water. Figure 1.3 shows that AOPs can be classified into electrocatalytic oxidation, ozonation, wet oxidation, Fenton or Fenton-like processes and photocatalytic oxidation (Akbari, et al., 2021). These techniques could be applied either independently or combined with other techniques not only to improve performance in the degradation process of organic pollutants but also to enhance the safety, efficacy and economy (Sonawane, et al., 2018).

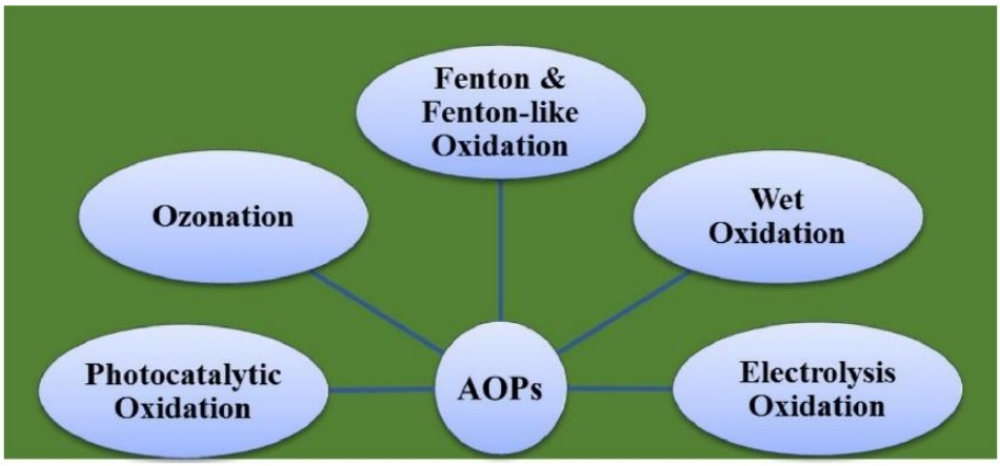

Figure 1.3: Advanced Oxidation Processes for the Removal of Antibiotics (Akbari, et al., 2021).

Among the AOPs, photocatalysis has been known as an effective and efficient method for the decomposition of antibiotic pollutants (Umar, et al., 2013). It can be described as a green technology that involves environmental detoxification and water clean-up (Moradi, et al., 2021). Organic contaminants can be removed from wastewater and be converted into harmless substances which are carbon dioxide (CO_2) and water (H_2O) with the aid of the photocatalyst (Li, et al., 2019; Li, et al., 2019). Some semiconductors such as SnO_2, ZnS, WO_3, TiO_2, and ZnO are applied as photocatalysts which is a material that can be activated by adsorbing a photon and has an ability of increasing the reaction rate without being consumed. Titanium oxide (TiO_2) is the commonly studied photocatalyst as it showed good performance to decompose organic pollutants and even achieve mineralization completely (Fujishima, et al., 2000). Due to the potential application of semiconductor oxide photocatalysts in environmental purification and solar energy confirmation, these applications have obtained much attention in recent years. In addition, photocatalysis can be categorized into homogeneous photocatalysis and heterogeneous photocatalysis (Panda, et al., 2022). However, heterogeneous photocatalysis has been verified as efficient in degrading organic compounds particularly antibiotics (Gaya and Abdullah, 2008). Generally, photocatalysis have been reported for various applications such as removal of toxic ions, water splitting, decomposition of organic contaminants, CO_2 reduction and others (Moradi, et al., 2021). The design and

fabrication of the novel semiconductor photocatalyst has hence been given much attention for the use for these applications (Moradi, et al., 2021).

1.3 Problem Statement

Oxytetracycline (OTC) is a type of tetracycline antibiotic that is frequently utilized for the treatment of infection disease (Watson and Preedy, 2012). The widespread application of the OTC in the farms and hospitals area has led to the appearance of OTC residues in the environment which contributed to environmental issues especially water pollution (Zhou, et al., 2020). Therefore, several damages have been brought to the ecosystem such as low water quality as eutrophication might happen, the growth of the aquatic life being affected, and causing bacteria to be more resistant to these antibiotics (Acevedo Barrios, et al., 2015). Wastewater that is discharged from the hospitals, large-scale animal farming, and antibiotic manufacturers is the main source that causes OTC to accumulate and bring up contamination to the environment (Liu, et al., 2021).

Due to the emergence of OTC contamination in the water source, various treatment methods or techniques including coagulation, membrane separation, absorption and biodegradation have been applied for elimination of antibiotic pollutants contained in aquatic environments (Chen, et al., 2013; Danner, et al., 2019; Ebele, et al., 2017; Hiller, et al., 2019; Huang, et al., 2019; Reis, et al., 2020; Szekeres, et al., 2018; Zhi, et al., 2019). However, they are low effective in antibiotic removal and high operational costs are required. In addition, antibiotic have a characteristic of low biodegradability, the regular conventional processes such as adsorption, precipitation, and coagulation that employed for wastewater treatment thus not capable enough to eliminate antibiotics from wastewater or water completely and they are evenly not applicable for some of the antibiotics (Cuerda-Correa, et al., 2019; Hiller, et al., 2019).

Advanced oxidation processes have shown a good ability in degrading and converting the antibiotics into biodegradable and non-toxic substances thereby decreasing the detrimental effects brought by antibiotic pollutants to the environment (WHO, 2014). A number of studies related to these techniques have been carried out and the result showed that these

techniques are considered as an effective treatment method for antibiotic wastewater (Giwa, et al., 2021).

Photocatalysis received major attention among the advanced oxidation processes because of its benefits of ease of operation and low cost (Prashanth, et al., 2021). Other than that, it has also been recognized as an effective removal method for degradation of organic pollutants particularly antibiotics using photocatalyst. Most of the semiconductor photocatalysts suffer serious drawbacks of low photocatalytic efficiency and low sunlight utilization (Wang, et al, 2016). Titanium dioxide (TiO_2) is the most studied photocatalyst as TiO_2 is low cost, nontoxic and high photocatalytic activity. However, fast recombination rate of electron-hole that generated during photoexcitation is the main limitation of TiO_2 (Dong, et al., 2015). Furthermore, photocatalytic application of TiO_2 is limited by its wide bandgap which is 3.2eV (about 4% of solar light) as this made it can only be applied as a photocatalyst under UV light which is considered as an expensive light source (ul Haq, et al., 2021). In fact, processes that are implemented based on industrial scale are required to be more cost effective and sustainable (Kutuzova, et al., 2021). The photocatalyst that is applicable under visible light is considered as the best. Therefore, different approaches such as co-doping, metal doping, non-metal doping, coupling of semiconductors, heterojunctions and composites materials have been introduced for the development of visible light-active photocatalysts with high photocatalytic efficiency (Imtiaz, et al., 2019).

Various visible light-driven photocatalysts are proposed and being studied by many researchers for the improvement of photocatalytic performance and at the same time achieve higher removal efficiency of antibiotics. In this project, the photocatalyst studied is silver vanadate (AgVA) and graphitic carbon nitride composite (g-C_3N_4) and its performance for the removal of OTC under visible light irradiation is investigated.

1.4 Aim and Objectives

The aim of this study is to investigate the performance of photocatalyst, silver vanadate and graphitic carbon nitride (AgVA/g-C_3N_4) composite for the removal of OTC. In order to achieve the aim of this study, various objectives have been identified and listed as below:

(i) To synthesize silver vanadate and graphitic carbon nitride (AgVA/g-C_3N_4) composite using wet chemical method.

(ii) To investigate the characterization of the prepared photocatalyst, AgVA/g-C_3N_4 composite by using XRD, FTIR, BET surface area, SEM and EDX.

(iii) To study the performance of the photocatalyst, AgVA/g-C_3N_4 composite for the removal of OTC under visible light irradiation.

1.5 Scope of the Study

In this project, AgVA/g-C_3N_4 composite was used as visible light-driven photocatalyst. Its' responsive reaction for the removal of oxytetracycline under visible light irradiation was investigated throughout the tasks. Besides that, the preparation method for pure AgVA, pure g-C_3N_4, and AgVA/g-C_3N_4 composite was studied through this project. Pure g-C_3N_4 was prepared using pyrolysis of urea whereas pure AgVA and AgVA/g-C_3N_4 composite was prepared using a wet chemical method. Next, the effect of weight percentage of AgVA on the photocatalytic efficiency of AgVA/g-C_3N_4 composite was examined through varying the weight percentage of AgVA (10, 30 and 50 wt%). As such, different weight percentage samples of AgVA/ g-C_3N_4 composite was prepared. In fact, the photocatalytic activity of a photocatalyst is greatly dependent on its degradation efficiency of the organic pollutants. Hence, the photocatalytic efficiency of the composites was studied through comparing the performance of the prepared photocatalysts for the removal of antibiotic, OTC under visible light irradiation. In addition, the prepared photocatalysts were characterized by XRD (X-ray diffraction), FTIR (Fourier-transform infrared spectroscopy), BET (Brunauer-Emmett-Teller) surface area, SEM (Scanning electron microscopy) and EDX (Energy dispersive X-ray).

CHAPTER 2

LITERATURE REVIEW

2.1 Antibiotic Pollutants

Antibiotics are considered as a chemical compound which are effectively used for the treatment of microbial infection disease (Manzetti and Ghisi, 2014). They are widely applicable as growth promoters in various sectors including aquaculture, livestock and agriculture (Gothwal and Shashidhar, 2015). Figure 2.1 shows the worldwide consumption of antibiotics in 5 different areas which are Western Pacific, Africa, European, Eastern Mediterranean and Americas.

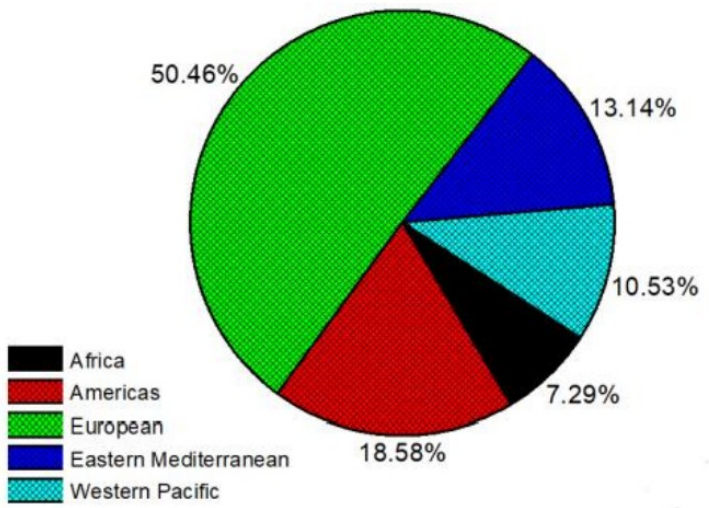

Figure 2.1: Worldwide Consumption of Antibiotics in Five Areas (World Health Organization, 2018).

Antibiotics that are applied for animal and human therapy might reach and accumulate in the environment which eventually lead to environmental problems such as plants, water, and soils contamination (Polianciuc, et al., 2020). Furthermore, antibiotic residues can cause disruption to the function of the human's digestive system, chronic toxic effects due to long term exposure and even alter the human microbiome (Ben, et al., 2019; Van Boeckel, et al., 2015; Larramendy and Soloneski, 2015). Municipal wastewater that contains antibiotics from human feces which is incompletely

metabolized and wastewater that is discharged from the pharmaceutical factory which consists of high quantity of antibiotics is the major source that led to residual antibiotic in the aquatic environment (Phoon, et al., 2020). In recent decades, drinking water and surface water in most of the areas of the world was reported for the presence of antibiotics (Chen, et al., 2019). Hence, various technologies for the removal of antibiotics from the wastewater and polluted water source have been developed. As shown in Figure 2.2, conventional wastewater treatment techniques can be classified into three categories which are physical, biological and chemical methods and three of them operate with each other for wastewater treatment. The typical conventional wastewater treatment process is shown in Figure 2.3.

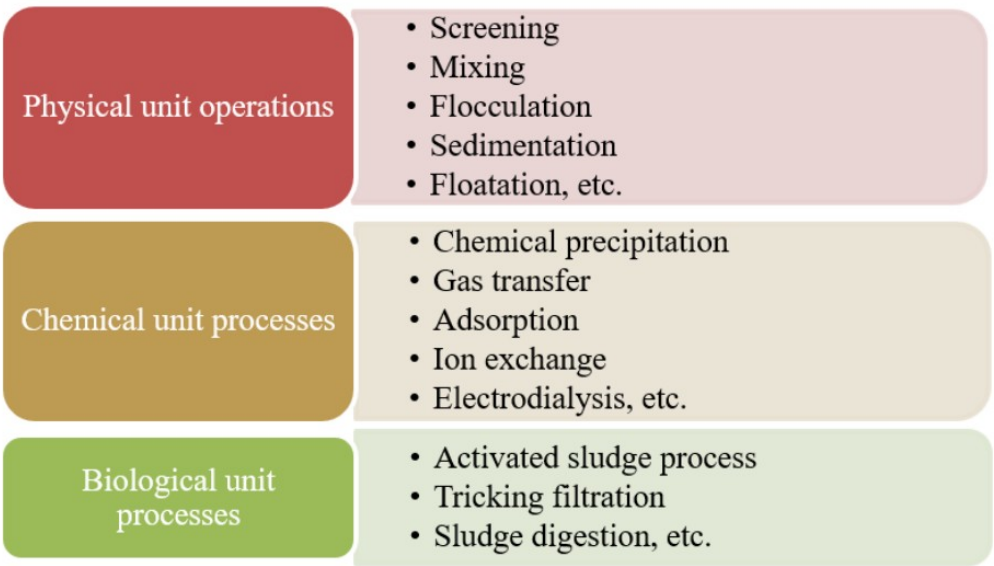

Figure 2.2: Conventional Wastewater Treatment Techniques (Parajuli, 2018).

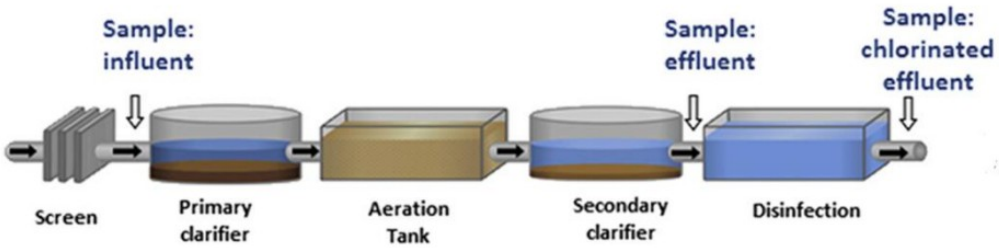

Figure 2.3: Typical Conventional Wastewater Treatment Process (Al-Jassim, et al., 2015).

The physical treatment methods included filtration, coagulation, adsorption, membrane treatment and sedimentation. Through physical wastewater treatment, the removal of pollutant substances can be accomplished with the presence of naturally occurring forces, for example electrical attraction, gravity and Van Der Waals forces (Phoon, et al., 2020). Wastewater treatment using biological methods refers to a process that transforms the organic pollutants which are biodegradable into additional biomass and simple substances by decomposing them utilizing normal cellular processes which are carried out by nematodes, bacteria and other microorganisms. Stabilization, activated sludge, anaerobic digestion, fungal treatment, aerated lagoons and trickling filters belong to biological treatment (Grady, et al., 2011).

Meanwhile, chemical wastewater treatment methods consist of ion exchange, reduction, catalysis, oxidation, electrolysis, and neutralization (Rao, et al., 2017). However, these conventional treatment methods are ineffective and inefficient as well to eliminate antibiotic pollutants. Chen, et al. (2019) reported that the stationary phase of organic substances can be alerted through treating wastewater by physical method but cannot be completely removed. Moreover, antibiotics with the characteristic of antibacterial effect causing the capability of traditional biological wastewater treatment in treating the antibiotic contaminated wastewater to be limited. Common chemical oxidation methods have low reaction efficiency and the use of the powerful oxidizing agent in large quantities is costly. In addition, Kumar and Pandey (2017) reported that the chemical oxidation method is limited to eliminate all organic compounds and is applicable for the removal of contaminants at high concentration. Table 2.1 summarizes the shortcomings of the existing conventional wastewater treatment methods.

Table 2.1: Shortcomings of the Existing Conventional Wastewater Treatment Technologies.

Conventional Technology		Drawback	Reference
Trickling filters	i.	Principal cost is high.	Gedda, et al., 2021
	ii.	Blockage of rotating arms.	
	iii.	Generation of great intense odour.	
Activated sludge process	i.	High operating cost.	
	ii.	Requirement in monitoring and controlling of the sludge concentration.	
Coagulation	i.	Producing a huge amount of sludge.	
	ii.	Low efficiency and high cost.	
Membrane filtration	i.	Due to membrane fouling, high maintenance cost is required.	Shah and Rather, 2021
	ii.	High Energy consumption.	
Adsorption	i.	Fast saturation.	
	ii.	High investment.	
	iii.	Non-destructive.	
Electrolysis	i.	High equipment cost.	
	ii.	Occurrence of inhibition of electrode.	
Chemical oxidation	i.	Pre-treatment process is needed.	
	ii.	Expensive.	
	iii.	Inefficiency in dye removal.	
	iv.	Toxic intermediates generation.	

According to the discussion above, conventional wastewater treatment methods require high operating costs and even could not treat the antibiotic contained in the wastewater effectively. This has led the conventional wastewater treatment plants (WWTPs) to be incapable of eliminating antibiotics and other pharmaceutical products from wastewater effectively. As a result, the treated effluent that discharged from WWTPs which contain high residues of antibiotic pollutants have caused pollution to the water streams (Gadipelly, et al., 2014). For instance, Lopez Penalver, et al. (2013) reported that antibiotics such as tetracycline, oxytetracycline and chlortetracycline have been detected in WWTP effluent with a concentration of 46-1300 ng/L, 240 ng/L and 270-970 ng/L respectively. Due to the emergence of antibiotics contamination in the aqueous systems, advanced oxidation processes (AOPs) have been developed as one alternative technique for the treatment of antibiotics in wastewater where the antibiotic pollutants are degraded through oxidation (Giler-Molina, 2020).

2.2 Oxytetracycline

Tetracyclines (TCs) are frequently used antibiotics for agricultural feed additives, animal disease control and human therapy because of their high-quality, broad-spectrum activity and low cost (Daghrir and Drogui, 2013). Oxytetracycline (OTC) with a molecular formula of $C_{22}H_{24}N_2O_9$ is one of the tetracycline groups of antibiotics which are commonly utilized throughout the world (Daghrir and Drogui, 2013). OTC can be applied for the treatment of infectious diseases such as respiratory infection, typhus, anthrax, plaque, malaria, and others (Hegde, et al., 2013). Figure 2.4 represents the chemical structure of OTC and Table 2.2 shows the properties of OTC.

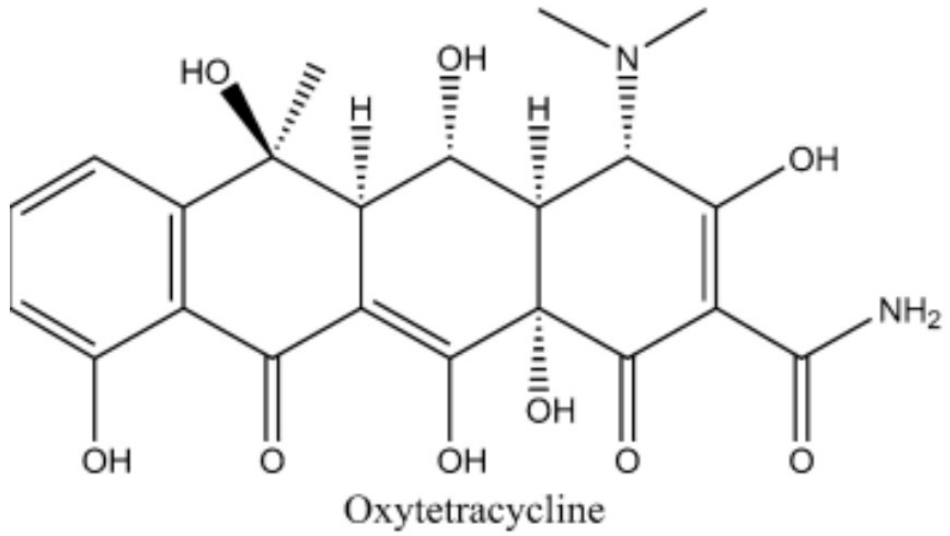

Figure 2.4: Chemical Structure of Oxytetracycline (Ahmad, et al, 2021).

Table 2.2: Properties of OTC (Xu, et al., 2021).

Compound	Abbreviation	Molecular weight (g/mol)	Melting point (℃)	Water solubility at 25 ℃ (mg/L)
Oxytetracycline	OTC	460.44	184.50	313

OTC has the benefits of high antibacterial activity and low costs which made it mainly applied in aquaculture and animal farm applications. However, absorption rates for OTC to be absorbed by animals and humans is scarce, leading to almost 70% to 90% of the metabolites and active ingredients being released into the aquatic environment (Massé et al., 2014). Wide usage of the OTC in a variety of sectors including hospitals, animal management centers, pharmaceutical factories and feedlots has led to widespread occurrence of OTC in the environment (Hou, et al., 2016). As proof, numerous studies have found OTC at a high concentration of 300 μg/kg in soils and about 15 μg/L in surface water and groundwater (Fatta-Kassinos, et al., 2011). The appearance of OTC residues might cause potential threat to the ecosystem in various ways, for example spread of antibiotic-resistant bacteria, low water quality, and inhibition of aquatic plant growth (Acevedo Barrios, et al., 2015; Van Der Grinten, et al., 2010). In fact, OTC has phytotoxic effects which can cause chromosomal anomaly and decrease the content of carotenoid pigments

and photosynthetic chlorophyll in plants. In addition, the OTC residues could inhibit the growth of plants once absorbed as it would interfere with physiological processes of the plants and lead to potential ecotoxicological effects (Polianciuc, et al., 2020). Other than that, accumulation of OTC in agricultural soil with a high level would reduce biomass production and delay germination by means of applying the contaminated manure to fertilize the farmland (Minden, et al., 2017).

Last but not least, antibiotic resistance which is considered as a global health security risk would happen while bacteria become resistant to the antibiotics that are used for the treatment of infections caused by them. In addition, the spread of antibiotic-resistant bacteria on agricultural land or in water resources could be the easy route for animals and humans to encounter these antibiotic-resistant bacteria (King, 2018). Consequently, the application of the relevant antibiotic for the treatments in human medicine may fail due to infections led by the antibiotic-resistant bacteria which could result in the increase of the case of mortality and duration of illness (Polianciuc, et al., 2020). In general, the occurrence of OTC residues in the environment over a long period of time might cause the generation of antibiotic resistant bacteria, antibiotic resistant genes and accelerate the development of antibiotic resistance which can threaten the ecological systems and human health (Kummerer, 2009).

The raising in the environmental problem particularly water contamination caused by antibiotic pollutants has therefore brought about the development of inexpensive but efficient treatment methods for the removal of antibiotic contaminants (Harja and Ciobanu, 2017). Photocatalysis which is an environmental protection technology with the benefits of efficiency, green, and energy saving has presently become a promising wastewater treatment technology for the removal of antibiotic contaminants.

2.3 Photocatalysis

In 1972, photocatalysis technology was proposed by Fujishima and Honda in their research on the topic 'Electrochemical Photolysis of water at a semiconductor electrode' which was published in Nature (website) (Fujishima and Honda, 1972). Photocatalysis is environmentally friendly, stable, and efficient when performing as environmental pollution control technology (Kudo and Miseki, 2009). This is because photocatalysis only required light irradiation to activate photocatalyst for the generation of electron-hole pairs to carry out photocatalytic reactions (Byrne, et al., 2018). In other words, photocatalysis can reduce or oxidize contaminants by stimulating electron transfer of a photocatalyst with the aid of solar energy (Motahari, et al., 2014; Deng, et al., 2020). Among the AOPs, this technology has been widely studied for the degradation of antibiotic pollutants. In general, there are two types of photocatalysis which are known as homogeneous photocatalysis and heterogeneous photocatalysis.

2.3.1 Homogeneous Photocatalysis

Photocatalytic reaction that involves the same phase of both photocatalyst and reactant is known as homogeneous photocatalysis (Ameta, et al., 2018). One example that used to describe the homogeneous photocatalysis is using the water-soluble carbon dots to degrade the aqueous organic dyes with the assistance of light (Baruah, et al., 2019). Next, ozone and photo-Fenton systems are the commonly used homogeneous photocatalyst (Panda, et al., 2022).

2.3.2 Heterogeneous Photocatalysis

Photocatalytic reaction that involves both reactant and photocatalyst which exist in different phases is known as heterogeneous photocatalysis. Heterogeneous photocatalysis which developed in the 1970s has been proven to be of interest as it is efficient in decomposing recalcitrant organic substances (Umar and Aziz, 2013). Recently, various studies on the application of heterogeneous photolysis with a viewpoint to mineralize and degrade recalcitrant organic substances (Umar and Aziz, 2013). There are various semiconductors that can be applied for heterogeneous photocatalysis

such as cadmium sulfide (CdS), ferric oxide (Fe_2O_3), tungsten trioxide (WO_3), magnesium oxide (MgO), titanium dioxide (TiO_2), and zinc oxide (ZnO). However, all of them have a larger band gap and narrow light absorption range which causes them to have a low efficiency of photoactivity and only be photoactive within the UV range (Imtiaz, et al., 2019; Molinari, et al., 2020). In fact, solar light consists of 46% visible light, 4% to 5% of UV light and the rest are Infrared irradiation. UV radiation that is costly can contribute to a rise in the wastewater remediation cost with a high percentage of 50% to 60% (Centi, et al., 2000).

Replacement of UV radiation with visible light has gained interest in order to minimize the cost spent for the energy consumption. Other than that, solar energy is an inexhaustible, costless and green energy source. Utilizing solar energy in an effective manner is important for reducing pollution, retarding global warming, and enhancing the sustainability of industry (Ge, et al., 2019). Thus, strategies such as metal or anion doping have been introduced to modify these UV-driven semiconductor photocatalysts into visible light-driven photocatalysts which are able to absorb lower energy photons and thus achieve maximum sunlight utilization (Phoon, et al., 2020). However, this method is not an appropriate way as dopants could act as the sites for recombination of electron-hole pairs which could reduce the photocatalytic activity to occur (Malik, et al., 2022). Therefore, researchers have given much attention to the fabrication of visible light-responsive photocatalysts with a high photocatalytic efficiency (Roy, et al., 2020).

2.3.3 Mechanism of Heterogeneous Photocatalysis

Figure 2.5 shows the photocatalytic reactions that take place over a heterogeneous photocatalyst. At the beginning of the reaction, the electron-hole pairs are being generated when a sufficient energy either equal or larger than the band gap energy (E_g) of the semiconductor is absorbed by the photocatalyst (Wang and Zhuan, 2020). The excited valence band (VB) electron transfers to the conduction band (CB), leaving hole behind in the VB. Thus, the photocatalyst with a narrow band gap is favourable to capture more visible-light photons. Second step is the separation of the electrons (e^-) and holes (h^+) that are generated during the photoexcitation process. However, the

number of the excited charge carriers will be reducing through the recombination process with the formation of heat or photons. Moreover, the photogenerated e^- and h^- can participate in several surface chemical reactions but these charge carriers might also be combined on the surface. Next, the separated e^- which has high reduction ability reduces oxygen (O_2) for the formation of superoxide radical ($^{\bullet}O_2^-$). Whereas the separated h^+ which has strong oxidation ability will react with the water molecule or hydroxyl ion (OH^-) for the formation of hydroxyl radical ($^{\bullet}OH$). The contaminants contained in the water will be absorbed on the surface of photocatalytic material resulting in the rise of the mobility of charge and further enhances the redox ability of photocatalysts. At the end of the reaction, organic pollutants could be degraded into harmless substances such as CO_2 and H_2O. In general, light harvesting, charge excitation, charge separation and transfer followed by surface electrocatalytic reaction are the four major processes that make up heterogeneous photocatalysis. The redox reaction as mentioned above can be written into equations from 2.1 to 2.9 as listed below (Ren, et al., 2021).

Photoexcitation

$$\text{Photocatalyst} + h\nu \rightarrow e^- + h^+ \qquad \text{(Equation 2.1)}$$

Reduction process for absorbed O_2

$$\mathbf{e^- + O_2 \rightarrow {}^{\bullet}O_2^-} \qquad \text{(Equation 2.2)}$$

Reaction of superoxide radical with H^+

$$\mathbf{{}^{\bullet}O_2^- + H^+ \rightarrow {}^{\bullet}OOH} \qquad \text{(Equation 2.3)}$$

Electrochemical reduction

$$^{\bullet}OOH + {}^{\bullet}OOH \rightarrow \mathbf{O_2 + H_2O_2} \qquad \text{(Equation 2.4)}$$

$$H_2O_2 + \mathbf{{}^{\bullet}O_2^- \rightarrow OH^- + O_2} + {}^{\bullet}OH \qquad \text{(Equation 2.5)}$$

$$\mathbf{H_2O_2 + h\nu \rightarrow 2}{}^{\bullet}OH \qquad \text{(Equation 2.6)}$$

Oxidation of H_2O

$$H_2O + h^+ \rightarrow H^+ + {}^{\bullet}OH \qquad \text{(Equation 2.7)}$$

Generation of free hydroxyl radicals

$$h^+ + OH^- \rightarrow {}^{\bullet}OH \qquad \text{(Equation 2.8)}$$

Degradation of organic pollutants

$$\text{Pollutants} + {}^{\bullet}OH\ ({}^{\bullet}OOH,\ e^-,\ h^+ \text{ or } {}^{\bullet}O_2^-) \rightarrow \text{degradation products} \qquad \text{(Equation 2.9)}$$

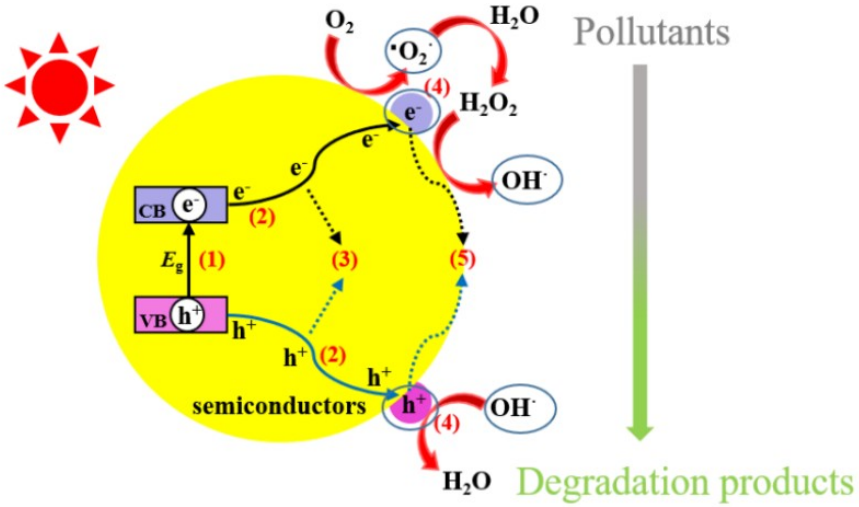

Figure 2.5: Photocatalytic Reaction Mechanism (Ren, et al., 2021).

In addition, light harvesting process is strongly related to the structure and surface morphology of photocatalysts which could usually be improved via constructing the hierarchical mesoporous or macroporous architectures so that the photocatalyst can be more effective in light utilization through its scattering effects and multiple reflection (Li, et al., 2016).

2.3.4 Advantages and Limitations of Photocatalysis

Inefficiency of conventional wastewater treatment technologies for the degradation of organic pollutants has resulted in the increasing of the pollution issue in various water resources such as sewage, drinking water, surface water and groundwater. Moreover, most of these technologies could contribute to high energy consumption and are complicate when performing the waste treatment process. Hence, technology with the characteristics of advanced, high efficiency of reclamation of wastewater, low cost, and even environmentally friendly is essential to be developed (Ren, et al., 2021). This is to ensure that the environment pollution could be controlled without affecting the well-being of the environment (Sinar Mashuri, et al., 2020). Photocatalysis which has shown various benefits and is promising, efficient and effective when being applied for the removal of organic compounds like antibiotic pollutants from wastewater has caused it to become an emerging technology for wastewater treatment. However, it also consists of numerous limitations. For example, most of the semiconductor photocatalysts is ineffective in visible light utilization due to their wide band gap. Moreover, semiconductor photocatalysts have the high recombination rate of electron-hole pairs which contributed to the low photocatalytic ability. Next, recovery of the nanosized photocatalysts are difficult to be carried out (Dong, et al., 2015). Table 2.3 shows the advantages and limitations of photocatalysis.

Table 2.3: Advantages and Limitations of Photocatalysis.

	Advantages		Limitations	Reference
i.	Green, eco-friendly and energy saving.	i.	Incomplete mineralization	Ahmad, et al., 2021
ii.	Long durability.	ii.	Not efficient in utilization of visible light.	
iii.	High mineralization rate.	iii.	Formation of intermediate compounds	Chen, et al., 2019
iv.	Used oxygen as oxidizer.	iv.	Application of UV light which is expensive and harmful as energy source	
v.	Photocatalyst is reusable and low cost.	v.	Limitation of mass transfer to the immobilized catalyst surface	Kumar, et al., 2014
vi.	Reaction conditions is mild.	vi.	Recombination rate of electron-hole pairs is high	Zhang, et al., 2019
vii.	Fast reaction speed.			
viii.	Photocatalyst can be excited by sunlight.			Zhang, et al., 2021
ix.	Complete degradation of organic compound			
x.	Without causing secondary pollution			

2.4 Photocatalyst

Photocatalyst refers to a semiconductor device that has the ability to decompose various chemicals (pharmaceuticals, petrochemicals, and organic compounds) and disinfect a variety of pathogens (protozoan cells, virus, bacteria, and fungi) (Ojha, 2020). Till today, development of an individual visible light responsive semiconductor photocatalyst with a high efficiency remains a significant challenge (Ge, et al., 2019). By using the most studied photocatalyst TiO_2 as example, its wide band gap and rapid recombination rate of electron-holes has limited it for only applicable under UV light. BiOX (X=Br or I), a visible-light driven semiconductor photocatalyst which has been developed in the recent year. It has a lower energy band gap however it will be suffering from electron-hole pairs recombination problem and the problem of photo-corrosion in aqueous media (Huizhong, et al., 2008).

In fact, a good photocatalyst should has the characteristics of high stability, excellent charge separation, rapid charge transfer, low cost, non-toxicity and good absorption in the visible spectrum (Kovacic, et al., 2020). In general, single semiconductor photocatalysts are facing two major issues which are wide band gaps and recombination of the photogenerated electron and hole pairs thereby decreasing photocatalytic and quantum efficiencies (Louangsouphom, et al., 2019; Soltani, et al., 2019). Hence, various modification strategies including co-catalyst, surface heterojunction, surface doping and exposure of highly reactive facets has been developed to overcome the issues suffered by most of the semiconductor photocatalysts and improve their photocatalytic efficiency (Zhao, et al., 2022). Some of the modification strategies are briefly discussed as below.

2.4.1 Surface Doping

Surface doping could result in the changing of the catalyst structure, expanding of the light absorption range, and decreasing of the carrier recombination rate which lead to the increases of the photocatalytic performance. In addition, surface doping causes an optical response through introducing electrons into semiconductor band gap which in turn contributes a

significant redshift. This approach can be classified into metal doping and non-metal doping (Zhao, et al., 2022).

Metal doping could improve both adsorption and photocatalytic decomposition efficiencies by introducing metal dopant on photocatalyst (Sinar Mashuri, et al., 2020). Cao, et al. (2018) reported that the addition of 1-8 wt% of $CoZr_6O_4(OH_4)BDC_{12}$ on the photocatalyst has successfully improved the process of adsorption and degradation from 9.9% to 78.5%. The two key parameters that affect the photocatalytic oxidation are type and doping quantity of transition metals. By adding optimum amount of dopant, the separation process of carriers could be accelerated. However, dopant would serve as a recombination center and decrease the photocatalytic efficiency if the dopant added is above optimal value (Zhao, et al., 2022).

In non-metal doping, photoactive performance of the catalyst is improved by dopants *via* changing the morphology. Non-metal doping such as fluorine, nitrogen, boron, sulphur and carbon has been widely evaluated previously (Zhao, et al., 2022). In addition, the doped state is positioned near to the edge of the valence band which is not utilized as a carrier. This has weakened the role of doped state as the recombination center. Table 2.4 shows a few examples of the synthesized non-metal and metal doped photocatalysts.

Table 2.4: Examples of the Synthesized Non-metal and Metal Doped Photocatalysts.

Dopant	**Photocatalyst**	**Efficiency changes after doping**	**Reference**
Ag/Ag_2O	TiO_2	7.5% → 23.3%	Xue, et al., 2021
Mg	OMS-2	68.4% → 97.2%	Fang, et al., 2017
V	TiO_2	0.3% → 12.7%	Devaraji, et al., 2014
F	TiO_2	77.3% → 81%	Khalilzadeh and Fatemi, 2016
N	TiO_2	77.3% → 92.1%	Khalilzadeh and Fatemi, 2016
N	TiO_2	33% → 38%	Kamaei, et al., 2018

2.4.2 Supported Co-catalyst

The transfer of the electron and hole between the semiconductor and co-catalyst not only accelerates the carrier's separation but could also achieve the spatial separation of oxidation and reduction reaction which improved both reaction efficiency and quantum efficiency. In addition, the presence of the co-catalyst could decrease the overpotential of the surface reaction and result in the increase of the surface reaction rate as the co-catalyst has abundance of surface-active sites on it (Zhao, et al., 2022). Wang, et al. (2020) reported that the improvement of both charge transfer and light absorption efficiency has been found in the synthesized photocatalyst, $WSe_2/g\text{-}C_3N_4$ with WSe_2 serving as a co-catalyst.

2.4.3 Surface Heterojunction

When two semiconductors which have the similar characteristics are combined with each other, an electrical field is generated at their contact surface. The generated electric field provides driving force which encourages the directional migration of charge carriers between different semiconductors which could promote the effective separation (Zhao, et al., 2022). During heterojunction photocatalysis, a photoproduced hole will migrate from a semiconductor which has a lower valence band energy level whereas a photoproduced electron will migrate from a semiconductor which has a higher conduction band energy level as shown in Figure 2.6. Table 2.5 shows the examples of heterojunction photocatalysts and their degradation efficiency.

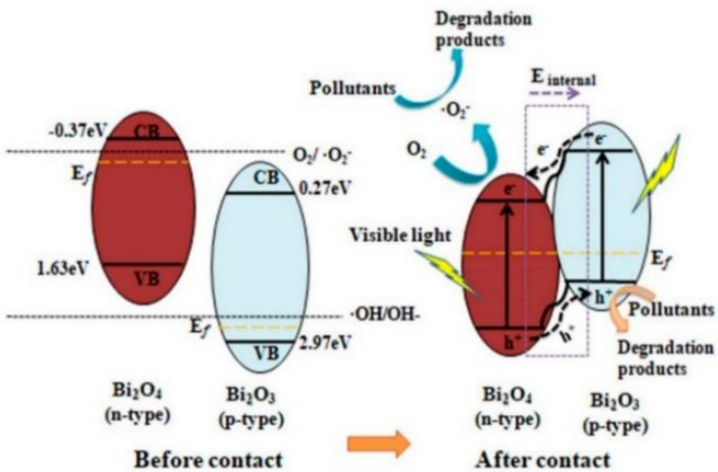

Figure 2.6: Binary Coupling Heterojunction Photocatalyst (Li, et al., 2020).

Table 2.5: Examples of the Heterojunction Photocatalysts and Their Photodegradation Efficiency after undergo Heterojunction Photocatalysis.

Heterostructure	**Photocatalyst**	**Efficiency changes**	**Reference**
Z-Scheme	$LaFeO_3$/g-C_3N_4	37% → 100%	Wu, et al., 2018
Z-Scheme	Au-TiO_2@NH_2-UiO-66	10% → 85%	Liu, et al., 2021
S-Scheme	Cu_2S/SnO_2	17.9% → 67.2%	Enesca and Isac, 2021

In fact, this strategy is known as semiconductor coupling and it has received great interest for photocatalysis as it allows for the construction of heterojunction which improving the separation of photoproduced electron-hole pairs effectively (Ifebajo, et al., 2019; Nguyen, et al., 2020).

2.5 Classification of Photocatalysts

In recent years, proper categorization of photocatalysts have become difficult due to the emergence of countless photocatalyst materials (Thongam and Chaturvedi, 2021). In general, photocatalysts can be classified into a few types which are non-metal semiconductors, metal oxides, multicomponent materials, ternary compounds, and metal sulphides as shown in Table 2.6.

Table 2.6: Difference Types of Photocatalysts and Their Examples.

Type of photocatalyst	Examples	Reference
Non-metal semiconductors	Graphene, g-C_3N_4	Zhang, et al., 2019 Wen, et al., 2017 Shi, et al., 2015
Metal oxides	Bi_2O_3, ZnO, In_2O_3, TiO_2, Fe_2O_3 or WO_3	Lee, et al., 2016 Kumar and Rao, 2017 Fagan, et al., 2016
Multicomponent materials	Graphene-heterojunctions g-C_3N_4-heterojunctions $BiVO_4/Bi_2O_2CO_3$ $Bi_2O_2CO_3/Bi_2O_4$ Bi_2S_3/ Bi_2O_4/ $Bi_2O_2CO_3$	Li, et al., 2018 Wen, et al., 2017 Huang, et al., 2016 Sun, et al., 2017 Madhusudan, et al., 2011
Ternary compounds	Tungstates ($ZnWO_4$ Bi_2WO_6)	Zhang, et al., 2018 Sethi, et al., 2018
	Titanates ($La_2Ti_2O_7$, $BaTiO_3$ or $SrTiO_3$)	Mourão, et al., 2015 Rastogi, et al., 2016 Hua, et al., 2015
	Metalates [$A_xB_yO_z$] (such as $BiVO_4$)	Thalluri, et al., 2016 Kubacka, et al., 2012
Metal sulphides	CdS, Bi_2S_3, MoS_2, ZnS or CuS	Mondal, et al., 2015 Lee and Wu, 2017 Wang, et al., 2015

2.6 Factors Affecting the Photocatalytic Efficiency

Though photocatalytic reaction can be performed under milder reaction conditions such as ambient pressure and temperature, short reaction times and require only fewer auxiliary additives (Molinari, et al., 2021), its photocatalytic performance of a photocatalyst on the degradation of organic pollutants is highly be affected by several parameters where these parameters could be categorized into two which are extrinsic and intrinsic as shown in Figure 2.7. Some of the intrinsic and extrinsic parameters that affect the photocatalytic ability of the photocatalyst have been briefly discussed below.

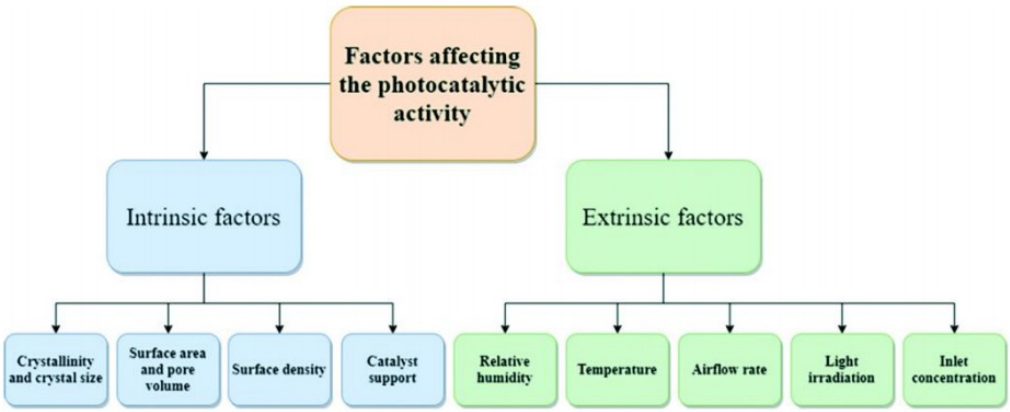

Figure 2.7: Parameters Affecting the Photocatalytic Performance (Zhao, et al., 2022).

2.6.1 Reaction Temperature

Photocatalytic process is usually be performed under room temperature. Various studies have proposed performing photocatalytic reaction within the temperature range of 20-80 ℃. For instance, Mozia (2010) has investigated and found that photodegradation rate could be increased at the optimum temperature range of 20-60 ℃. While for a temperature which exceeds 80 ℃ is found to be unfavourable for the photocatalytic reaction as it will promote the recombination of electron-hole pairs.

2.6.2 pH of Solution

In fact, pH could influence the size of aggregates, surface charges on the photocatalyst, and the position of conductance and valence bands (Chong, et al., 2010). Hence, pH of the solution has played a significant role as it controls the degradation efficiency of the contaminants (Joerin, et al., 2009).

2.6.3 Photocatalyst Loading

Overall photocatalysis reaction rate is highly dependent on the concentration of the photocatalyst (Umar and Aziz, 2013). This is because increasing the photocatalyst loading will bring about the increase of the surface area of photocatalyst available for the absorption and degradation which promote the degradation rate of the pollutants (Zhang, et al., 2018). Thus, reaction rate is increasing with catalyst concentration. However, the increasing of the catalyst concentration above a certain dose would cause a decrease in the reaction rate (Zhang, et al., 2019).

2.6.4 Light Wavelength and Intensity (Light Irradiation)

Light irradiation has a higher impact on the photocatalytic performance of a photocatalyst. The energy band gap (E_g) is correlated with the wavelength of the light source. The E_g which is lower than the energy band of the photocatalyst would result in the electrons fail to be excited and hence cause the oxidation of organic compounds on the photocatalyst surface is difficult to take place (Zhao, et al., 2022). In addition, light intensity is associated with the photocatalytic reaction rate. This can be proven by the fact that a power-law relationship can be observed between the light intensity and the reaction rate when the light intensity increases (Deng, 2018).

2.6.5 Structure and Size of the Photocatalyst

A significant factor to be considered in the photodegradation process is surface morphology such as agglomerate size and particle size. This is due to there being a direct relationship between surface coverage of the photocatalyst and organic compounds (Guillard, et al., 2003). In fact, photodegradation reactions occur only in the absorbed phase of the photocatalyst thus the reaction rate is

controlled by the number of photons that strike to the photocatalyst (Gaya and Abdullah, 2008; Kogo, et al., 1980).

2.7 Silver Vanadate (AgVA)

Recently, band structure control technique has been developed by researchers to synthesis non-TiO_2-based visible light responsive photocatalysts such as $CoFe_2O_4$ (Choudhary, et al., 2019), Ag_3VO_4 (Vu, et al., 2014), $BiWO_6$ (Zhang, et al., 2014), $BiVO_4$ (Malathi, et al., 2018) and $AgVO_3$ (Vu, et al., 2014). Among these photocatalysts, silver vanadate (AgVA) has gained remarkable attention due to its electrochemical, excellent antibacterial and photophysical properties as well as photocatalytic activity (Vu, et al., 2014; Wu, et al., 2015; McNulty, et al., 2016). Moreover, AgVA possesses higher photocatalytic ability, suitable band gaps and stability which made it become a promising visible-light active photocatalyst (Lu, et al., 2017). Other than that, it is found that AgVA has the characteristics of ease of preparation and well crystallization (Guo, et al., 2019). In addition, AgVA not only has potential application as a photocatalyst but also applicable in rechargeable high-energy density lithium-ion batteries (Takeuchi, et al., 2001).

2.7.1 Characteristics of AgVA

In fact, AgVA with a chemical formula of $AgVO_3$ is the most prevalent form of solid-phase silver vanadate oxides. Figure 2.8 shows the chemical structure of $AgVO_3$.

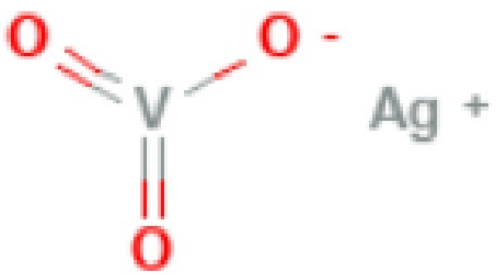

Figure 2.8: Chemical Structure of $AgVO_3$ (PubChem, 2022).

$AgVO_3$ is considered as an efficient visible light-driven photocatalyst because of its nanocrystalline nature, favourable morphology, and visible light absorption capacity (Hu, et al., 2008). $AgVO_3$ could further be distributed into α-$AgVO_3$ and β-$AgVO_3$. The α-$AgVO_3$ can be described as a metastable phase, generated instantaneously below the melting point while cooled slowly and frozen quickly. The β-$AgVO_3$ is considered as a stable compound which has a monoclinic spatial group (de Campos, et al., 2021). In addition, the α-$AgVO_3$ phase would begin to transform into the β-$AgVO_3$ phase above the temperature of 200°C (Kittaka, et al., 1999). Figure 2.9 shows the structure of α-$AgVO_3$ (a) and β-$AgVO_3$ (b).

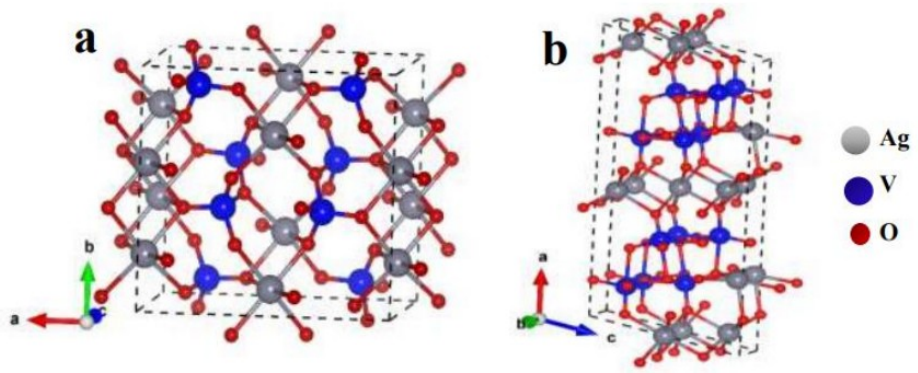

Figure 2.9: The Structure of (a) α-$AgVO_3$ and (b) β-$AgVO_3$ (Vali, et al., 2019).

2.7.2 Synthesis Method of AgVA

The most common synthesis method of AgVA is the hydrothermal method. Ordinarily, assistance of a surfactant, silver-vanadium ratio, hydrothermal time and hydrothermal temperature could affect photocatalytic performance and tune the structures of AgVA (Guo, et al., 2018). Many researchers have synthesized AgVA successfully using the hydrothermal method. For instance, Chen, et al. (2019) synthesized rod-like silver vanadate using the hydrothermal method. Hu, et al. (2008) reported that monoclinic structure Ag_3VO_4 could be prepared using hydrothermal method. Song, et al. (2009) used the hydrothermal method to prepare β-$AgVO_3$ nanoribbons with lengths of about 200μm to 300μm. Xu, et al. (2012) synthesized monoclinic phase structure β-$AgVO_3$ nanowires with length up to 300μm and diameter in the range of 200-700 μm. Through varying the hydrothermal conditions such as molar ratio of

silver to vanadium, pH values of the precursor solution, hydrothermal temperature and hydrothermal time, AgVA products with unique properties could be obtained. In general, the hydrothermal method has numerous benefits such as high purity, good crystallinity, controllable particle size, energy conservation, easy-to-control operating parameters and simple operation process. However, hydrothermal synthesis has a major drawback of time consuming as a few hours to a few days is required to synthesize the desired sample (Guo, et al., 2018). Besides the hydrothermal method, other methods have also been developed to synthesize AgVA such as ultrasonic-assisted synthesis, thermal decomposition method, soft chemical in-site synthesis techniques and microemulsion method.

Thermal decomposition method possesses many advantages like low cost, solventless, well crystallized products and simple operation. Thermal decomposition process could be performed by calcining the grinded raw materials for a certain time in a muffle furnace to obtain the desired sample product (Guo, et al., 2018). Sivakumar, et al. (2015) synthesized $AgVO_3$ nanorods using thermal decomposition method. They mix and grinded silver nitrate, ammonium metavanadate and 1-dodecenol follow by calcinating the mixtures at temperature of 450^{o}C for 5 h. The products obtained are nano sized $AgVO_3$ rods.

2.7.3 Application of Metal Vanadate Based Photocatalyst

Researchers found that hybrid or doped photocatalysts are more active than single semiconductor photocatalysts during the photocatalysis process. This has resulted in the synthesis of the nanostructure hybrid photocatalyst that has attracted great attention in the recent year. Vanadate can be described as oxyanion of vanadium, most of the vanadate compounds have a maximum oxidation state of +5 (Akhoondi, et al., 2021). Numerous applications have been developed for ternary vanadate one-dimensional which are production of electrochemical sensors, photocatalytic process and lithium batteries as well as its good photocatalytic and electrochemical properties (Monfort and Plesch, 2018; Josephine et al., 2020). Vanadates which have the attractive structural features received much attention due to their potential applications in the photocatalysis process. In general, vanadates provide the benefits of simple

preparation methods and close band gaps. There are numerous semiconductors shown capability for the absorption of visible light (Martinez-de La Cruz and Perez, 2010). Among them, bismuth vanadate ($BiVO_4$) which is considered as a layered vanadium type has gained much attention as a semiconductor photocatalyst due to its narrow band gap of 2.4-2.5 eV, specific electronic structure, controllable crystalline aspect and potential application for water oxidation and organic degradation. However, its photocatalytic performance is relatively low due to the poor surface absorption content, poor mobility of the charge carrier, low electron transfer rate and slow oxidation of water (Wang, et al., 2019). Besides $BiVO_4$, copper vanadate (CuVA) which has an energy band gap of 2 eV is also one of the promising materials that could be applied as a photocatalyst. It is the composite of 2 major chemical elements which are copper (Cu) and vanadium (V) (Hassan, et al., 2019). Though CuVA possesses less energy band gap and excellent properties of photochemical and electrochemical (Ghiyasiyan-Arani, et al., 2016; Sivakumar, et al., 2014), it still suffers low photocatalytic ability due to its low visible light absorption. Recently, several approaches have been developed in order to solve the defects of a single semiconductor photocatalyst and fabricate photocatalyst with high photocatalytic efficiency. Table 2.7 shows some examples of metal vanadate based photocatalysts and their applications.

Table 2.7: Examples of Metal Vanadate Based Photocatalysts and Their Applications.

Types of metal vanadate based photocatalysts	Application	Efficiency	Light source	Reference
$AgVO_3/g\text{-}C_3N_4$	-For the removal of tetracycline, TC	Degradation efficiency of 70% under 30 minutes of visible light irradiation.	300 W Xenon (Xe) lamp	Chen, et al., 2019
$AgVO_3/g\text{-}C_3N_4$	-For the removal of Rhodamine B, RhB	Degradation efficiency of 73% under 60 minutes of visible light irradiation.	300 W Xenon (Xe) lamp	Shi, et al., 2015
$AgVO_3/g\text{-}C_3N_4$	-For the removal of nitric oxide, NO	Degradation efficiency of 65% under 60 minutes of visible light irradiation.	300 W Xenon (Xe) lamp	Liu, et al., 2019
$AgVO_3/g\text{-}C_3N_4$	-For the removal of methyl orange, MO	Degradation efficiency of 54% under 60 minutes of visible light irradiation.	Light with wavelength, $\lambda \geq 420$ nm	Ye, et al., 2017
$BiVO_4/InVO_4$/CNQDs nanocomposite	-Rhodamine B, RhB photolysis	RhB removal-100%	300 W Xe lamp	Lin, et al., 2016

Table 2.7: Continued (Examples of Metal Vanadate Based Photocatalysts and Their Applications).

Types of metal vanadate based photocatalysts	**Application**	**Efficiency**	**Light source**	**Reference**
Z-scheme heterojunction V_2O_5/g-C_3N_4	-For the decomposition of contaminants such as methyl orange (MO), methylene blue (MB), tetracycline (TC), Rhodamine B (RhB)	RhB removal-95.5%	250 W Xe lamp	Hong, et al., 2016
g-C_3N_4/$Ag_2VO_2PO_4$ Z-scheme	-For the photocatalytic decomposition of methyl orange and phenol in the aqueous solution.	40% photodegraded	100 W halogen lamp	Zhang, et al., 2018
Z-scheme composite $BiVO_4$-Ru/$SrTiO_3$:Rh	-For solar water splitting	Quantum yield of 1.6% under 420 nm.	300 W Xe lamp	Jia, et al., 2014

2.8 Graphitic Carbon Nitride (g-C_3N_4)

Graphitic carbon nitride has a chemical formula of g-C_3N_4 and its chemical structure is shown in Figure 2.10. Based on Figure 2.10, several surface functionalities could be found on the structure of g-C_3N_4 (Thomas, et al., 2008). It can be described as a polymeric material which consists of nitrogen, carbon and hydrogen (impurity), connected through tris-triazine-based patterns (Zhu, et al., 2014).

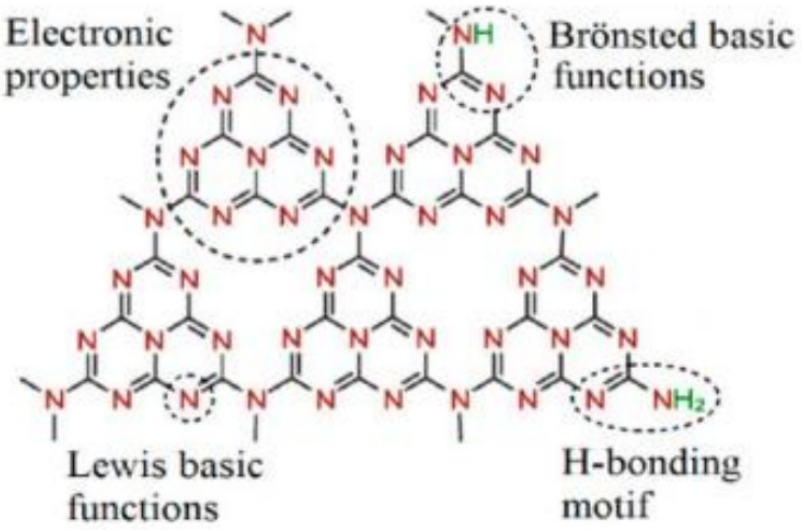

Figure 2.10: Chemical Structure of Graphitic Carbon Nitride, g-C_3N_4 (Chen, et al., 2019).

The g-C_3N_4 which is a non-metallic organic polymer semiconductor substance has wonderful conductivity. Next, it has several promising properties such as unique structural, optical, physicochemical and electric properties which encourage the g-C_3N_4 based materials involved in the energy, electronic and catalytic applications (Xu, et al., 2015; Xu, et al., 2014). In addition, g-C_3N_4 has an appropriate electronic band structure which makes it widely applied in numerous areas such as organic synthesis, CO_2 reduction, photocatalytic water splitting, disinfectant and pollutant degradation. Thus, the development of g-C_3N_4 based photocatalysts has received great interest for various applications via suitable modification which is able to overcome its shortcoming as stated below and at the same time maximize its photocatalytic efficiency (Wen, et al., 2017).

2.8.1 Characteristics of g-C_3N_4

Graphitic carbon nitride has become an attractive polymer photocatalyst in the recent year due to its' characteristic of moderate band gap of 2.7eV which caused g-C_3N_4 to become one of a visible light-driven photocatalyst (Qi, et al., 2020). Moreover, the VB and CB of g-C_3N_4 is situated at the suitable position of 1.3eV and -1.4eV respectively which greatly encourages g-C_3N_4 to absorb some portion of visible light. By this, water is split into oxygen (O_2) and hydrogen (H_2) whereas carbon dioxide is reduced into energy rich compounds which is to cope with energy crises and decompose several inorganic and organic contaminants into harmless substances. Moreover, g-C_3N_4 possess a characteristic of chemical and thermal stabilities that are highly attractive under harsh conditions of chemical and heat environments. Other than that, g-C_3N_4 also has numerous advantages such as non-toxic, metal free, environmentally friendly, low cost and high adaptability to large-scale changes in pH (Wen, et al., 2017). However, g-C_3N_4 suffers the same shortcoming of fast recombination of photogenerated electron-hole pairs and low visible light absorption as seen in many other semiconductor photocatalysts. Other than that, g-C_3N_4 has moderate oxidation ability, low charge mobility which affect the delocalization of electrons, and low surface area which result in small active sites for interfacial photoreaction (Yin, et al., 2015; Zhang, et al., 2011). These limitations caused g-C_3N_4 to have low photocatalytic efficiency. Thus, further modification is required to improve the photocatalytic efficiency of g-C_3N_4.

2.8.2 Synthesis Method of g-C_3N_4

Synthesis method of graphitic carbon nitride, g-C_3N_4 including methods of sonochemical (Huang, et al., 2015; Kumar, et al., 2014), soft-templating synthesis (Yan, 2012), template-directed solid-state (Zimmerman, et al., 2021; Savateev and Dontsova, 2016), solvent hot method and thermal polymerization (Mo, et al., 2015). Among these methods, the most common synthesis method of g-C_3N_4 is through a fractional thermal polymerization method using different precursors, usually nitrogen-rich materials such as dicyandiamide, guanidine carbonate, thiourea, ammonium thiocyanate, urea

and melamine (Alaghmandfard and Ghandi, 2022). Figure 2.11 shows the general preparation process of the sample of g-C_3N_4 with different raw materials using thermal polymerization method.

Figure 2.11: General Preparation Process of the Sample of g-C_3N_4 using Simple Thermal Polymerization Method (Gao, et al., 2021).

In fact, the synthesized g-C_3N_4 would show different photocatalytic activities, morphology and band gap due to the use of different raw materials under different temperatures (Zhao, et al., 2018). As shown in Figure 2.12, preparation of g-C_3N_4 with different precursors using thermal condensation method will have their respective optimum calcination temperatures.

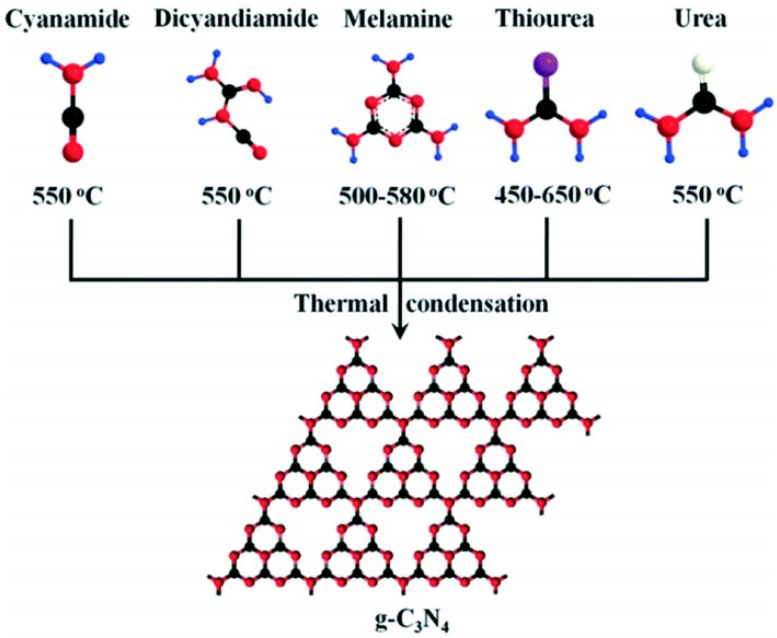

Figure 2.12: Preparation of g-C_3N_4 with Different Precursors using Thermal Condensation Method under Different Calcination Temperature (Iqbal, et al., 2018).

2.8.3 Application of g-C_3N_4 Based Photocatalyst

The g-C_3N_4 is a novel metal-free polymeric semiconductor, and it is unique from other semiconductors as it could be readily used to generate several greatly tailorable hybrid photocatalysts with controllable pore structure, morphologies, sizes, compositions, thickness and size distribution (Wen, et al., 2017). Thus, the design and fabrication of high effective g-C_3N_4-based photocatalysts through suitable modification have received great interest for several applications in photocatalysis and other fields like supercapacitor, lithium battery, electrocatalysis, photo-electrocatalysis, and solar cell. Other than that, g-C_3N_4-based photocatalysts have emerged as ideal candidates due to its applications of CO_2 reduction, degradation of pollutants, and photocatalytic water oxidation and reduction. Generally, g-C_3N_4-based photocatalysts are capable in solving the environmental and energy issues (Wen, et al., 2017). Table 2.8 shows the examples of g-C_3N_4-based photocatalysts and their capability for environmental remediation. According to Table 2.8, it is noted that g-C_3N_4-based heterojunction photocatalysts could be widely applied for the photocatalytic degradation of contaminants

especially liquid-phase contaminants like methylene blue (MB), tetracycline hydrochloride, Rhodamine B (RhB), phenol and methyl orange (MO).

Table 2.8: Examples of g-C_3N_4 Based Photocatalysts and Their Capability for Environmental Remediation.

Types of g-C_3N_4 based photocatalysts	**Type of contaminants**	**Degradation efficiency**	**Reference**
ZnO/g-C_3N_4	Phenol	Phenol removal-99.5%	Rosli, et al., 2018
$Ti_3C_2T_x$/g-C_3N_4	Tetracycline hydrochloride	Tetracycline hydrochloride removal-77%	Yi, et al., 2020
g-C_3N_4/AC	Phenol	Phenol removal- 100%	Chen, et al., 2016
g-C_3N_4/Ti_3C_2/TiO_2	Tetracycline hydrochloride	Tetracycline hydrochloride degradation-78.34%	Diao, et al., 2020
$BiVO_4$/PDA/g-C_3N_4	Glyphosate	Glyphosate degradation-100%	Huo, et al., 2018
g-C_3N_4/Ti_3C_2/black phosphorus	Ciprofloxacin	Ciprofloxacin removal-99%	Zhou, et al., 2021
g-C_3N_4/ $BiVO_4$	Methylene blue	Higher degradation efficiency than pure g-C_3N_4 and $BiVO_4$	Cheng, et al., 2017
In_2O_3/g-C_3N_4	Rhodamine B	RhB removal-99%	Chen and Zhang, 2014
SiO_2/g-C_3N_4	Rhodamine B	RhB removal-94.3%	Lin, et al., 2015
TiO_2/g-C_3N_4	Rhodamine B	RhB removal-82%	Zhang, et al., 2015
g-C_3N_4/SnO_2	Methyl orange	MO removal-73%	Zang, et al, 2014
g-C_3N_4/Ag_2O	Methyl orange Phenol	MO removal-90% Phenol removal-82%	Xu, et al., 2013
ZnO/g-C_3N_4	Methylene blue	Methylene blue removal-98.3%	Adhikari, et al., 2015

2.9 Research Gap

According to the literature review, g-C_3N_4 and $AgVO_3$ are considered as an ideal semiconductor photocatalyst as both of them are applicable under visible light and have narrow energy band gaps. The combination of g-C_3N_4 and $AgVO_3$ not only could produce a greatly active heterojunction composite namely silver vanadate and graphitic carbon nitride composite, $AgVO_3$/g-C_3N_4. Meanwhile, the drawbacks faced by g-C_3N_4 and $AgVO_3$ as a single semiconductor photocatalyst could also be overcome. However, it is found that the research which applied $AgVO_3$/g-C_3N_4 composite for the degradation of antibiotics is very scant. In section 2.7.3, Chen, et al. (2019) firstly reported the use of $AgVO_3$/g-C_3N_4 composite for the degradation of antibiotic, tetracycline. Other researchers tended to apply $AgVO_3$/g-C_3N_4 composite for the removal of dye. Thus, it is of great value to investigate the photocatalytic ability of $AgVO_3$/g-C_3N_4 composite and its degradation efficiency for the decomposition of antibiotics.

In this project, $AgVO_3$/g-C_3N_4 composite was synthesized through the wet chemical method. Oxytetracycline was used as act as the source of pollutant and the photocatalytic degradation experiment was carried out to examine the photocatalytic performance of the $AgVO_3$/g-C_3N_4 composite for the removal of OTC under LED light irradiation.

CHAPTER 3

METHODOLOGY AND WORK PLAN

This chapter involves all the materials and chemicals required for the synthesis of pure AgVA, pure g-C_3N_4 and AgVA/g-C_3N_4 composite photocatalysts with different weight percentage of AgVA (10, 30, and 50 wt%). Besides, the preparation method for all of the photocatalysts is also discussed. Other than that, the methodology on the investigation of photocatalytic efficiency of the AgVA/g-C_3N_4 composite for the removal of oxytetracycline is outlined. In addition, the techniques applied to investigate the characterization of AgVA/g-C_3N_4 composite photocatalyst are discussed in this chapter.

3.1 List of Materials and Chemicals

The chemicals required throughout this research are determined and their specification is tabulated in Table 3.1 accordingly.

Table 3.1: List of Chemicals and Their Specification.

Chemicals	**Chemical formula**	**Brand**	**Purity, %**	**Usage**
Urea powder	CH_4N_2O	Fisher Scientific	99.0-100.5	Synthesis of g-C_3N_4
Silver nitrate	$AgNO_3$	Sigma-Aldrich	≥99.9	Synthesis of AgVA
Ammonium metavanadate	NH_4VO_3	Sigma-Aldrich	≥99.9	Synthesis of AgVA
Oxytetracycline hydrochloride	$C_{22}H_{24}N_2O_9$•HCl	Sigma-Aldrich	94.5-102	Source of pollutant
Ammonium hydroxide	NH_4OH	Sigma-Aldrich	28.0-30.0	pH Adjuster
Sodium hydroxide	NaOH	Sigma-Aldrich	≥98.0	pH Adjuster
Hydrochloric acid	HCl	Merck	37	pH Adjuster

Table 3.1: Continued (List Chemicals and Their Specification).

Chemicals	**Chemical formula**	**Brand**	**Purity, %**	**Usage**
Isopropanol	C_3H_8O	Sigma-Aldrich	≥99.5	For washing purpose (remove organic compounds)
Dimethyl sulfoxide	C_2H_6OS	Univar	99	Scavenging experiment
Ethylenediaminetetraacetic Acid Disodium Salt	$C_{10}H_{16}N_2Na_2O_8^{+2}$	Bio Basic Inc.	99	Scavenging experiment
Isopropanol	C_3H_8O	Bendosen	83.5	Scavenging experiment
Benzoquinone	$C_6H_4O_2$	Sigma-Aldrich	>98	Scavenging experiment

3.2 Experimental Flowchart

The overall process flow of this project is summarized in Figure 3.1. The experimental flowchart can be categorized into three sections as following:

i) Photocatalysts synthesis method.

ii) Characterization of the photocatalysts synthesized.

iii) Photocatalytic efficiency of photocatalysts synthesized for the removal of oxytetracycline.

iv) Scavenging experiment to identify the most reactive oxidizing radicals.

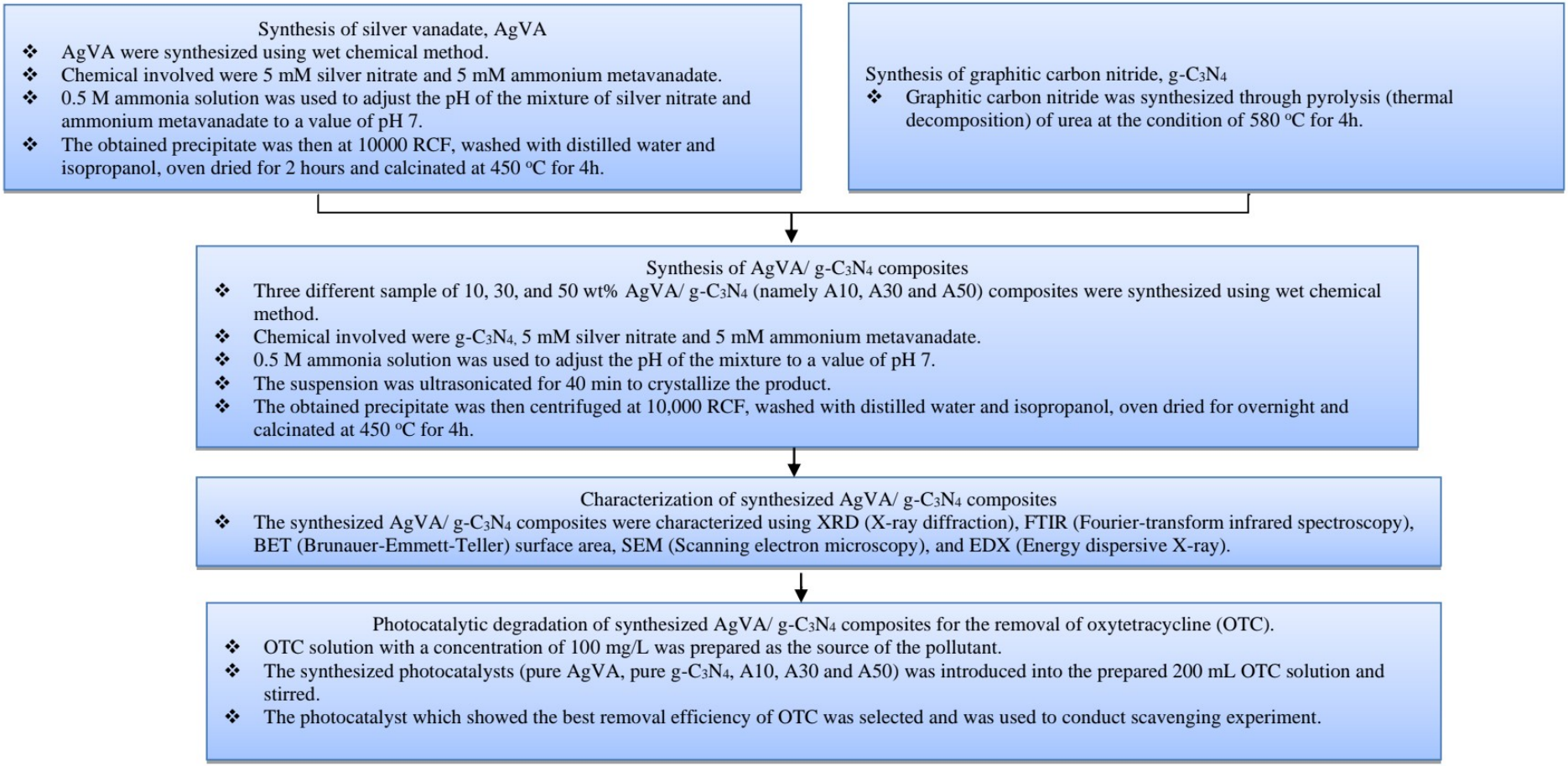

Figure 3.1: Overall Experimental Flowchart

3.3 Synthesis of Pure Silver Vanadate, AgVA

Silver vanadate, AgVA was synthesized using a wet chemical method (Singh, et al., 2010). The chemical used to prepare AgVA including silver nitrate, $AgNO_3$ and ammonium metavanadate, NH_4VO_3. Firstly, 125 mL of 5 mM silver nitrate was prepared. Then, 125 mL of 5 mM ammonium metavanadate were added dropwise into silver nitrate solution under constant stirring at the temperature of 25°C (room temperature). 0.5 M ammonia solution was used to adjust the pH of the mixture to a value of pH 7. The mixture was then ultra-sonicated for 30 min for the crystallization to occur. The obtained precipitate was centrifuged at 10,000 RCF, rinsed with distilled water and 99% isopropanol multiple times and dried in the oven for a few hours. Lastly, the obtained sample was calcined in furnace at 450 °C for 4 h. Figure 3.2 shows the preparation step for pure silver vanadate, AgVA.

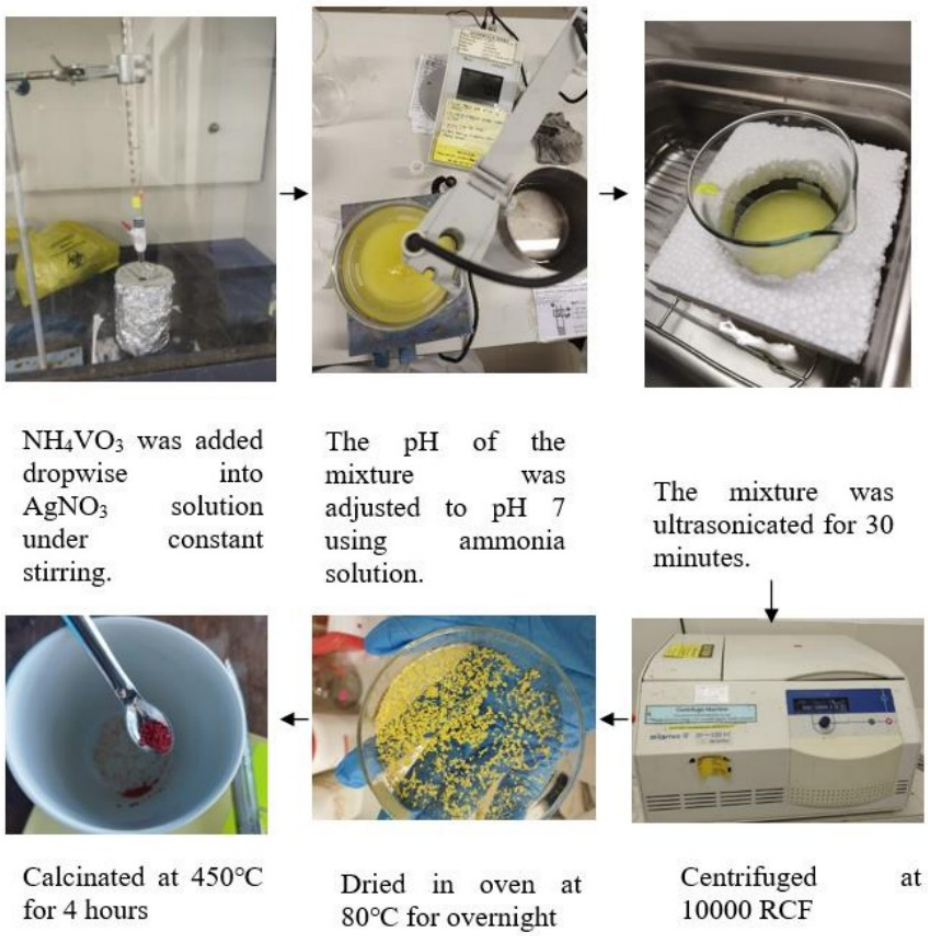

Figure 3.2: Preparation Step of Pure Silver Vanadate, AgVA.

3.4 Synthesis of Graphitic Carbon Nitride, g-C_3N_4

Graphitic carbon nitride, g-C_3N_4 was synthesized using thermal treatment of urea (urea pyrolysis) (Yang, et al., 2021). Firstly, 20 g of the urea power was weighed and placed into an alumina crucible with a cover. A piece of aluminium foil was used to wrap the alumina crucible and the wrapped crucible was then put into furnace to calcinate at 580 ^oC for 4 h to complete the reaction as shown in Figure 3.3. At the end of the reaction, products with the appearance of pale yellowish colour were collected and crushed using pestle and mortar into fine powder.

***Important note**:* wrapping of the alumina crucible before placing it into the furnace is an important step for the preparation of g-C_3N_4 as the formation of ammonia vapor from the thermal decomposition of urea is crucial for the generation of g-C_3N_4. Without covering the alumina crucible, the vapor generated will escape which causes the reaction to not occur.

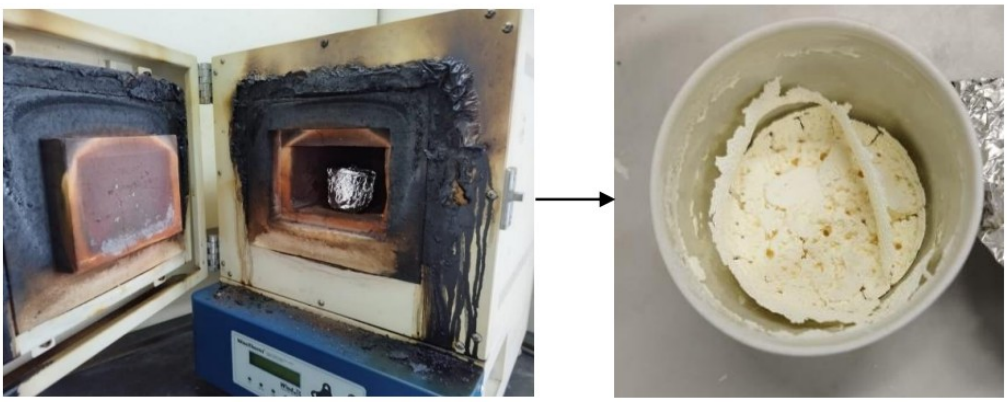

Figure 3.3: Pyrolysis of Urea in Programmable Furnace at 580 ℃ for 4 h.

3.5 Synthesis of AgVA/g-C_3N_4 Composites

The AgVA/g-C_3N_4 composite can be synthesized using the wet chemical method. Three different sample of AgVA/g-C_3N_4 composite was prepared through varying the weight percentage of AgVA to 10, 30, and 50 wt% and the composites are named as A10, A30 and A50 respectively. In order to produce 50 wt% AgVA/g-C_3N_4 composite, 81.697 mg of g-C_3N_4 were dispersed into 125 mL of 5 mM silver nitrate through sonification for 5 min. 125 mL of 5 mM concentration of ammonium metavanadate were added drop by drop into the suspension under constant stirring at room temperature. 0.5 M ammonia, NH_3 solution was used to adjust the mixture to pH 7. The yield of AgVA was found decreasing drastically while using high concentration of ammonia solution or sodium hydroxide to increase the pH of the mixture. The suspension was ultrasonicated for 40 min to crystallize the product. The obtained precipitate was centrifuged at 10,000 RCF and rinsed with distilled water and 99% isopropanol few times to remove the organic compounds. The sample was then oven dried for overnight followed by the calcination in furnace at 450 ^oC for 4 h.

Another two AgVA/g-C_3N_4 composites with the weight percentage of 10 and 30 wt% AgVA were prepared using the similar route. For each composite, the feed quantity of g-C_3N_4 was adjusted depending on the mass ratio and yield of AgVA.

3.6 Characterization of AgVA/g-C_3N_4 Composites

The photocatalyst characterization techniques applied in this research including Scanning electron microscopy (SEM), Fourier-transform infrared spectroscopy (FTIR), Brunauer-Emmett-Teller surface area (BET), X-ray diffraction (XRD), and energy dispersive X-ray (EDX). X-Ray diffraction (XRD) is a powerful-analytical technique that has been applied for studying the crystalline structure of the synthesized photocatalyst composites. In this study, XRD analysis is carried out using Copper (Cu) source which has a wavelength of 1.54 Å to act as the target in the diffractometer. The operating condition of XRD was set to operate at 40.0 kV and 30.0 mA. Moreover, the diffraction pattern of the synthesized photocatalysts has been collected within the angles range of 10° and 80° with a scanning speed of 2 degree per minutes. Scanning Electron Microscopy (SEM) is referred to a powerful imaging technique used to examine the surface structure and morphology of samples at high magnification. Fourier Transform Infrared Spectroscopy (FTIR) is a technique used to analyse the infrared region of the electromagnetic spectrum. By performing the FTIR, the functional groups and chemical bonds present in the sample could be determined. The Brunauer-Emmett-Teller (BET) surface area is to quantify the total surface area of a solid material, which is an important parameter for understanding its properties and performance in various applications. The BET surface area is determined by measuring the amount of gas absorb by a solid material at different pressures and temperature.

In summary, the purpose of carrying out the characterization work is to study the physical and chemical properties of the prepared photocatalysts which are pure AgVA, pure g-C_3N_4, A10, A30 and A50. As the physicochemical properties of the prepared photocatalysts are greatly related to their photocatalytic ability in the degradation process. The respective function of the previous mentioned technique is summarized in Table 3.2.

Table 3.2: Application of the Photocatalyst Characterization Techniques.

Techniques	Application	Equipment model
XRD	-Fast analytical technique -To investigate the crystallographic structure of a sample such as molecular structure, crystallite size and atomic arrangement.	Shimadzu XRD-6000
SEM	-To characterize the surface features -To investigate the morphological changes such as distribution of nanoparticles, shape and pore size.	Hitachi Model S-3400N
FTIR	-To determine the functional groups and chemical bonds present in the sample	Nicolet IS10 FTIR
BET	-To determine the surface area -Commonly applied in the study of surface morphological	Micromeritics
EDX	-Chemical microanalysis technique -To determine the elemental composition and lattice spacing of a sample	Hitachi Model S-3400N

3.7 Photocatalytic Degradation of Oxytetracycline

In this section, the photodegradation of OTC was examined over the as-synthesized pure AgVA, pure g-C_3N_4, A10, A30 and A50 under visible light irradiation. A constant weight of 50 mg for all the synthesized photocatalysts are used to conduct the photodegradation test on the removal of OTC under the visible light source provided by the 30W LED light bulb. The detailed procedures were discussed as follows.

At first, OTC solution with a concentration of 100 mg/L (100 ppm) was prepared as the source of the pollutant. 0.1 M ammonia solution was used to adjust the solution to pH 5. 50 mg of A10 was introduced into the prepared 200 mL OTC solution and stirred. Before carrying out the photodegradation

experiment, the solution was stirred overnight in the dark condition where a box wrapped with aluminium foil to reach adsorption-desorption equilibrium.

The photocatalysts involved in the photocatalytic experiment include AgVA, g-C_3N_4, A10, A30 and A50. In the photocatalytic degradation test, the 30 W LED light was switched on and the timer was started. The constant variable is the distance between the light bulb and the surface of the solution where a distance of 10 cm was fixed. At the time of 0, 30, 60, 90, 120, 150, 180, 240, 300, and 360 min, an aliquot (3 mL) of OTC was collected and filtered using a 0.21 μm syringe filter to remove the solid. The concentration of OTC in the sample collected was then examined using the UV-vis spectrophotometer (Agilent Cary 100). In addition, the photodegradation experiment was carried out at room temperature by placing the beaker in a homemade water bath. The similar steps as above were repeated by replacing A10 with AgVA, g-C_3N_4, A30, and A50 for comparison.

The photocatalyst which showed the best removal efficiency of OTC was selected and was used in further study. Figure 3.4 shows the experiment setup for the photocatalytic degradation of OTC by using synthesized photocatalysts under visible light irradiation.

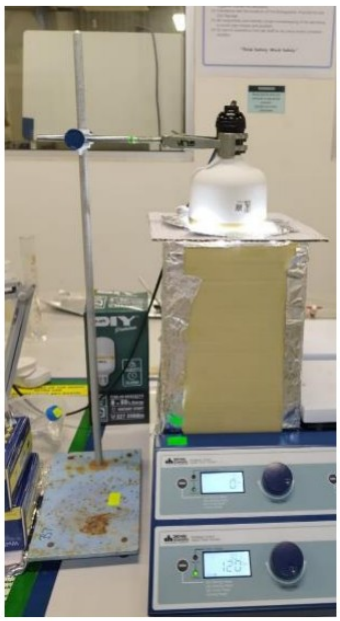

Figure 3.4: Experiment Setup for the Photocatalytic Degradation of OTC.

3.8 Identification of OTC Concentrations

The OTC concentrations were quantified by using Ultraviolet-visible spectrophotometer (Agilent Cary 100) at maximum wavelength of 274 nm. Five standard solutions with 20, 40, 60, 80 and 100 ppm of OTC were prepared to plot calibration curves of OTC as shown in Figure 3.5.

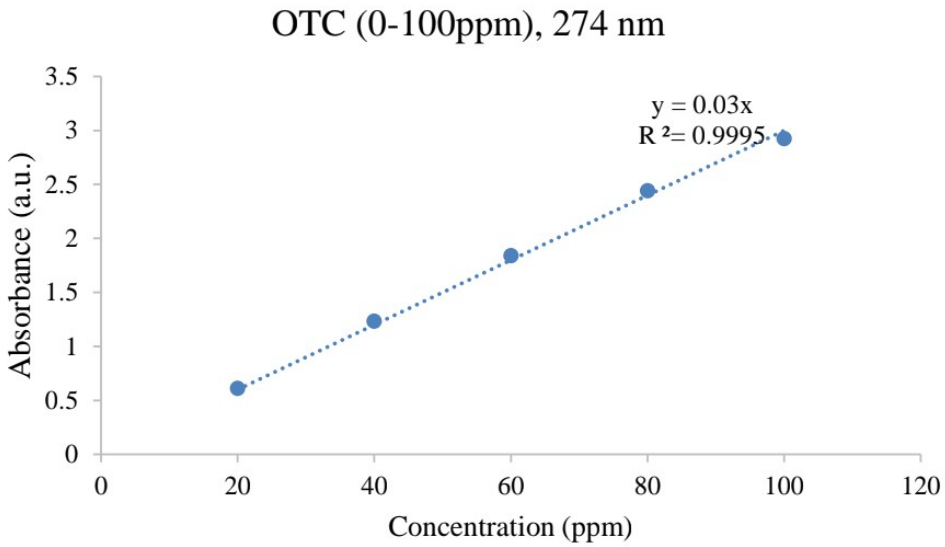

Figure 3.5: Calibration Curve of OTC ranging from 0 to 100 ppm at 274 nm.

3.9 Scavenging Experiment

Scavenging Experiment was carried out to determine the active species of radicals which contributed to the efficiency of photocatalytic degradation of OTC. In this experiment, the scavengers involved are isopropanol (IPA), dimethyl sulfoxide (DMSO), benzoquinone (BQ), and ethylenediaminetetraacetic acid disodium salt (EDTA-2Na$^+$). 0.05 g of the photocatalyst with best photocatalytic performance was selected to undergo scavenging experiments with 5 mM of each scavenger. The procedure of the scavenging experiment is similar to the photocatalytic degradation experiment. In addition, DMSO, IPA, EDTA-2Na$^+$ and BQ was used to analyse e^-, $^{\bullet}OH$, h^+ and $^{\bullet}O_2^-$ respectively.

CHAPTER 4

RESULTS AND DISCUSSION

In this section, the results obtained from the analysis, characterization, and application work are discussed. In order to improve the photocatalytic performance, AgVA was used to modify g-C_3N_4 and produce composite photocatalysts namely A10, A30, and A50 which had different weight percentages of AgVA. The characterization work was performed to investigate the physicochemical properties of pure AgVA, pure g-C_3N_4, A10, A30, and A50. It is important to carry out the characterization work on each of the synthesized photocatalysts as it helps to analyse and determine the crystallographic structure, surface features, elemental composition, and lattice spacing of the synthesized photocatalysts. The equipment involved in these characterization works are XRD, SEM, EDX, FTIR, and BET.

Besides, photodegradation experiment was performed where the degradation ability of the prepared photocatalysts on the removal of antibiotic, OTC was examined and the photocatalyst that possessed the best performance was further used to perform the scavenging experiment in order to identify the active species of radicals present in the selected composite photocatalyst.

4.1 X-Ray Diffraction (XRD) Analysis

Figure 4.1 shows the XRD pattern of pure g-C_3N_4 where diffraction peaks with low intensity occurred around 13.0°. This peak could most likely be due to the structure of the tri-s-triazine unit with interplanar spacing. Moreover, an obvious diffraction peak appeared around 27.7°. This peak was likely to be attributed to the conjugated aromatic system. Both of the two distinct crystalline diffraction peaks of 13.0° and 27.7° corresponded to the (1 0 0) and (0 0 2) crystallographic planes of the tetragonal phase of g-C_3N_4 respectively (JCPDS 87-1526) (Cao, et al., 2017). Since no other obvious peaks from possible impurities are observed, it could be concluded that pure g-C_3N_4 was synthesized successfully.

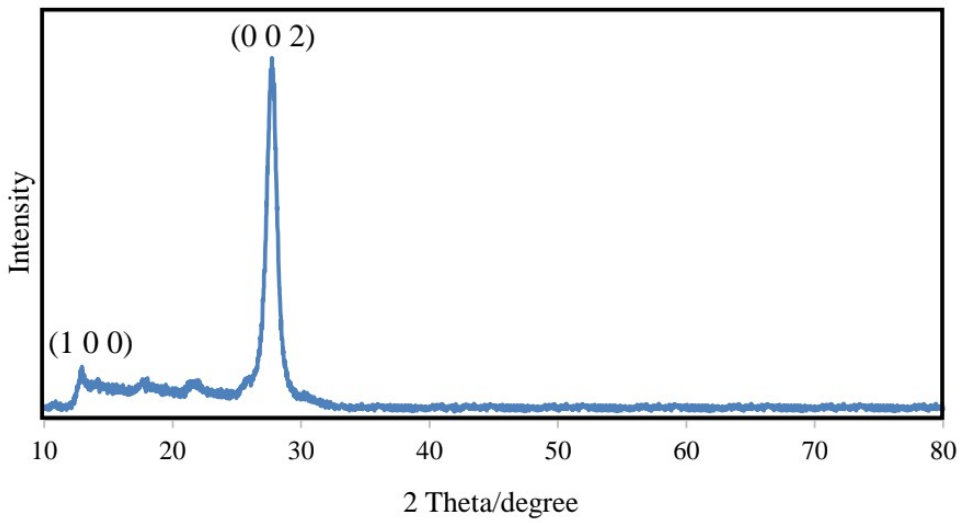

Figure 4.1: XRD Pattern of Pure g-C_3N_4.

The XRD pattern of the synthesized pure AgVA is shown in Figure 4.2. Based on Figure 4.2, the diffraction peak could be indexed to the pure AgVA phase which is also further confirmed by the standard data (JCPDS No. 29-1154). It could be observed that the XRD pattern of the pure AgVA sample showed diffraction peaks at around 22.6°, 28.4°, 30.0°, 32.9°, 33.6°, 34.5°, 34.9°, 51.0°, 55.03° which could be indexed to the AgVA (0 0 2), (-2 1 1), (5 0 1), (-4 1 1), (-1 1 2), (-6 0 2), (1 1 2), (0 2 0), and (-5 1 4) planes, respectively (JCPDS No. 29-1154) (Xiang, et al., 2016; Zhang, et al., 2018). These peaks indicated that the synthesized AgVA was well crystallized. Moreover, the diffraction peaks of the pure AgVA were observed to have a high intensity which implied the good crystallinity of the synthesized AgVA.

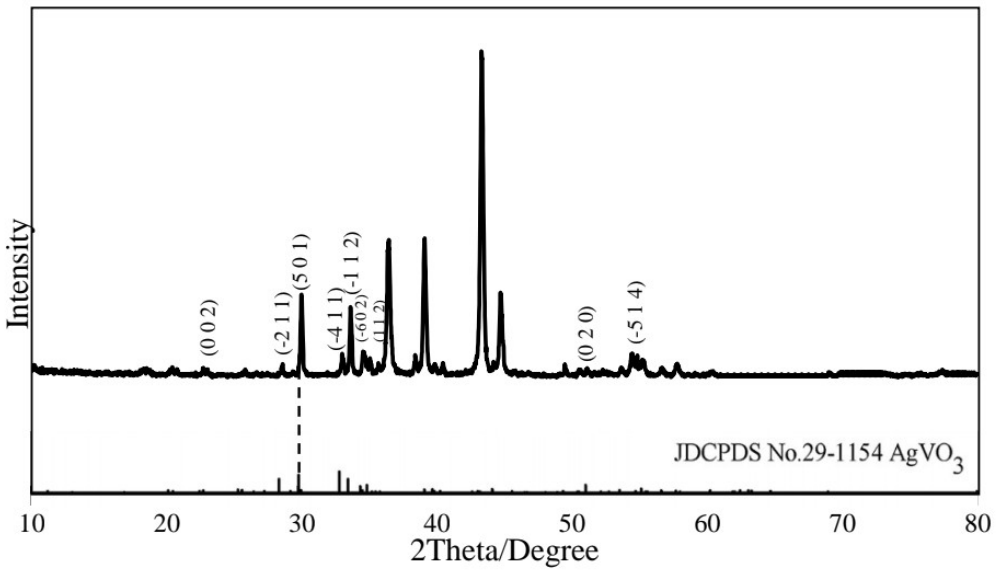

Figure 4.2: XRD Pattern of Pure AgVA.

In order to have a better observation, the XRD patterns of all the as-prepared samples have been placed together as shown in Figure 4.3. Based on the XRD analysis result of A50, the characteristic peaks of g-C_3N_4 at position 27.7° could not be observed which might be due to the fact that the content of g-C_3N_4 is relatively low in the sample of A50 and thus difficult for XRD to detect. Whereas XRD patterns for A30 and A10 have shown main characteristic peaks of both AgVA and g-C_3N_4, indicating the presence of these two components in the synthesized composite. In addition, it could clearly be observed that the intensity of the g-C_3N_4 diffraction peaks became weaker in the order of A10, A30 followed by A50 as a result of the increasing AgVA weight percentage. Overall, the XRD result suggests the co-existence of AgVA and g-C_3N_4 in the composite of A10, A30, and A50, indicating AgVA has successfully been coupled into g-C_3N_4.

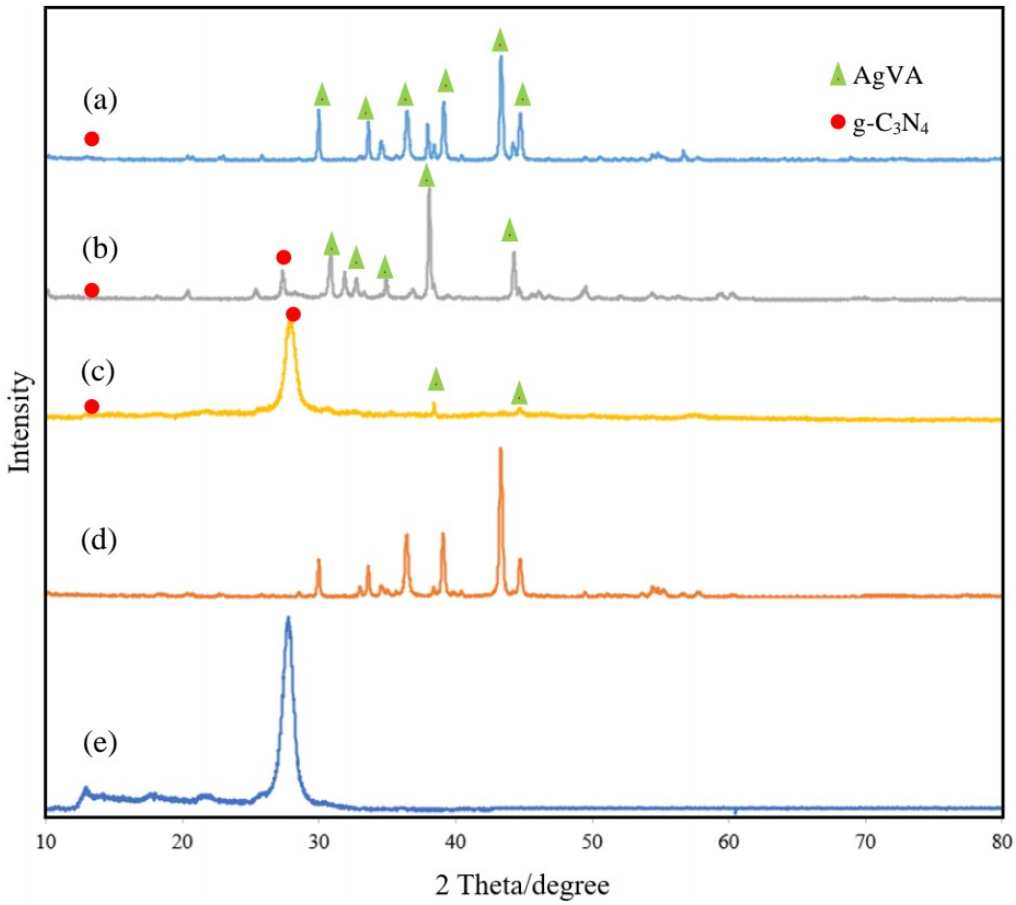

Figure 4.3: XRD Pattern of (a) A50, (b) A30, (c) A10, (d) Pure AgVA, (e) Pure g-C_3N_4.

4.2 Scanning Electron Microscopy (SEM)

Figure 4.4 (a) to (c) shows the SEM image for the sample of pure g-C_3N_4 where numerous tiny pores are generated within the loose layered g-C_3N_4. In other words, the synthesized pure g-C_3N_4 exhibits a two-dimensional structure with typical irregular porosity. Figure 4.4 (d) to (f) show the SEM image sample of pure AgVA at different magnifications. According to Chen, et al. (2018), the morphologies of the silver vanadate would be influenced by the pH value and molar ratios of Ag/V. Chen, et al. (2018) reported that AgVA that is synthesized with a molar ratio of Ag:V = 1:1 and at a pH value of 7 would show its morphology as a rod-like structure. Based on its SEM images, the synthesized pure AgVA exists in a rod-like shape which has similar findings to Chen, et al. (2018). Thus, it is concluded that a nanorod of silver vanadate has been synthesized successfully.

Figure 4.4 (g)-(i), (j)-(l), and (m)-(o) show the morphology of samples A10, A30, and A50 respectively at different magnifications of 5000X, 10000X, and 15000X. Based on the SEM images of A10 and A30, it shows that AgVA effectively inherits the g-C_3N_4 sheet structure where the AgVA nanorods are randomly dispersed on the g-C_3N_4 matrix, filling its holes and cavities, and therefore constructing a composite material. Moreover, the lamellar structure properties of pure g-C_3N_4 are compatible with the abundance of gauze-like corrugated and wrinkled layered structures present in the SEM images of A10 and A30. With the increasing weight percentage of AgVA, a significant morphological variation could be observed as shown in Figure 4.4 (g)-(i), (j)-(l), and (m)-(o) whereby the structure of g-C_3N_4 gradually decreased and was replaced by a large number of rod-like structures of AgVA. This variation could be observed clearly in the SEM image of A50 as shown in Figure 4.4 (m)-(o).

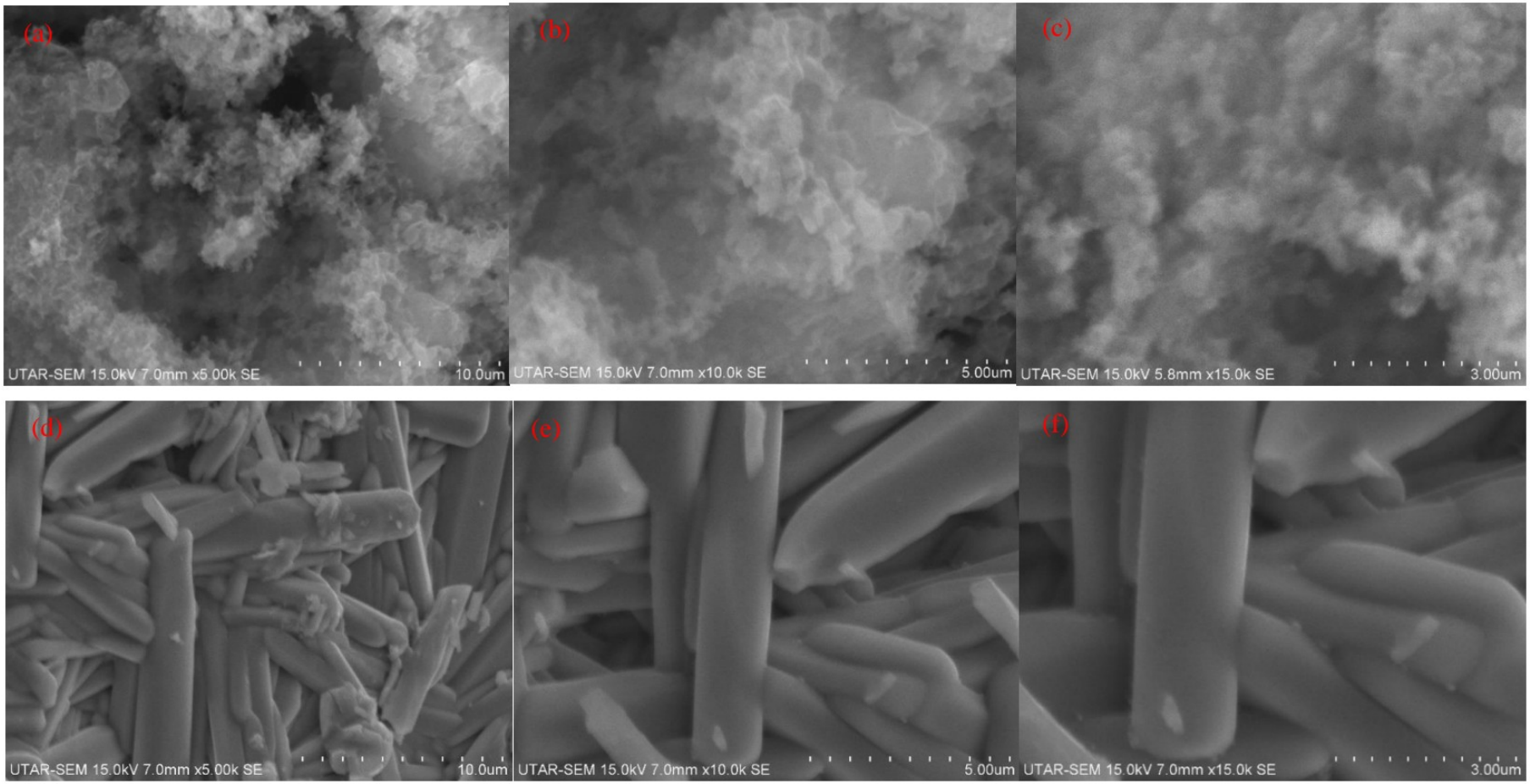
(a)
UTAR-SEM 15.0kV 7.0mm x5.00k SE
10.0um
(b)
UTAR-SEM 15.0kV 7.0mm x10.0k SE
5.00um
(c)
UTAR-SEM 15.0kV 5.8mm x15.0k SE
3.00um
(d)
UTAR-SEM 15.0kV 7.0mm x5.00k SE
10.0um
(e)
UTAR-SEM 15.0kV 7.0mm x10.0k SE
5.00um
(f)
UTAR-SEM 15.0kV 7.0mm x15.0k SE
3.00um

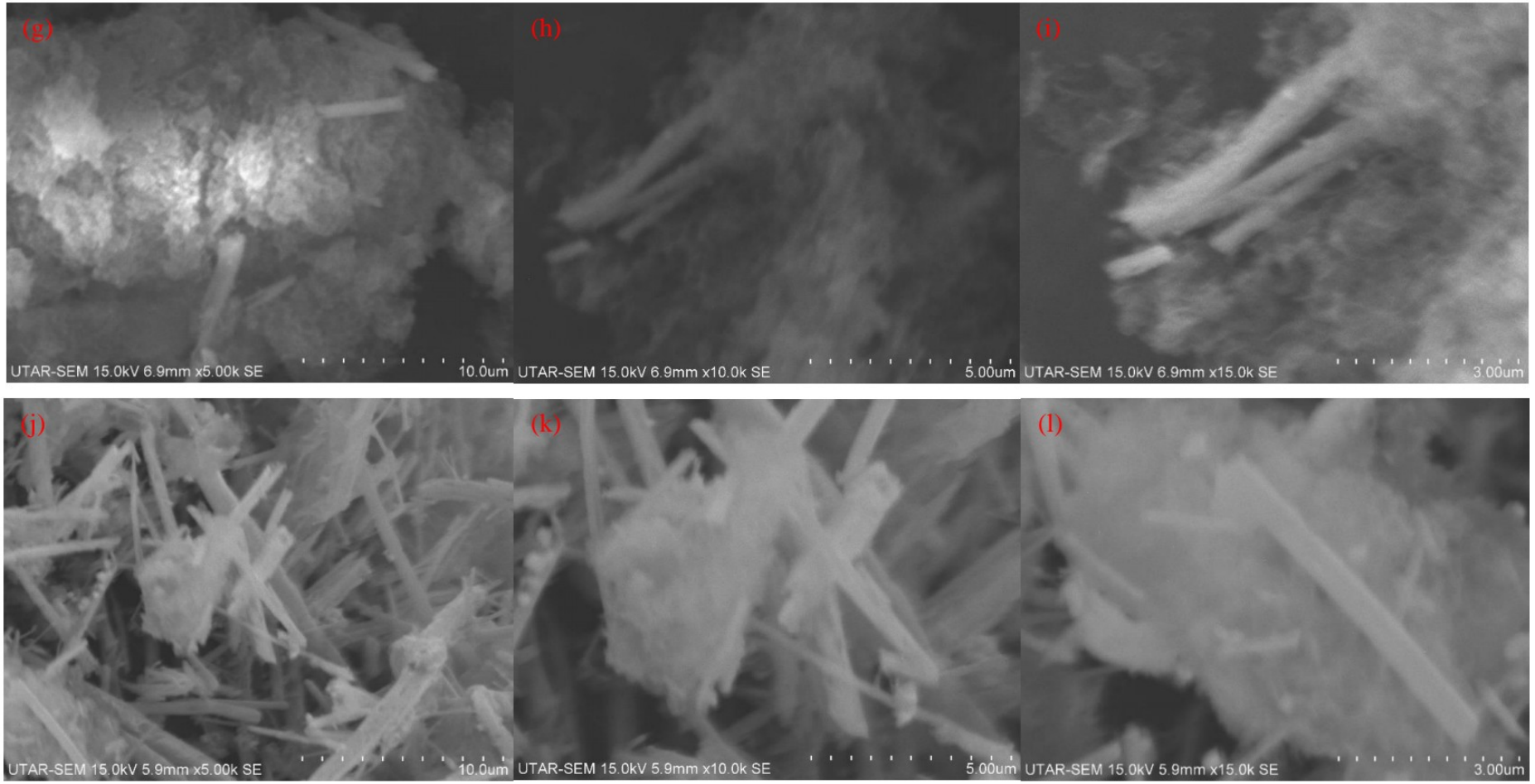
(g)
UTAR-SEM 15.0kV 6.9mm x5.00k SE
10.0um
(h)
UTAR-SEM 15.0kV 6.9mm x10.0k SE
5.00um
(i)
UTAR-SEM 15.0kV 6.9mm x15.0k SE
3.00um
(j)
UTAR-SEM 15.0kV 5.9mm x5.00k SE
10.0um
(k)
UTAR-SEM 15.0kV 5.9mm x10.0k SE
5.00um
(l)
UTAR-SEM 15.0kV 5.9mm x15.0k SE
3.00um

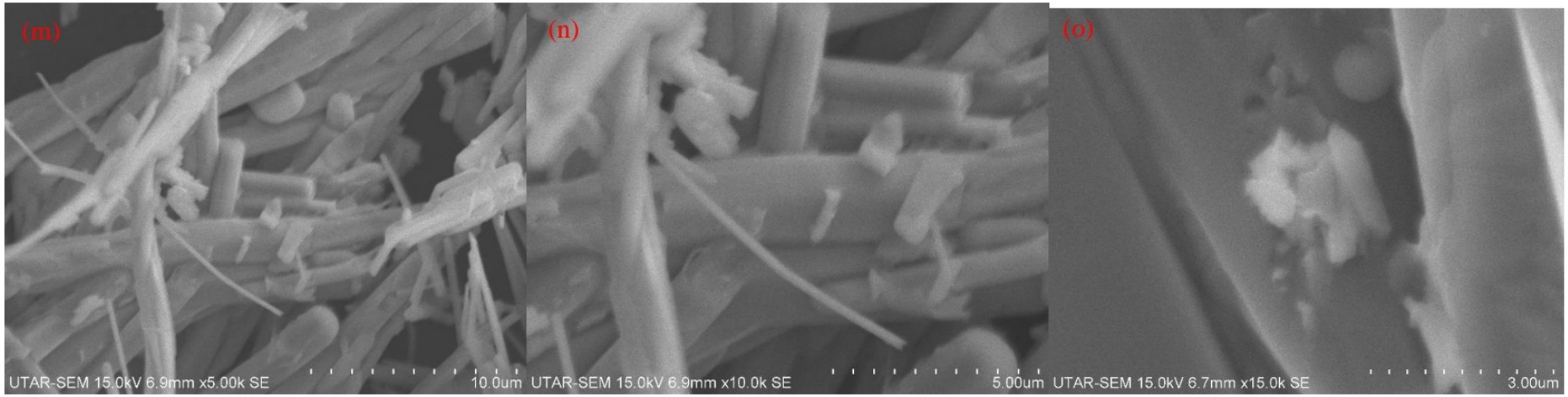

Figure 4.4: SEM Image of (a)-(c) pure g-C_3N_4, (d)-(f) pure AgVA, (g)-(i) A10, (j)-(l) A30, and (m)-(o) A50.

4.3 Energy Dispersive X-Ray (EDX) Analysis

In this section, the elemental composition of all the synthesized photocatalysts, including pure AgVA, pure g-C_3N_4, A10, A30, and A50 were examined using the EDX detector. According to the EDX analysis, it could be noted that there are three elements present in the AgVA which are silver (Ag), vanadium (V), and oxygen (O). Whereas the three elements existing in the sample of pure g-C_3N_4 consist of carbon (C), nitrogen (N) and oxygen (O). Theoretically, only C and N atoms are expected to be detected in its elemental composition. The presence of O elements was assigned to the occurrence of the reaction when urea came into contact with air in the atmosphere. Furthermore, the presence of these five elements (C, N, O, V, and Ag) have been confirmed for all three synthesized composite photocatalysts (A10, A30, and A50). In addition, it could be concluded that there are no impurities generated in the synthesized photocatalyst as no other elements are detected. The elemental composition of all the synthesized photocatalysts obtained from EDX analysis are summarized in Table 4.1 and their EDX analysis reports are attached in Appendix A accordingly.

Table 4.1: Elemental Composition of Synthesized Photocatalysts.

Photocatalyst	**Elemental Composition (%)**				
	Carbon	Nitrogen	Oxygen	Vanadium	Silver
Pure g-C_3N_4	52.01	39.76	08.23	-	-
Pure AgVA	-	-	50.41	25.95	23.64
A10	46.11	38.05	11.37	02.19	02.28
A30	39.06	16.98	26.13	09.12	08.17
A50	05.22	02.84	42.82	26.56	22.57

4.4 Fourier transform infrared (FTIR)

The FTIR spectra of the synthesized photocatalysts (pure g-C_3N_4, pure AgVA, A10, A30 and A50) are illustrated in Figure 4.5, where all of them were examined in the spectra region within 4000 to 400 cm^{-1}.

For pure g-C_3N_4, the sharp peak present at 803.68 cm^{-1} was assigned to the C-N and C-C stretching vibrations as well as the triazine units. The broad absorption bands appeared in the region of 3400-3000 cm^{-1} corresponding to the N-H stretching and O-H stretching vibrations from the absorbed water molecule, H_2O (Hummers and Offerman, 1958; Hoffmann, et al., 1995). Moreover, the complex spectra observed in the region between 1800 to 900 cm^{-1} corresponded to s-triazine derivatives such as bridging C-NH-C or trigonal C-N(-C)-C whereas the peaks observed at approximately 1531.69 and 1625.86 cm^{-1} were attributed to the C=N stretching vibrations (Lotsch, et al., 2007; Li, et al., 2010; Narkbuakaew and Sujaridworakun, 2020).

The FTIR spectrum of pure AgVA revealed characteristic bands for VO vibrations within the range of 400-1000 cm^{-1} (Sediri and Gharbi, 2009). There was a strong and relative absorption that could be observed at 760.93 cm^{-1} which was attributed to symmetric V-O stretching vibration (Frost, et al., 2005). Furthermore, the existence of V-O stretching vibration in AgVA also caused a peak to appear at 455.76 cm^{-1} (Akbarzadeh and Amin, 2015).

According to Figure 4.5, the FTIR spectra of A10, A30, and A50 resembled the characteristic peaks of pure AgVA and pure g-C_3N_4, however the majority of the vibration bands were slightly shifted from their original positions because of the strong interaction between AgVA and g-C_3N_4. Other than that, the respective transmittances of the vibration bands of AgVA and g-C_3N_4 were found to change with the composition. Moreover, it is interesting to note that the vibrational bands of the g-C_3N_4 arising at 803.68 cm^{-1} dominated the FTIR spectrum of A10. The strong vibrational band of AgVA at position of 760.93 cm^{-1} almost disappeared. This might be due to the fact that the AgVA nanorods were covered by g-C_3N_4 as shown in the obtained SEM image of A10 in Figure 4.4 (g)-(i). Whereas in the cases of A30 and A50, the nanorods were not completely covered by g-C_3N_4 due to the higher content of AgVA which results in a low energy shoulder at the g-C_3N_4 mode. In addition,

the FTIR analysis reports for all the prepared photocatalysts are attached in Appendix B accordingly.

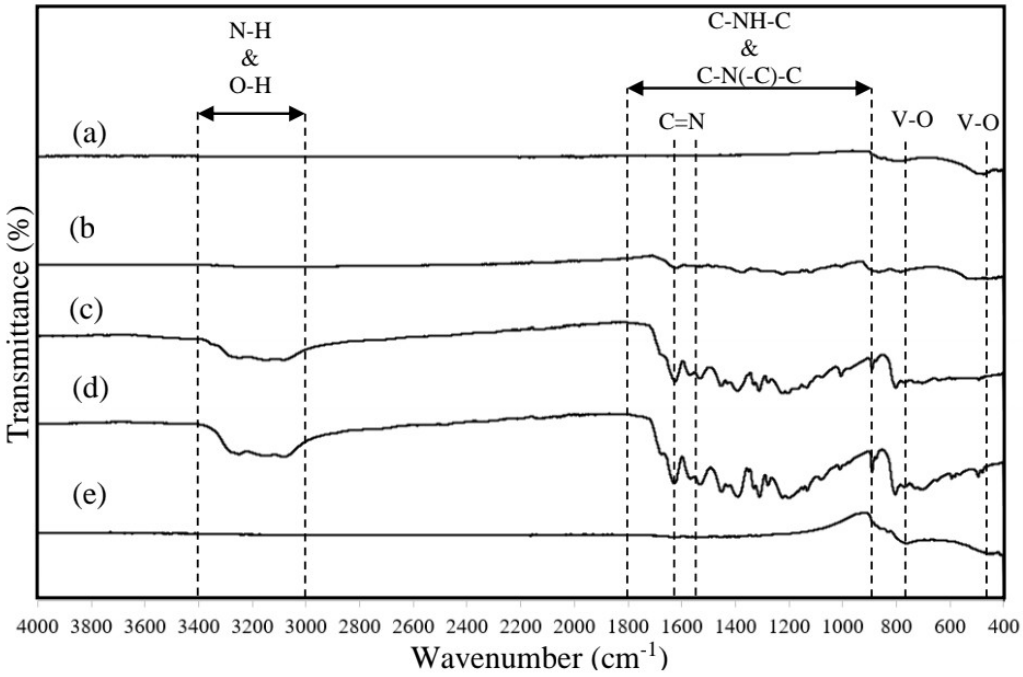

Figure 4.5: FTIR Spectrum of (a) A50, (b) A30, (c) A10, (d) Pure g-C_3N_4, and (e) Pure AgVA.

4.5 Brunauer-Emmett-Teller Surface Area (BET)

In this section, the synthesized photocatalyst pure g-C_3N_4 and composite photocatalyst (A10) which showed the excellent photocatalytic performance among all the synthesized photocatalysts is selected to undergo this BET characterization work. Their BET surface area, pore volume and average particle size of the as-synthesized pure g-C_3N_4 and A10 are then summarized in Table 4.2.

According to Table 4.2, the BET surface area was significantly increased from 70.0935 m^2/g to 125.9222 m^2/g upon the formation of the AgVA/g-C_3N_4 heterostructure system. Moreover, the average particle size obtained for g-C_3N_4 and A10 was 85.5999 nm and 47.6485 nm respectively. Whereas the total pore volume of pores was also increased from 0.1480 cm^3/g (pure g-C_3N_4) to 0.2615 cm^3/g. It is worth mentioning that the large BET surface, small particle size, and large pore volume were highly favourable as they were beneficial for enhancing the photodegradation activity of the composite photocatalyst. This was justified by the fact that the high specific surface area of a designed composite photocatalyst would offer a large number of active sites (Nasri, et al., 2022). As such, the photocatalytic performance could be improved as more active sites were available for pollutant absorption.

Table 4.2: BET Surface Area, Average Particle Size and Total Pore Volume of Pure g-C_3N_4 and A10.

Sample	**BET surface area (m^2/g)**	**Average particle size (nm)**	**Pore volume (cm^3/g)**
Pure g-C_3N_4	70.0935	85.5999	0.1480
A10	125.9222	47.6485	0.2615

4.6 Application of Photodegradation of Oxytetracycline under Visible Light Irradiation.

The variation of photocatalytic degradation of OTC over different photocatalysts of pure AgVA, pure g-C_3N_4, A10, A30 and A50 are illustrated in Figure 4.6. Based on Figure 4.6, an apparent increase in absorbance could be observed for pure AgVA and pure g-C_3N_4. This might be due to the formation of partial oxidation products or radicals, reaction intermediates that give rise to an increase in pollutant absorbance. Moreover, it is interesting to note that there is also an increase in pollutant absorbance for A10, A30 and A50 during the first 2 hours of treatment which is also assigned to the formation of photodegradation intermediate products of OTC that could give rise to absorbance at 274 nm (Zhang, et al., 2021; Ibad, et al., 2017; Kosslick, et al., 2021). Thereafter, a progressive decrease was observed as a result of the degradation of OTC and intermediates. Figure 4.7 shows the possible degradation intermediates and pathways that might be formed during the OTC degradation process.

According to Figure 4.7, several reactions such as decarboxamidation, dehydration, demethylation, hydroxylation and ring opening reactions might be involved in the OTC decomposition process. When the aromatic ring of OTC is attacked by the $^{\bullet}OH$ active species, OTC 1 and OTC 2 are produced through hydroxylation reaction. Furthermore, OTC 3 could be generated from OTC by removing the N-methyl group in the demethylation route (Liu, et al., 2016), whereas OTC 4 is produced from OTC after the loss of water through the dehydration reaction. In addition, OTC 3 could undergo two degradation pathways. Firstly, it could transform into OTC 5 by losing both the hydroxyl and N-methyl group. Subsequently, OTC 5 further decomposes for the formation of OTC 6 via a decarboxamidation pathway. OTC 6 could then undergo dehydration to form OTC 7, followed by deamination to generate OTC 8. The double bond bearing on OTC 8 would then be attacked by reactive oxygen species including $^{\bullet}O_2^-$ and $^{\bullet}OH$, leading to the production of OTC 9 and OTC 10 through the ring opening. After that, OTC 10 could further transform into OTC 11 via dehydration and decarboxylation pathways. Another OTC 3 degradation pathway involves fragmentation, leading to the

formation of OTC 12 by removing hydroxyl, carboxamide, N-methyl, and amide groups. Then, OTC 12 experiences ring opening to generate OTC 13, which could then undergo decarboxylation, dehydration, and demethylation for the formation of OTC 14. The intermediates OTC 11 and OTC 14 go through demethylation, dehydration, and ring-opening reactions during this process, which are oxidized to produce a number of by-products (OTC 15 to OTC 19) (Shaojun, et al., 2008; Ren, et al., 2020; Chen, et al., 2016).

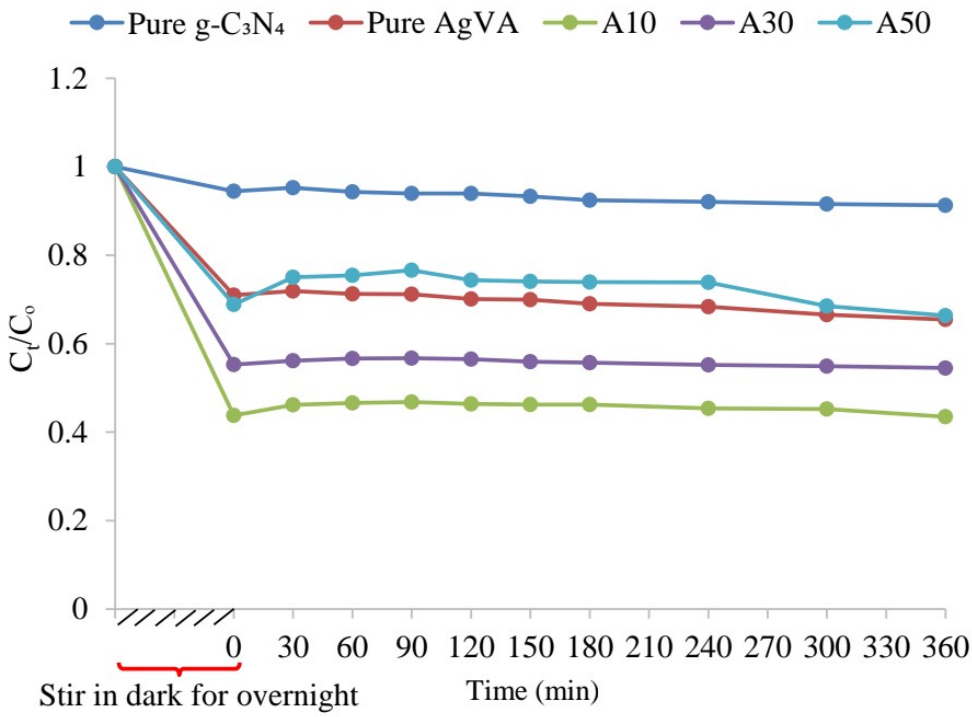

Figure 4.6: Photocatalytic Degradation of OTC over Pure AgVA, Pure g-C_3N_4, A10, A30 and A50.

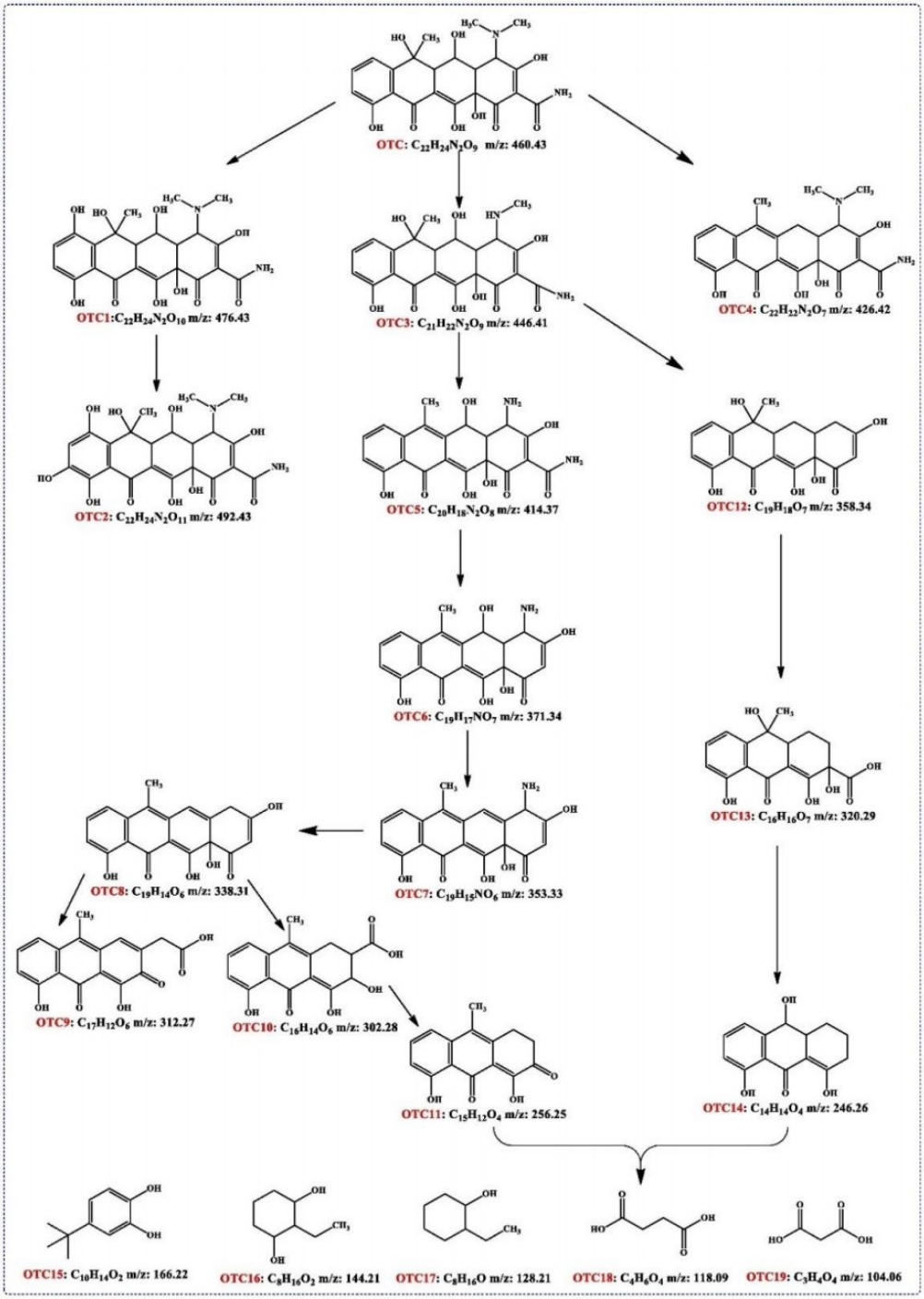

Figure 4.7: Possible Degradation Intermediates and Pathways that might be formed during OTC Degradation Process (Zhang, et al., 2021).

Moreover, the OTC degradation rate could be evaluated using equation 4.1 as expressed below:

$$\text{OTC degradation rate (\%)} = \frac{C_o - C_t}{C_o} * \mathbf{100}\% \qquad \text{(Equation 4.1)}$$

Where:

C_0 = initial concentration of OTC (ppm)

C_t =concentration of OTC at degradation time equal to t (ppm)

The OTC degradation efficiency after 6 hours of treatment with different photocatalysts of pure AgVA, pure g-C_3N_4, A10, A30, and A50 was then calculated using equation 4.1 and summarized in Figure 4.8. According to Figure 4.8, the OTC degradation rate of pure AgVA and pure g-C_3N_4 were 34.55 % and 8.71 % respectively, indicating that pure AgVA offered higher photodegradation performance as compared to pure g-C_3N_4. However, the OTC degradation efficiency of both components was considered low. This unsatisfied OTC degradation efficiency could be contributed by the low electron-hole separation efficiency of AgVA and the rapid electron-hole recombination of g-C_3N_4. Other than that, the OTC degradation rate was increasing from A50 to A30 followed by A10. The addition of AgVA to g-C_3N_4 which formed the heterojunction photocatalyst had greatly improved the degradation performance on the removal of OTC. This could be evidenced by the fact that the OTC degradation rate has improved to 56.52 % as shown in Figure 4.8. Overall, A10, A30 and A50 provided an OTC degradation rate of 56.52 %, 45.49 %, and 33.65 % respectively.

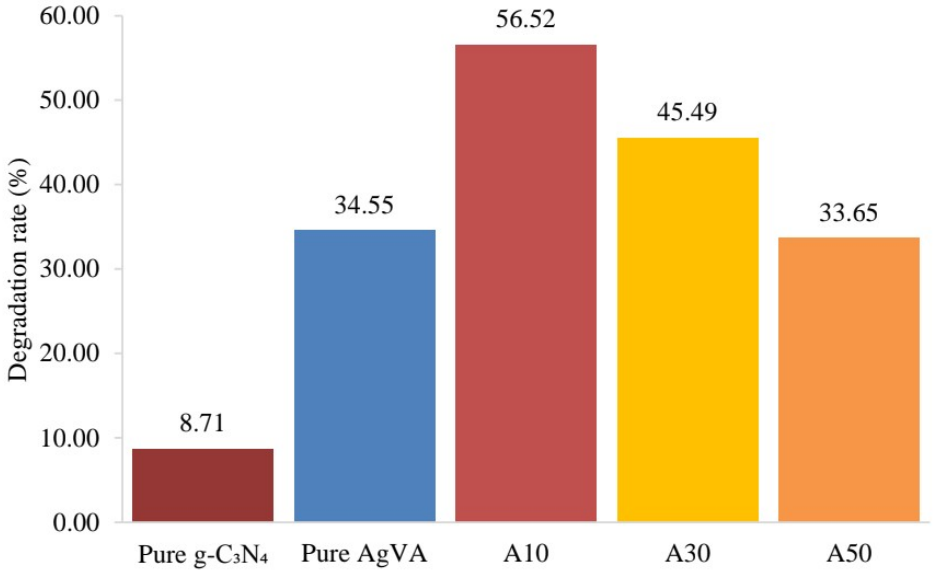

Figure 4.8: OTC Degradation Rate for Pure g-C_3N_4, Pure AgVA, A10, A30 and A50.

Other than that, the rate constant of photocatalytic degradation of OTC under visible light irradiation were investigated by pseudo-first-order kinetic equation which could be written as Equation 4.2. The reaction rate constant, k_1 in the unit of min^{-1} obtained for pure g-C_3N_4, pure AgVA, A10, A30 and A50 are then summarized in Figure 4.9.

$$ln\left(\frac{C_0}{C_t}\right) = k_1 t \qquad \text{(Equation 4.2)}$$

Where:

k_1: First order kinetic rate constant, min^{-1}

t: Degradation time, min

Based on Figure 4.9, it could be observed clearly that the photocatalytic activity of A10 is the most superior among all the synthesized photocatalysts. Whereas A30 has the second highest photocatalytic performance followed by pure AgVA, A50 and pure g-C_3N_4. Other than that, the reaction rate constant of A10 is 0.0034 min^{-1} which is 11.3 times and 2.1 times higher than pure g-C_3N_4 (0.0003 min^{-1}) and pure AgVA (0.0016 min^{-1}),

respectively. Thus, it could be concluded that the photocatalytic performance of the single components of pure g-C_3N_4 and pure AgVA could be enhanced through coupling them which resulted in the formation of heterojunction photocatalysts.

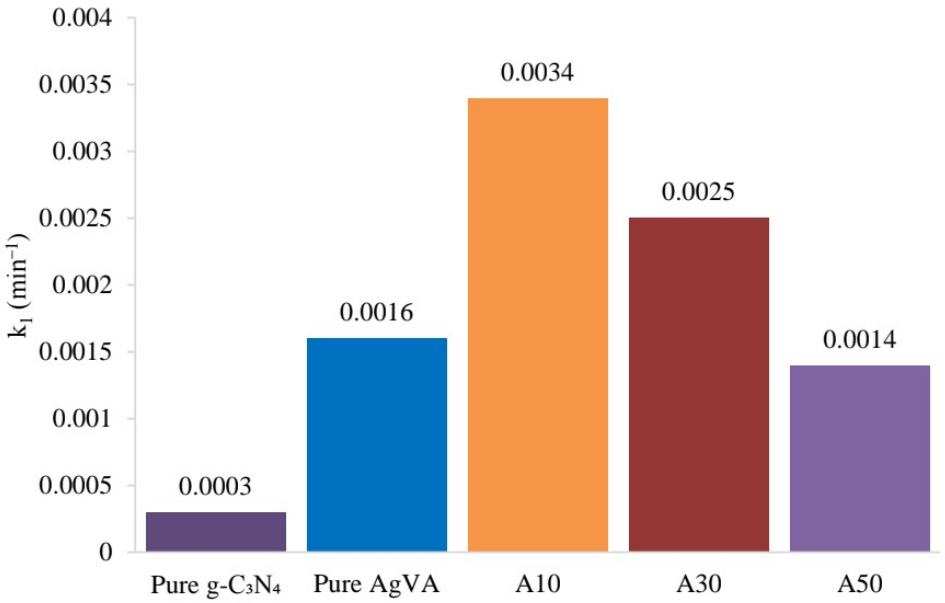

Figure 4.9: Reaction Rate Constant of Pure g-C_3N_4, Pure AgVA, A10, A30 and A50.

Besides, the pseudo-second order kinetic which exists in linear form could be written as Equation 4.3. The second order kinetic constant, k_2 obtained for all the photocatalysts is then illustrated in Figure 4.10.

$$\frac{1}{C_t} - \frac{1}{C_o} = k_2 t \qquad \text{(Equation 4.3)}$$

Where:

k_2: Second order kinetic rate constant, min^{-1}

According to Figure 4.10, the second order reaction constant is increasing in the order of pure g-C_3N_4, A50, pure AgVA, A30, and A10. as they have the second order reaction constant of 0.000004, 0.00002, 0.00002, 0.00003, and 0.00005 min^{-1}, respectively. Thus, it is further confirmed that

A10 has the highest photocatalytic performance in OTC degradation as its second order reaction constant is 12.5 and 2.5 times higher than pure g-C_3N_4 and pure AgVA respectively.

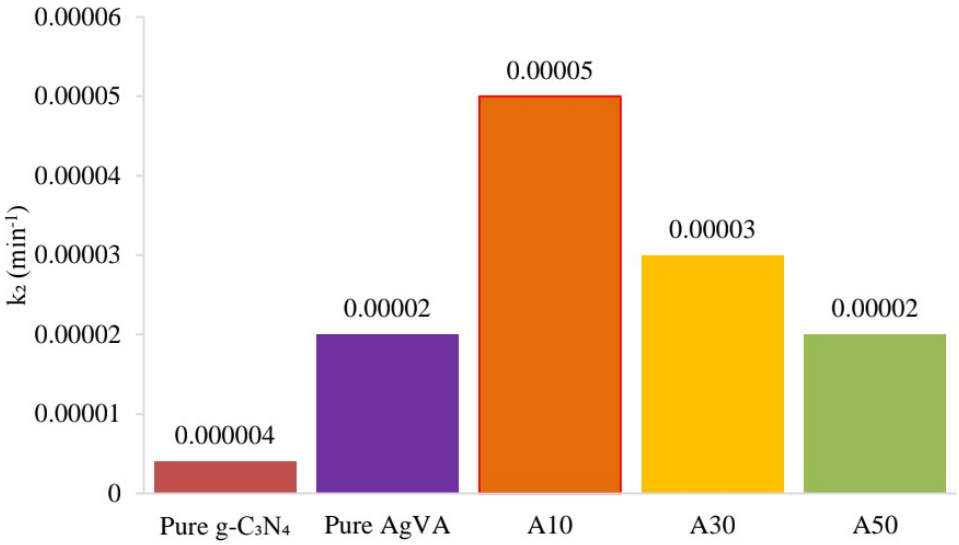

Figure 4.10: Second Order Reaction Rate Constant of Pure g-C_3N_4, Pure AgVA, A10, A30 and A50.

Table 4.3 summarizes the rate constants (k_1 and k_2) obtained and their regression coefficient, R^2 for the pseudo-first order and pseudo-second order models. According to Table 4.3, the pseudo-second-order model has a higher regression coefficient (R^2) value as compared to the pseudo-first-order model where its R^2 is ranged from 0.6675 to 0.8178. This high R^2 indicates that OTC degradation over the synthesized photocatalysts is well fitted to the pseudo-second-order model.

Table 4.3: Kinetic Parameters for OTC Removal over Synthesized Photocatalysts.

Photocatalysts	**Pseudo-first-order**		**Pseudo-second-order**	
	k_1 (min^{-1})	**R^2**	**k_2 (min^{-1})**	**R^2**
Pure g-C_3N_4	0.0003	0.8128	0.000004	0.8178
AgVA	0.0016	0.7239	0.00002	0.7379
A10	0.0034	0.6629	0.00005	0.6675
A30	0.0025	0.6667	0.00003	0.6714
A50	0.0014	0.7166	0.00002	0.7261

In fact, it is important to achieve saturation or adsorption by stirring the mixture of OTC solution and photocatalyst in dark conditions before performing the photocatalytic degradation test as this could help to differentiate the contribution of adsorption and photocatalytic degradation of the synthesized photocatalysts. Based on Figure 4.6, a significant decrease in the OTC concentration could be observed in dark conditions where the OTC concentration was reduced from 100 ppm to about 54.51 ppm. This implied that the synthesized photocatalyst (A10) offered good absorption capacity for the OTC to be absorbed. However, a slow OTC degradation rate over A10 was observed under visible light irradiation. The light source used was a 30W LED light bulb and the amount of photocatalyst applied in the OTC photodegradation test was only 50 mg. Thus, the slow degradation rate might be due to the insufficient light intensity and the insufficient amount of photocatalyst used.

4.7 Possible Photocatalytic Mechanism of AgVA/g-C_3N_4

Figure 4.11 displays a possible photocatalytic mechanism of AgVA/g-C_3N_4 for the degradation of OTC under visible light irradiation. In fact, the charge transfer between heterojunctions is greatly based on the conduction band (CB) and valence band (VB) potential. The conduction energy levels of g-C_3N_4 and AgVA are -1.2 eV and 0.26 eV respectively. Under visible light irradiation, both g-C_3N_4 and AgVA generated electron-hole (e-h) pairs. The photogenerated e^- excited by g-C_3N_4 was transferred from g-C_3N_4 to AgVA conduction band due to the low conduction energy level of g-C_3N_4. Whereas the produced light-generating h^+ was transferred from AgVA valence band to the g-C_3N_4. This indicates that AgVA could be applied as a photogenerated e^- transfer medium that decreased the probability of recombination of photogenerated e-h pairs and increased the separation efficiency of the photogenerated charge carriers in AgVA/g-C_3N_4 (Chen, et al., 2019). After that, the photoexcited e^- in the CB of g-C_3N_4 reduced O_2 to superoxide anion radical ($^{\bullet}O_2^-$) and the photogenerated h^+ in the VB of AgVA oxidized OH^- and H_2O to $^{\bullet}OH$. These active radicals produced then turned OTC into corresponding degradation.

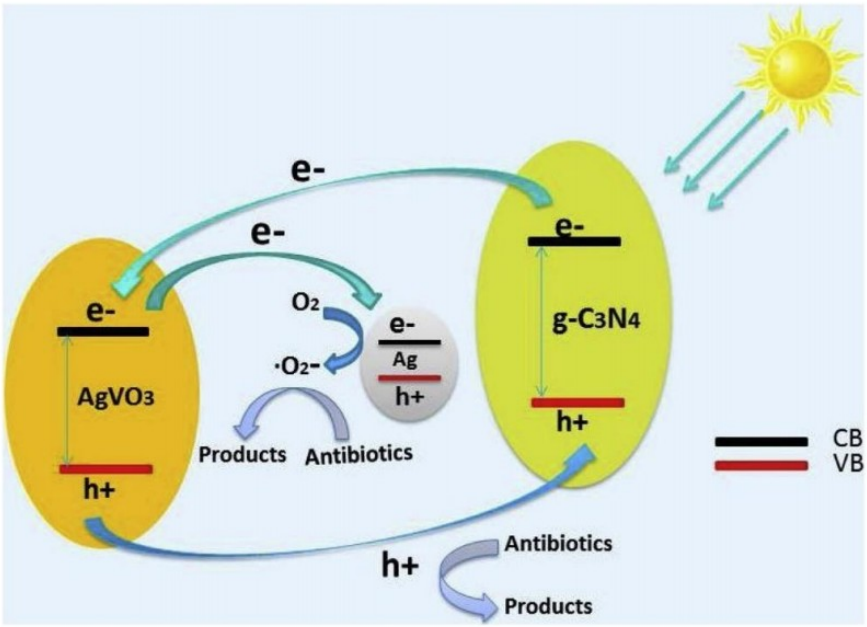

Figure 4.11: Possible Photocatalytic Mechanism of AgVA/g-C_3N_4 for the Degradation of OTC under Visible Light Irradiation (Chen, et al., 2019).

4.8 Scavenging Test

Based on the discussion in section 4.7, a couple of active species such as hydroxyl radical ($^{\bullet}OH$), reductive conduction band electrons (e^-), superoxide anion radical ($^{\bullet}O_2^-$), and oxidative valence band holes (h^+) could contribute to the photocatalytic degradation process, however the contribution varies depending on the type of catalysts. In this section, photodegradation of OTC over A10 in the presence of e^-, $^{\bullet}OH$, h^+ and $^{\bullet}O_2^-$ scavengers (DMSO, IPA, EDTA-$2Na^+$ and BQ respectively) is studied in order to examine the active species involved in the A10 which shown the best photocatalytic performance among all the synthesized photocatalysts in the previous experiment (photodegradation test). Figure 4.12 illustrates the effect of scavengers on the photodegradation of OTC over A10 whereas Figure 4.13 summarizes the OTC degradation efficiency over A10 after adding scavengers of EDTA, BQ, IPA and DMSO. In order to have a better comparison for the impact of scavengers on the OTC degradation over A10 composite, the OTC degradation efficiency of A10 without the scavenger was added into the graph to act as the control.

According to Figure 4.12 and Figure 4.13, the OTC removal rate dropped to 31.01% and 15.19% after introducing EDTA and BQ whereas the presence of the IPA and DMSO resulted in OTC removal rates of 53.69% and 44.86% respectively. The dramatically decreased in OTC degradation efficiency due to the adding of BQ implies that $^{\bullet}O_2^-$ radicals played an essential role in the photocatalytic degradation of OTC. The second active species that contributes the most OTC degradation efficiency is h^+ as the degradation efficiency has been decreased to 31.01% due to the addition of EDTA. However, the addition of the IPA and DMSO only slightly affected the photodegradation of OTC by A10 composite, indicating that the e^- and $^{\bullet}OH$ participated in the OTC photodegradation but they are not the main active species. Hence, it could be concluded that the contributing reactive species which responsible to the OTC photodegradation are arranged in the order of $^{\bullet}O_2^-$ followed by h^+, e^-, and $^{\bullet}OH$.

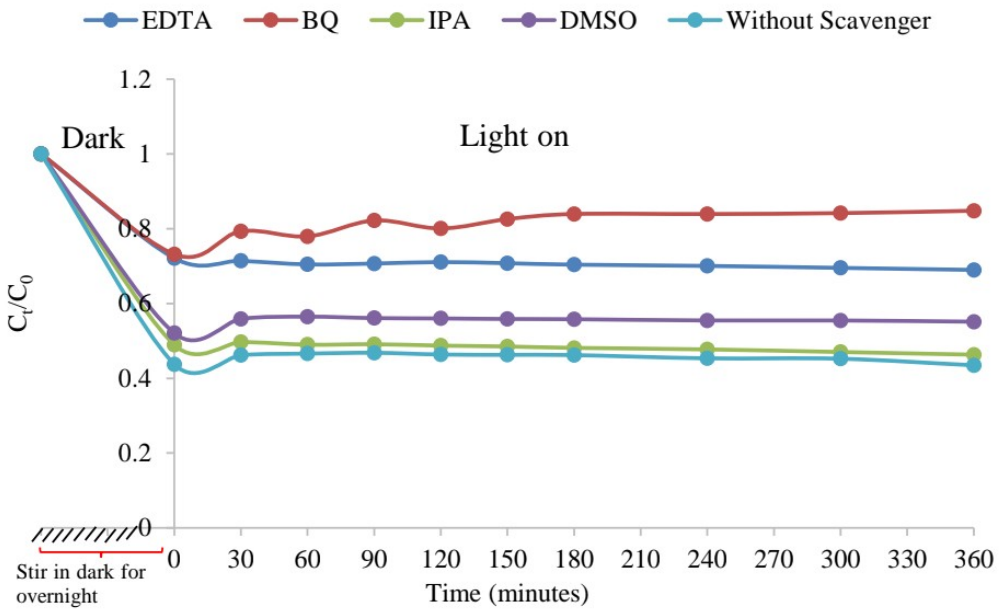

Figure 4.12: The Effect of Scavengers on the Photodegradation of OTC over A10.

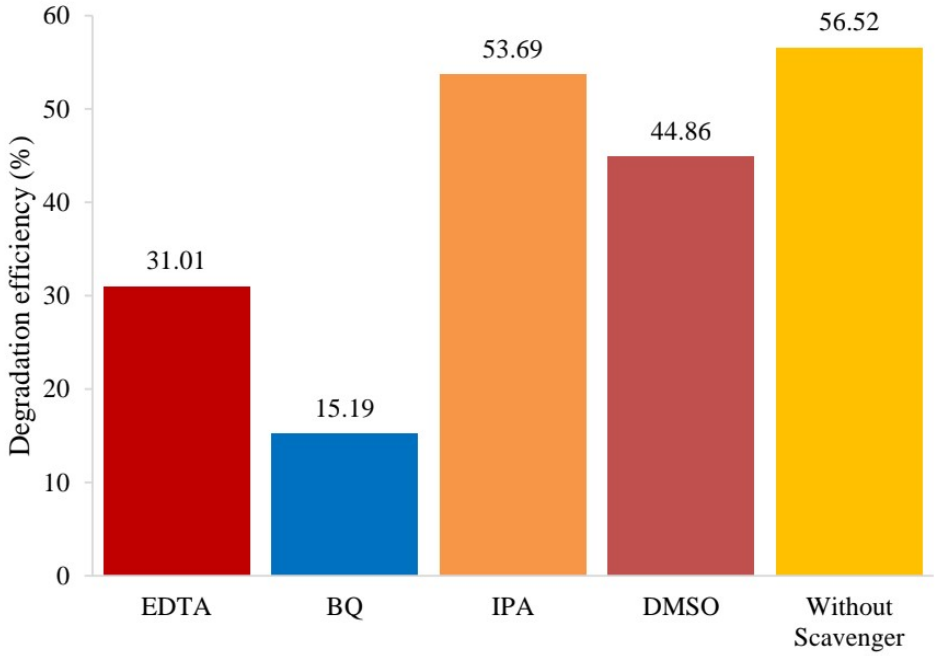

Figure 4.13: OTC Degradation Efficiency over A10 after Adding Scavengers of EDTA, BQ, IPA, DMSO and Without Scavenger (Control).

CHAPTER 5

CONCLUSIONS AND RECOMMENDATIONS

5.1 Conclusions

The AgVA/g-C_3N_4 composite photocatalyst with different weight percentages of 10 wt%, 30 wt% and 50 wt% of AgVA had successfully been synthesized using wet chemical method. The synthesized composite photocatalysts were named as A10, A30, and A50. One-dimensional nanorods AgVA were evenly dispersed on the two-dimensional nanosheet of g-C_3N_4. The coexistence of both g-C_3N_4 and AgVA in the synthesized composite photocatalysts was confirmed by performing characterization work using FTIR, SEM, BET, XRD and EDX. From the XRD result, it could be observed that the characteristic peaks of both AgVA and g-C_3N_4 were detected in all the synthesized composite photocatalysts. According to the FTIR spectrum, the absorption bands observed at wavenumber of 1531.69, 1625.86, 760.93, and 455.76 cm^{-1} indicated the presence of both AgVA and g-C_3N_4. This has greatly showed that AgVA was successfully incorporated with g-C_3N_4 for the formation of AgVA/g-C_3N_4 heterojunction. Based on the SEM image of A10 photocatalyst, the AgVA nanorod was covered by the g-C_3N_4. Moreover, the synthesized A10 composite photocatalyst was found to have a smaller average particle size, higher total pore volume and larger BET surface area as compared to g-C_3N_4. These characteristics indicated the coupling of AgVA into g-C_3N_4 could enhance the photocatalytic efficiency as compared to the single components. Apart from these, the elemental composition of the synthesized photocatalysts were identified using EDX technique. There were three elements that had been detected in pure g-C_3N_4 including C, N and O. Theoretically, only C and N atoms are expected to detect in its elemental composition. The presence of O elements was assigned to the occurrence of the reaction when urea came into contact with air in the atmosphere. For AgVA, the elements detected consist of Ag, V and O which implied that there were no any impurities presented during the synthesizing process. The elemental composition of all the prepared

composite photocatalysts consisted of C, N, O, Ag, and V which further indicated that AgVA was successfully coupled into g-C_3N_4.

The photocatalytic degradation activity of the synthesized AgVA/g-C_3N_4 composite photocatalyst was markedly higher than the single component of pure AgVA and pure g-C_3N_4. Through photodegradation of OTC under visible light irradiation where the light source was provided by a 30W LED light bulb, the highest photocatalytic effect and rate was found with A10 among all the synthesized photocatalysts. The degradation efficiency of A10 composites to degrade 100 ppm of OTC was found to be 56.52 %. Through performing scavenging test, the active species which contributed to most of the photocatalytic activity of A10 in OTC degradation was found with superoxide radicals ($^{\bullet}O_2^-$) followed by h^+, e^-, and $^{\bullet}OH$. In conclusion, the OTC photodegradation test indicated that the decrease in the OTC concentration was due to the adsorption and photocatalytic degradation of the synthesized photocatalyst, A10. Thus, the synthesized AgVA/g-C_3N_4 composite photocatalyst in the present work could be a practical way to be applied in industry today for the removal of OTC contained in the wastewater.

5.2 Recommendations for future work

Due to time constraint, there are several recommendations given for the further work regarding this study not only to enhance the accuracy and reliability of the experiment result but also potentially enhance the practicability of the AgVA/g-C_3N_4 composite photocatalyst to be applied in the industry. The recommendations are discussed as follows.

i. Optimization of photocatalytic degradation conditions is suggested to be performed in order to achieve high OTC degradation efficiency. This is because the photocatalytic degradation of OTC is greatly influenced by numerous parameters such as reaction temperature, pH, photocatalyst loading and its particle size, and light intensity.

ii. To perform reaction cycling runs for the OTC photocatalytic degradation over the as-synthesized AgVA/g-C_3N_4 composite

photocatalyst under visible light irradiation in order to determine its stability.

iii. To carry out more characterization for the photocatalysts such as high-resolution transmission electron microscopy (HETEM) and X-ray photoelectron spectroscopy (XPS) to further understand their structure and morphology.

iv. To carry out gas chromatography-mass spectrometry analysis to further study the intermediate products of OTC presence during the degradation process.

v. To study the effect of the pH and the calcination temperature on the structure and morphology of the photocatalysts.

REFERENCES

Acevedo Barrios, R.L., Severiche Sierra, C.A. and Jaimes Morales, J.D.C., 2015. Bacterias resistentes a antibióticos en ecosistemas acuáticos. *Producción+ Limpia*, *10*(2), pp.160-172.

Ahmad, F., Zhu, D. and Sun, J., 2021. Environmental fate of tetracycline antibiotics: degradation pathway mechanisms, challenges, and perspectives. *Environmental Sciences Europe*, *33*(1), pp.1-17.

Akbari, M.Z., Xu, Y., Lu, Z. and Peng, L., 2021. Review of antibiotics treatment by advance oxidation processes. *Environmental Advances*, *5*, p.100111.

Akbarzadeh-T, N. and Amiri-O, L., 2015. Synthesis and characterization of barium-vanadium oxide nanocomposite using a facile thermolysis approach. *Oriental Journal of Chemistry*, *31*(4), p.2247.

Akhoondi, A., Feleni, U., Bethi, B., Idris, A.O. and Hojjati-Najafabadi, A., 2021. Advances in metal-based vanadate compound photocatalysts: synthesis, properties and applications. *Synthesis and Sintering*, *1*(3), pp.151-168.

Alaghmandfard, A. and Ghandi, K., 2022. A Comprehensive Review of Graphitic Carbon Nitride (g-C3N4)–Metal Oxide-Based Nanocomposites: Potential for Photocatalysis and Sensing. *Nanomaterials*, *12*(2), p.294.

Al-Jassim, N., Ansari, M.I., Harb, M. and Hong, P.Y., 2015. Removal of bacterial contaminants and antibiotic resistance genes by conventional wastewater treatment processes in Saudi Arabia: Is the treated wastewater safe to reuse for agricultural irrigation?. *Water research*, *73*, pp.277-290.

Ambler Campus. (2021). *Why Water Is So Important*. [online] Available at: https://ambler.temple.edu/community/earthfest/celebrating-earth/world-water-day/why-water-so-important.

Ameta, R., Solanki, M.S., Benjamin, S. and Ameta, S.C., 2018. Photocatalysis. In *Advanced oxidation processes for wastewater treatment* (pp. 135-175). Academic Press.

Arikan, O.A., Mulbry, W. and Rice, C., 2009. Management of antibiotic residues from agricultural sources: use of composting to reduce chlortetracycline residues in beef manure from treated animals. *Journal of Hazardous materials*, *164*(2-3), pp.483-489.

Baruah, A., Chaudhary, V., Malik, R. and Tomer, V.K., 2019. Nanotechnology based solutions for wastewater treatment. In *Nanotechnology in Water and wastewater treatment* (pp. 337-368). Elsevier.

Ben, Y., Fu, C., Hu, M., Liu, L., Wong, M.H. and Zheng, C., 2019. Human health risk assessment of antibiotic resistance associated with antibiotic residues in the environment: A review. *Environmental research*, *169*, pp.483-493.

Byrne, C., Subramanian, G. and Pillai, S.C., 2018. Recent advances in photocatalysis for environmental applications. *Journal of environmental chemical engineering*, *6*(3), pp.3531-3555.

Cao, J., Qin, C., Wang, Y., Zhang, H., Sun, G. and Zhang, Z., 2017. Solid-state method synthesis of SnO2-decorated g-C3N4 nanocomposites with enhanced gas-sensing property to ethanol. *Materials*, *10*(6), p.604.

Cao, J., Yang, Z.H., Xiong, W.P., Zhou, Y.Y., Peng, Y.R., Li, X., Zhou, C.Y., Xu, R. and Zhang, Y.R., 2018. One-step synthesis of Co-doped UiO-66 nanoparticle with enhanced removal efficiency of tetracycline: Simultaneous adsorption and photocatalysis. *Chemical Engineering Journal*, *353*, pp.126-137.

Centi, G., Perathoner, S., Torre, T. and Verduna, M.G., 2000. Catalytic wet oxidation with H2O2 of carboxylic acids on homogeneous and heterogeneous Fenton-type catalysts. *Catalysis Today*, *55*(1-2), pp.61-69.

Chen, A., Chen, Y., Ding, C., Liang, H. and Yang, B., 2015. Effects of tetracycline on simultaneous biological wastewater nitrogen and phosphorus removal. *Rsc Advances*, *5*(73), pp.59326-59334.

Chen, B., Liang, X., Huang, X., Zhang, T. and Li, X., 2013. Differentiating anthropogenic impacts on ARGs in the Pearl River Estuary by using suitable gene indicators. *Water research*, *47*(8), pp.2811-2820.

Chen, D., Li, B., Pu, Q., Chen, X., Wen, G. and Li, Z., 2019. Preparation of Ag-AgVO3/g-C3N4 composite photo-catalyst and degradation characteristics of antibiotics. *Journal of hazardous materials*, *373*, pp.303-312.

Chen, H., Jing, L., Teng, Y. and Wang, J., 2018. Multimedia fate modeling and risk assessment of antibiotics in a water-scarce megacity. *Journal of hazardous materials*, *348*, pp.75-83.

Chen, L.Y. and Zhang, W.D., 2014. In2O3/g-C3N4 composite photocatalysts with enhanced visible light driven activity. *Applied surface science*, *301*, pp.428-435.

Chen, M., Guan, R. and Yang, S., 2019. Hybrids of fullerenes and 2D nanomaterials. *Advanced Science*, *6*(1), p.1800941.

Chen, Q., Wu, S. and Xin, Y., 2016. Synthesis of Au–CuS–TiO2 nanobelts photocatalyst for efficient photocatalytic degradation of antibiotic oxytetracycline. *Chemical Engineering Journal*, *302*, pp.377-387.

Chen, Y., Huang, W., He, D., Situ, Y. and Huang, H., 2014. Construction of heterostructured g-C3N4/Ag/TiO2 microspheres with enhanced photocatalysis performance under visible-light irradiation. *ACS applied materials & interfaces*, *6*(16), pp.14405-14414.

Chong, M.N., Jin, B., Chow, C.W. and Saint, C., 2010. Recent developments in photocatalytic water treatment technology: a review. *Water research*, *44*(10), pp.2997-3027.

Choudhary, S., Bisht, A. and Mohapatra, S., 2019. Facile synthesis, morphological, structural, photocatalytic and optical properties of CoFe2O4 nanostructures. *SN Applied Sciences*, *1*(12), pp.1-12.

Cuerda-Correa, E.M., Alexandre-Franco, M.F. and Fernández-González, C., 2019. Advanced oxidation processes for the removal of antibiotics from water. An overview. *Water*, *12*(1), p.102.

Daghrir, R. and Drogui, P., 2013. Tetracycline antibiotics in the environment: a review. *Environmental chemistry letters*, *11*(3), pp.209-227.

Danner, M.C., Robertson, A., Behrends, V. and Reiss, J., 2019. Antibiotic pollution in surface fresh waters: occurrence and effects. *Science of the Total Environment*, *664*, pp.793-804.

de Campos, M.R., Botelho, A.L. and Dos Reis, A.C., 2021. Nanostructured silver vanadate decorated with silver particles and their applicability in dental materials: A scope review. *Heliyon*, *7*(6), p.e07168.

Deng, F., Luo, Y., Li, H., Xia, B., Luo, X., Luo, S. and Dionysiou, D.D., 2020. Efficient toxicity elimination of aqueous Cr (VI) by positively-charged BiOClxI1-x, BiOBrxI1-x and BiOClxBr1-x solid solution with internal hole-scavenging capacity via the synergy of adsorption and photocatalytic reduction. *Journal of hazardous materials*, *383*, p.121127.

Deng, Y., 2018. Developing a Langmuir-type excitation equilibrium equation to describe the effect of light intensity on the kinetics of the photocatalytic oxidation. *Chemical Engineering Journal*, *337*, pp.220-227.

Devaraji, P., Sathu, N.K. and Gopinath, C.S., 2014. Ambient oxidation of benzene to phenol by photocatalysis on Au/Ti0. 98V0. 02O2: role of holes. *Acs Catalysis*, *4*(9), pp.2844-2853.

Diao, Y., Yan, M., Li, X., Zhou, C., Peng, B., Chen, H. and Zhang, H., 2020. In-situ grown of g-C3N4/Ti3C2/TiO2 nanotube arrays on Ti meshes for efficient degradation of organic pollutants under visible light irradiation. *Colloids and Surfaces A: Physicochemical and Engineering Aspects*, *594*, p.124511.

Dong, H., Zeng, G., Tang, L., Fan, C., Zhang, C., He, X. and He, Y., 2015. An overview on limitations of TiO2-based particles for photocatalytic degradation of organic pollutants and the corresponding countermeasures. *Water research*, *79*, pp.128-146.

Ebele, A.J., Abdallah, M.A.E. and Harrad, S., 2017. Pharmaceuticals and personal care products (PPCPs) in the freshwater aquatic environment. *Emerging contaminants*, *3*(1), pp.1-16.

Enesca, A. and Isac, L., 2021. Photocatalytic Activity of Cu2S/WO3 and Cu2S/SnO2 Heterostructures for Indoor Air Treatment. *Materials*, *14*(13), p.3656.

Fagan, R., McCormack, D.E., Dionysiou, D.D. and Pillai, S.C., 2016. A review of solar and visible light active TiO2 photocatalysis for treating bacteria, cyanotoxins and contaminants of emerging concern. *Materials Science in Semiconductor Processing*, *42*, pp.2-14.

Fang, S., Li, Y., Yang, Y., Chen, J., Liu, H. and Zhao, X., 2017. Mg-doped OMS-2 nanorods: a highly efficient catalyst for purification of volatile organic compounds with full solar spectrum irradiation. *Environmental Science: Nano*, *4*(9), pp.1798-1807.

Fatta-Kassinos, D., Meric, S. and Nikolaou, A., 2011. Pharmaceutical residues in environmental waters and wastewater: current state of knowledge and future research. *Analytical and bioanalytical chemistry*, *399*(1), pp.251-275.

Frost, R.L., Erickson, K.L., Weier, M.L. and Carmody, O., 2005. Raman and infrared spectroscopy of selected vanadates. *Spectrochimica Acta Part A: Molecular and Biomolecular Spectroscopy*, *61*(5), pp.829-834.

Fujishima, A. and Honda, K., 1972. Electrochemical photolysis of water at a semiconductor electrode. *nature*, *238*(5358), pp.37-38.

Fujishima, A., Rao, T.N. and Tryk, D.A., 2000. Titanium dioxide photocatalysis. *Journal of photochemistry and photobiology C: Photochemistry reviews*, *1*(1), pp.1-21.

Gadipelly, C., Pérez-González, A., Yadav, G.D., Ortiz, I., Ibáñez, R., Rathod, V.K. and Marathe, K.V., 2014. Pharmaceutical industry wastewater: review of the technologies for water treatment and reuse. *Industrial & Engineering Chemistry Research*, *53*(29), pp.11571-11592.

Gao, Y., Duan, J., Zhai, X., Guan, F., Wang, X., Zhang, J. and Hou, B., 2021. Extraordinary photodegradation performance of graphitic carbon nitride derived from tin foil–wrapped urea. *Journal of Nanoparticle Research*, *23*(2), pp.1-14.

Gaya, U.I. and Abdullah, A.H., 2008. Heterogeneous photocatalytic degradation of organic contaminants over titanium dioxide: a review of fundamentals, progress and problems. *Journal of photochemistry and photobiology C: Photochemistry reviews*, *9*(1), pp.1-12.

Ge, J., Zhang, Y., Heo, Y.J. and Park, S.J., 2019. Advanced design and synthesis of composite photocatalysts for the remediation of wastewater: A review. *Catalysts*, *9*(2), p.122.

Gedda, G., Balakrishnan, K., Devi, R.U., Shah, K.J. and Gandhi, V., 2021. Introduction to conventional wastewater treatment technologies: limitations and recent advances. *Advances in Wastewater Treatment I.; Gandh, V., Shah, KL, Eds*, pp.1-36.

Giler-Molina, J.M., Zambrano-Intriago, L.A., Quiroz-Fernández, L.S., Napoleão, D.C., dos Santos Vieira, J., Simões Oliveira, N. and Rodríguez-Díaz, J.M., 2020. Degradation of oxytetracycline in aqueous solutions: Application of homogeneous and heterogeneous advanced oxidative processes. *Sustainability*, *12*(21), p.8807.

Giwa, A., Yusuf, A., Balogun, H.A., Sambudi, N.S., Bilad, M.R., Adeyemi, I., Chakraborty, S. and Curcio, S., 2021. Recent advances in advanced oxidation processes for removal of contaminants from water: A comprehensive review. *Process Safety and Environmental Protection*, *146*, pp.220-256.

Gopal, G., Alex, S.A., Chandrasekaran, N. and Mukherjee, A., 2020. A review on tetracycline removal from aqueous systems by advanced treatment techniques. *RSC advances*, *10*(45), pp.27081-27095.

Gothwal, R. and Shashidhar, T., 2015. Antibiotic pollution in the environment: a review. *Clean–Soil, Air, Water*, *43*(4), pp.479-489.

Grady Jr, C.L., Daigger, G.T., Love, N.G. and Filipe, C.D., 2011. *Biological wastewater treatment*. CRC press.

Guillard, C., Lachheb, H., Houas, A., Ksibi, M., Elaloui, E. and Herrmann, J.M., 2003. Influence of chemical structure of dyes, of pH and of inorganic salts on their photocatalytic degradation by TiO2 comparison of the efficiency of powder and supported TiO2. *Journal of Photochemistry and Photobiology A: Chemistry*, *158*(1), pp.27-36.

Guo, J., Liang, J., Yuan, X., Jiang, L., Zeng, G., Yu, H. and Zhang, J., 2018. Efficient visible-light driven photocatalyst, silver (meta) vanadate: synthesis, morphology and modification. *Chemical Engineering Journal*, *352*, pp.782-802.

Hariganesh, S., Vadivel, S., Maruthamani, D. and Rangabhashiyam, S., 2020. Disinfection by-products in drinking water: Detection and treatment methods. In *Disinfection By-products in Drinking Water* (pp. 279-304). Butterworth-Heinemann.

Harja, M. and Ciobanu, G., 2017. Removal of oxytetracycline from aqueous solutions by hydroxyapatite as a low-cost adsorbent. In *E3S Web of Conferences* (Vol. 22, p. 00062). EDP Sciences.

Hassan, A., Iqbal, T., Tahir, M.B. and Afsheen, S., 2019. A review on copper vanadate-based nanostructures for photocatalysis energy production. *International Journal of Energy Research*, *43*(1), pp.9-28.

Hegde, K., Mathew, N., Shivashankara, A.R., Prabhu, A.N. and Baliga, M.S., 2013. Hepatoprotective effects of picroliv: The ethanolic extract fraction of the endangered indian medicinal plant Picrorhiza kurroa royle ex. Benth. In *Bioactive Food as Dietary Interventions for Liver and Gastrointestinal Disease* (pp. 685-695). Academic Press.

Hiller, C.X., Hübner, U., Fajnorova, S., Schwartz, T. and Drewes, J.E., 2019. Antibiotic microbial resistance (AMR) removal efficiencies by conventional and advanced wastewater treatment processes: A review. *Science of the Total Environment*, *685*, pp.596-608.

Hoffmann, M.R., Martin, S.T., Choi, W. and Bahnemann, D.W., 1995. Environmental applications of semiconductor photocatalysis. *Chemical reviews*, *95*(1), pp.69-96.

Hong, Y., Jiang, Y., Li, C., Fan, W., Yan, X., Yan, M. and Shi, W., 2016. In-situ synthesis of direct solid-state Z-scheme V2O5/g-C3N4 heterojunctions with enhanced visible light efficiency in photocatalytic degradation of pollutants. *Applied Catalysis B: Environmental*, *180*, pp.663-673.

Hou, J., Wang, C., Mao, D., Luo, Y., 2016a. The occurrence and fate of tetracyclines in two pharmaceutical wastewater treatment plants of Northern China. Environ. Sci. Pollut. Res. Int. 23, 1722–1731

Hu, X., Hu, C. and Qu, J., 2008. Preparation and visible-light activity of silver vanadate for the degradation of pollutants. *Materials Research Bulletin*, *43*(11), pp.2986-2997.

Hua, Z., Zhang, X., Bai, X., Lv, L., Ye, Z. and Huang, X., 2015. Nitrogen-doped perovskite-type La2Ti2O7 decorated on graphene composites exhibiting efficient photocatalytic activity toward bisphenol A in water. *Journal of colloid and interface science*, *450*, pp.45-53.

Huang, Y., Fan, W., Long, B., Li, H., Zhao, F., Liu, Z., Tong, Y. and Ji, H., 2016. Visible light Bi2S3/Bi2O3/Bi2O2CO3 photocatalyst for effective degradation of organic pollutions. *Applied Catalysis B: Environmental*, *185*, pp.68-76.

Huang, Y., Wang, Y., Bi, Y., Jin, J., Ehsan, M.F., Fu, M. and He, T., 2015. Preparation of 2D hydroxyl-rich carbon nitride nanosheets for photocatalytic reduction of CO 2. *RSC Advances*, *5*(42), pp.33254-33261.

Huang, Y.H., Liu, Y., Du, P.P., Zeng, L.J., Mo, C.H., Li, Y.W., Lü, H. and Cai, Q.Y., 2019. Occurrence and distribution of antibiotics and antibiotic resistant genes in water and sediments of urban rivers with black-odor water in Guangzhou, South China. *Science of the total environment*, *670*, pp.170-180.

Huizhong, A.N., Yi, D.U., Tianmin, W.A.N.G., Cong, W.A.N.G., Weichang, H.A.O. and ZHANG, J., 2008. Photocatalytic properties of biox (X= Cl, Br, and I). *Rare Metals*, *27*(3), pp.243-250.

Hummers Jr, W.S. and Offeman, R.E., 1958. Preparation of graphitic oxide. *Journal of the american chemical society*, *80*(6), pp.1339-1339.

Ibad, M.F., Kosslick, H., Tomm, J.W., Frank, M. and Schulz, A., 2017. Impact of the crystallinity of mesoporous polymeric graphitic carbon nitride on the photocatalytic performance under UV and visible light. *Microporous and Mesoporous Materials*, *254*, pp.136-145.

Ifebajo, A.O., Oladipo, A.A. and Gazi, M., 2019. Efficient removal of tetracycline by CoO/CuFe2O4 derived from layered double hydroxides. *Environmental Chemistry Letters*, *17*(1), pp.487-494.

Imtiaz, F., Rashid, J. and Xu, M., 2019. Semiconductor nanocomposites for visible light photocatalysis of water pollutants. *Concepts of semiconductor photocatalysis*.

Iqbal, W., Yang, B., Zhao, X., Rauf, M., Waqas, M., Gong, Y., Zhang, J. and Mao, Y., 2018. Controllable synthesis of graphitic carbon nitride nanomaterials for solar energy conversion and environmental remediation: the road travelled and the way forward. *Catalysis Science & Technology*, *8*(18), pp.4576-4599.

Irfan, S., Li, L., Saleemi, A.S. and Nan, C.W., 2017. Enhanced photocatalytic activity of La 3+ and Se 4+ co-doped bismuth ferrite nanostructures. *Journal of Materials Chemistry A*, *5*(22), pp.11143-11151.

Jia, Q., Iwase, A. and Kudo, A., 2014. BiVO 4–Ru/SrTiO 3: Rh composite Z-scheme photocatalyst for solar water splitting. *Chemical Science*, *5*(4), pp.1513-1519.

Jiang, L., Hu, X., Yin, D., Zhang, H. and Yu, Z., 2011. Occurrence, distribution and seasonal variation of antibiotics in the Huangpu River, Shanghai, China. *Chemosphere*, *82*(6), pp.822-828.

Joerin, F., Desthieux, G., Beuze, S.B. and Nembrini, A., 2009. Participatory diagnosis in urban planning: Proposal for a learning process based on geographical information. *Journal of Environmental Management*, *90*(6), pp.2002-2011.

Josephine, A.J., Dhas, C.R., Venkatesh, R., Arivukarasan, D., Christy, A.J., Monica, S.E.S. and Keerthana, S., 2020. Effect of pH on visible-light-driven photocatalytic degradation of facile synthesized bismuth vanadate nanoparticles. *Materials Research Express*, *7*(1), p.015036.

Kamaei, M., Rashedi, H., Dastgheib, S.M.M. and Tasharrofi, S., 2018. Comparing photocatalytic degradation of gaseous ethylbenzene using N-doped and pure TiO2 nano-catalysts coated on glass beads under both UV and visible light irradiation. *Catalysts*, *8*(10), p.466.

Katuri, K.P., Ali, M. and Saikaly, P.E., 2019. The role of microbial electrolysis cell in urban wastewater treatment: integration options, challenges, and prospects. *Current opinion in biotechnology*, *57*, pp.101-110.

Kaus, N.H., 2020. Photocatalysis for organic wastewater treatment: From the basis to current challenges for society. *Catalysts*, *10*(11), p.1260.

Khalilzadeh, A. and Fatemi, S., 2016. Spouted bed reactor for VOC removal by modified nano-TiO2 photocatalytic particles. *Chemical Engineering Research and Design*, *115*, pp.241-250.

King, A., 2018. *Why antibiotic pollution is a global threat*. Retrieved from https://www.chemistryworld.com/news/why-antibiotic-pollution-is-a-global-threat/3009021.article

Kittaka, S., Matsuno, K. and Akashi, H., 1999. Crystal Structure ofα-AgVO3and Phase Relation of AgVO3. *Journal of Solid State Chemistry*, *142*(2), pp.360-367.

Kogo, K., Yoneyama, H. and Tamura, H., 1980. Photocatalytic oxidation of cyanide on platinized titanium dioxide. *The Journal of Physical Chemistry*, *84*(13), pp.1705-1710.

Kolaczkowski, S.T., Plucinski, P., Beltran, F.J., Rivas, F.J. and McLurgh, D.B., 1999. Wet air oxidation: a review of process technologies and aspects in reactor design. *Chemical Engineering Journal*, *73*(2), pp.143-160.

Kosslick, H., Wang, Y., Ibad, M.F., Guo, X., Lütgens, M., Lochbrunner, S., Frank, M., Liem, N.Q. and Schulz, A., 2021. High-Performance Room-Light-Driven β-AgVO3/mpg-C3N4 Core/Shell Photocatalyst Prepared by Mechanochemical Method. *Advances in Chemical Engineering and Science*, *11*(4), pp.290-315.

Kovacic, Z., Likozar, B. and Hus, M., 2020. Photocatalytic CO2 reduction: A review of ab initio mechanism, kinetics, and multiscale modeling simulations. *ACS catalysis*, *10*(24), pp.14984-15007.

Kraemer, S.A., Ramachandran, A. and Perron, G.G., 2019. Antibiotic pollution in the environment: from microbial ecology to public policy. *Microorganisms*, *7*(6), p.180.

Kubacka, A., Fernandez-Garcia, M. and Colon, G., 2012. Advanced nanoarchitectures for solar photocatalytic applications. *Chemical reviews*, *112*(3), pp.1555-1614.

Kudo, A. and Miseki, Y., 2009. Heterogeneous photocatalyst materials for water splitting. *Chemical Society Reviews*, *38*(1), pp.253-278.

Kumar, A. and Pandey, G., 2017. A review on the factors affecting the photocatalytic degradation of hazardous materials. *Mater. Sci. Eng. Int. J*, *1*(3), pp.1-10.

Kumar, S., Ahlawat, W., Bhanjana, G., Heydarifard, S., Nazhad, M.M. and Dilbaghi, N., 2014. Nanotechnology-based water treatment strategies. *Journal of nanoscience and nanotechnology*, *14*(2), pp.1838-1858.

Kumar, S., Surendar, T., Kumar, B., Baruah, A. and Shanker, V., 2014. Synthesis of highly efficient and recyclable visible-light responsive mesoporous gC 3 N 4 photocatalyst via facile template-free sonochemical route. *RSC advances*, *4*(16), pp.8132-8137.

Kümmerer, K., 2009. Antibiotics in the aquatic environment–a review–part II. *Chemosphere*, *75*(4), pp.435-441.

Kurt, A., Mert, B.K., Özengin, N., Sivrioğlu, Ö. and Yonar, T., 2017. Treatment of antibiotics in wastewater using advanced oxidation processes (AOPs). *Physico-chemical wastewater treatment and resource recovery*, *175*.

Kutuzova, A., Dontsova, T. and Kwapinski, W., 2021. Application of TiO2-Based Photocatalysts to Antibiotics Degradation: Cases of Sulfamethoxazole, Trimethoprim and Ciprofloxacin. *Catalysts*, *11*(6), p.728.

Larramendy, M. and Soloneski, S. eds., 2015. *Emerging Pollutants in the Environment: Current and Further Implications*. BoD–Books on Demand.

Le Page, G., Gunnarsson, L., Snape, J. and Tyler, C.R., 2018. Antibiotic risk assessment needs to protect both environmental and human health.

Lee, G.J. and Wu, J.J., 2017. Recent developments in ZnS photocatalysts from synthesis to photocatalytic applications—A review. *Powder technology*, *318*, pp.8-22.

Lee, K.M., Lai, C.W., Ngai, K.S. and Juan, J.C., 2016. Recent developments of zinc oxide based photocatalyst in water treatment technology: a review. *Water research*, *88*, pp.428-448.

Li, C., Ma, Y., Zheng, S., Hu, C., Qin, F., Wei, L., Zhang, C., Duo, S. and Hu, Q., 2020. One-pot synthesis of Bi2O3/Bi2O4 pn heterojunction for highly efficient photocatalytic removal of organic pollutants under visible light irradiation. *Journal of Physics and Chemistry of Solids*, *140*, p.109376.

Li, X., Shen, R., Ma, S., Chen, X. and Xie, J., 2018. Graphene-based heterojunction photocatalysts. *Applied Surface Science*, *430*, pp.53-107.

Li, X., Yu, J. and Jaroniec, M., 2016. Hierarchical photocatalysts. *Chemical Society Reviews*, *45*(9), pp.2603-2636.

Li, Y., Zhang, J., Wang, Q., Jin, Y., Huang, D., Cui, Q. and Zou, G., 2010. Nitrogen-rich carbon nitride hollow vessels: synthesis, characterization, and their properties. *The Journal of Physical Chemistry B*, *114*(29), pp.9429-9434.

Li, Z., Meng, X. and Zhang, Z., 2019. Fabrication of surface hydroxyl modified gC 3 N 4 with enhanced photocatalytic oxidation activity. *Catalysis Science & Technology*, *9*(15), pp.3979-3993.

Li, Z., Meng, X. and Zhang, Z., 2019. Fewer-layer BN nanosheets-deposited on Bi2MoO6 microspheres with enhanced visible light-driven photocatalytic activity. *Applied Surface Science*, *483*, pp.572-580.

Lin, B., Xue, C., Yan, X., Yang, G., Yang, G. and Yang, B., 2015. Facile fabrication of novel SiO2/g-C3N4 core–shell nanosphere photocatalysts with enhanced visible light activity. *Applied Surface Science*, *357*, pp.346-355.

Lin, X., Xu, D., Zheng, J., Song, M., Che, G., Wang, Y., Yang, Y., Liu, C., Zhao, L. and Chang, L., 2016. Graphitic carbon nitride quantum dots loaded on leaf-like InVO4/BiVO4 nanoheterostructures with enhanced visible-light photocatalytic activity. *Journal of Alloys and Compounds*, *688*, pp.891-898.

Liotta, L.F., Gruttadauria, M., Di Carlo, G., Perrini, G. and Librando, V., 2009. Heterogeneous catalytic degradation of phenolic substrates: catalysts activity. *Journal of hazardous materials*, *162*(2-3), pp.588-606.

Liu, C., Tan, L., Zhang, L., Tian, W. and Ma, L., 2021. A review of the distribution of antibiotics in water in different regions of China and current antibiotic degradation pathways. *Frontiers in Environmental Science*, 6(5), p.221.

Liu, D., Chen, D., Li, N., Xu, Q., Li, H., He, J. and Lu, J., 2019. Integration of 3D macroscopic graphene aerogel with 0D-2D AgVO3-g-C3N4 heterojunction for highly efficient photocatalytic oxidation of nitric oxide. *Applied Catalysis B: Environmental*, *243*, pp.576-584.

Liu, H., Chang, X., Liu, X., Li, G., Zhang, W. and An, T., 2021. Boosting the photocatalytic degradation of ethyl acetate by a Z-scheme Au–TiO 2@ NH 2-UiO-66 heterojunction with ultrafine Au as an electron mediator. *Environmental Science: Nano*, *8*(9), pp.2542-2553.

Liu, Y., He, X., Fu, Y. and Dionysiou, D.D., 2016. Kinetics and mechanism investigation on the destruction of oxytetracycline by UV-254 nm activation of persulfate. *Journal of Hazardous Materials*, *305*, pp.229-239.

Lopez Penalver, J.J., Gomez Pacheco, C.V., Sanchez Polo, M. and Rivera Utrilla, J., 2013. Degradation of tetracyclines in different water matrices by advanced oxidation/reduction processes based on gamma radiation. *Journal of Chemical Technology & Biotechnology*, *88*(6), pp.1096-1108.

Lotsch, B.V., Döblinger, M., Sehnert, J., Seyfarth, L., Senker, J., Oeckler, O. and Schnick, W., 2007. Unmasking melon by a complementary approach employing electron diffraction, solid-state NMR spectroscopy, and theoretical calculations—structural characterization of a carbon nitride polymer. *Chemistry–A European Journal*, *13*(17), pp.4969-4980.

Louangsouphom, B., Wang, X., Song, J. and Wang, X., 2019. Low-temperature preparation of a N-TiO2/macroporous resin photocatalyst to degrade organic pollutants. *Environmental Chemistry Letters*, *17*(2), pp.1061-1066.

Lu, C.S., Chen, C.C., and Chi, H.T., 2017. Synthesis of silver vanadates ($AgVO_3$, Ag_3VO_4, and $Ag_4V_2O_7$) by controlled hydrothermal method and their photocatalytic properties. *Journal of material sciences & Engineering,* p.64.

Madhusudan, P., Ran, J., Zhang, J., Yu, J. and Liu, G., 2011. Novel urea assisted hydrothermal synthesis of hierarchical BiVO4/Bi2O2CO3 nanocomposites with enhanced visible-light photocatalytic activity. *Applied Catalysis B: Environmental*, *110*, pp.286-295.

Malathi, A., Madhavan, J., Ashokkumar, M. and Arunachalam, P., 2018. A review on BiVO4 photocatalyst: activity enhancement methods for solar photocatalytic applications. *Applied Catalysis A: General*, *555*, pp.47-74.

Malik, A.S., Liu, T., Rittiruam, M., Saelee, T., Da Silva, J.L., Praserthdam, S. and Praserthdam, P., 2022. On a high photocatalytic activity of high-noble alloys Au–Ag/TiO2 catalysts during oxygen evolution reaction of water oxidation. *Scientific reports*, *12*(1), pp.1-13.

Manzetti, S. and Ghisi, R., 2014. The environmental release and fate of antibiotics. *Marine pollution bulletin*, *79*(1-2), pp.7-15.

Martinez-de La Cruz, A. and Perez, U.G., 2010. Photocatalytic properties of BiVO4 prepared by the co-precipitation method: degradation of rhodamine B and possible reaction mechanisms under visible irradiation. *Materials research bulletin*, *45*(2), pp.135-141.

Massé, D.I., Cata Saady, N.M. and Gilbert, Y., 2014. Potential of biological processes to eliminate antibiotics in livestock manure: an overview. *Animals*, *4*(2), pp.146-163.

Masterflex, 2021. *The Importance of Wastewater Treatment - Masterflex*. [online] Available at: https://www.masterflex.com/tech-article/importance-of-wastewater-treatment [Accessed 1st July 2022].

McNulty, D., Ramasse, Q. and O'Dwyer, C., 2016. The structural conversion from α-AgVO 3 to β-AgVO 3: Ag nanoparticle decorated nanowires with application as cathode materials for Li-ion batteries. *Nanoscale*, *8*(36), pp.16266-16275.

Minden, V., Deloy, A., Volkert, A.M., Leonhardt, S.D. and Pufal, G., 2017. Antibiotics impact plant traits, even at small concentrations. *AoB Plants*, *9*(2).

Mo, Z., She, X., Li, Y., Liu, L., Huang, L., Chen, Z., Zhang, Q., Xu, H. and Li, H., 2015. Synthesis of gC 3 N 4 at different temperatures for superior visible/UV photocatalytic performance and photoelectrochemical sensing of MB solution. *RSC advances*, *5*(123), pp.101552-101562.

Mohan, R., Ravichandran, K., Nithya, A., Jothivenkatachalam, K., Ravidhas, C. and Sakthivel, B., 2014. Influence of spray flux density on the photocatalytic activity and certain physical properties of ZnO thin films. *Journal of Materials Science: Materials in Electronics*, *25*(6), pp.2546-2553.

Molinari, R., Lavorato, C. and Argurio, P., 2020. Visible-light photocatalysts and their perspectives for building photocatalytic membrane reactors for various liquid phase chemical conversions. *Catalysts*, *10*(11), p.1334.

Molinari, R., Lavorato, C. and Argurio, P., 2021. The Evolution of Photocatalytic Membrane Reactors over the Last 20 Years: A State of the Art Perspective. *Catalysts*, *11*(7), p.775.

Mondal, C., Singh, A., Sahoo, R., Sasmal, A.K., Negishi, Y. and Pal, T., 2015. Preformed ZnS nanoflower prompted evolution of CuS/ZnS p–n heterojunctions for exceptional visible-light driven photocatalytic activity. *New Journal of Chemistry*, *39*(7), pp.5628-5635.

Monfort, O. and Plesch, G., 2018. Bismuth vanadate-based semiconductor photocatalysts: a short critical review on the efficiency and the mechanism of photodegradation of organic pollutants. *Environmental Science and Pollution Research*, *25*(20), pp.19362-19379.

Moradi, Z., Jahromi, S.Z. and Ghaedi, M., 2021. Design of active photocatalysts and visible light photocatalysis. In *Interface Science and Technology* (Vol. 32, pp. 557-623). Elsevier.

Motahari, F., Mozdianfard, M.R., Soofivand, F. and Salavati-Niasari, M., 2014. NiO nanostructures: synthesis, characterization and photocatalyst application in dye wastewater treatment. *RSC advances*, *4*(53), pp.27654-27660.

Mour ão, H.A., Lopes, O.F., Ribeiro, C. and Mastelaro, V.R., 2015. Rapid hydrothermal synthesis and pH-dependent photocatalysis of strontium titanate microspheres. *Materials Science in Semiconductor Processing*, *30*, pp.651-657.

Mozia, S., 2010. Photocatalytic membrane reactors (PMRs) in water and wastewater treatment. A review. *Separation and purification technology*, *73*(2), pp.71-91.

Narkbuakaew, T. and Sujaridworakun, P., 2020. Synthesis of Tri-S-Triazine Based g-C3N4 Photocatalyst for Cationic Rhodamine B Degradation under Visible Light. *Topics in Catalysis*, *63*(11-14), pp.1086-1096.

Nasri, M.S.I., Samsudin, M.F.R., Tahir, A.A. and Sufian, S., 2022. Effect of MXene loaded on g-C3N4 photocatalyst for the photocatalytic degradation of methylene blue. *Energies*, *15*(3), p.955.

Nguyen, T.D., Nguyen, V.H., Nanda, S., Vo, D.V.N., Nguyen, V.H., Van Tran, T., Nong, L.X., Nguyen, T.T., Bach, L.G., Abdullah, B. and Hong, S.S., 2020. BiVO4 photocatalysis design and applications to oxygen production and degradation of organic compounds: a review. *Environmental Chemistry Letters*, *18*(6), pp.1779-1801.

Nguyen, V.H., Mousavi, M., Ghasemi, J.B., Van Le, Q., Delbari, S.A., Namini, A.S., Asl, M.S., Shokouhimehr, M., Jang, H.W. and Mohammadi, M., 2021. RETRACTED: g-C3N4 nanosheet adorned with Ag3BiO3 as a perovskite: An effective photocatalyst for efficient visible-light photocatalytic processes.

Ojha, A., 2020. Nanomaterials for removal of waterborne pathogens: Opportunities and challenges. *Waterborne pathogens*, pp.385-432.

Panda, D., Venkatesh, N. and Sakthivel, P., 2022. MXene-based materials for remediation of environmental pollutants. In *Mxenes and their Composites* (pp. 553-594). Elsevier.

Parajuli, S., 2018. Conventional wastewater treatment. [online] Available at: https://www.slideshare.net/SitalParajuli/conventional-wastewater-treatment [Accessed 16 July 2022].

Pena, A., Paulo, M., Silva, L.J.G., Seifrtová, M., Lino, C.M. and Solich, P., 2010. Tetracycline antibiotics in hospital and municipal wastewaters: a pilot study in Portugal. *Analytical and bioanalytical chemistry*, *396*(8), pp.2929-2936.

Phoon, B.L., Ong, C.C., Saheed, M.S.M., Show, P.L., Chang, J.S., Ling, T.C., Lam, S.S. and Juan, J.C., 2020. Conventional and emerging technologies for removal of antibiotics from wastewater. *Journal of hazardous materials*, *400*, p.122961.

Polianciuc, S.I., Gurzău, A.E., Kiss, B., Ştefan, M.G. and Loghin, F., 2020. Antibiotics in the environment: causes and consequences. *Medicine and pharmacy reports*, *93*(3), p.231.

Prashanth, V., Jayasree, P., Rajput, P. and Remya, N., 2021. Solar photocatalysis and its application for emerging contaminant removal from wastewater. In *Advanced Oxidation Processes for Effluent Treatment Plants* (pp. 69-85). Elsevier.

PubChem (n.d.). *Silver vanadium trioxide*. [online] pubchem.ncbi.nlm.nih.gov. Available at: https://pubchem.ncbi.nlm.nih.gov/compound/Silver-vanadium-trioxide#section=Structures [Accessed 17 Aug. 2022].

Qi, K., Liu, S.Y. and Zada, A., 2020. Graphitic carbon nitride, a polymer photocatalyst. *Journal of the Taiwan Institute of Chemical Engineers*, *109*, pp.111-123.

Quaik, S., Embrandiri, A., Ravindran, B., Hossain, K., Al-Dhabi, N.A., Arasu, M.V., Ignacimuthu, S. and Ismail, N., 2020. Veterinary antibiotics in animal manure and manure laden soil: Scenario and challenges in Asian countries. *Journal of King Saud University-Science*, *32*(2), pp.1300-1305.

Rao, M.N., Sultana, R. and Kota, S.H., 2017. Chapter 5–hazardous waste. *Solid and Hazardous Waste Management*, pp.159-207.

Rastogi, M., Kushwaha, H.S. and Vaish, R., 2016. Highly efficient visible light mediated azo dye degradation through barium titanate decorated reduced graphene oxide sheets. *Electronic Materials Letters*, *12*(2), pp.281-289.

Reis, A.C., Kolvenbach, B.A., Nunes, O.C. and Corvini, P.F., 2020. Biodegradation of antibiotics: the new resistance determinants–part I. *New biotechnology*, *54*, pp.34-51.

Ren, G., Han, H., Wang, Y., Liu, S., Zhao, J., Meng, X. and Li, Z., 2021. Recent advances of photocatalytic application in water treatment: a review. *Nanomaterials*, *11*(7), p.1804.

Ren, Z., Chen, F., Wen, K. and Lu, J., 2020. Enhanced photocatalytic activity for tetracyclines degradation with Ag modified g-C3N4 composite under visible light. *Journal of Photochemistry and Photobiology A: Chemistry*, *389*, p.112217.

Roberts, J.A., Norris, R., Paterson, D.L. and Martin, J.H., 2012. Therapeutic drug monitoring of antimicrobials. *British journal of clinical pharmacology*, *73*(1), pp.27-36.

Roy, J.S., Dugas, G., Morency, S., Ribeiro, S.J. and Messaddeq, Y., 2020. Enhanced photocatalytic activity of silver vanadate nanobelts in concentrated sunlight delivered through optical fiber bundle coupled with solar concentrator. *SN Applied Sciences*, *2*(2), pp.1-11.

Santaeufemia, S., Torres, E., Mera, R. and Abalde, J., 2016. Bioremediation of oxytetracycline in seawater by living and dead biomass of the microalga Phaeodactylum tricornutum. *Journal of hazardous materials*, *320*, pp.315-325.

Savateev, A. and Dontsova, D., 2016. Baking 'crumbly'carbon nitrides with improved photocatalytic properties using ammonium chloride. *RSC advances*, *6*(4), pp.2910-2913.

Sediri, F. and Gharbi, N., 2009. Controlled hydrothermal synthesis of VO2 (B) nanobelts. *Materials Letters*, *63*(1), pp.15-18.

Sethi, Y.A., Praveen, C.S., Panmand, R.P., Ambalkar, A., Kulkarni, A.K., Gosavi, S.W., Kulkarni, M.V. and Kale, B.B., 2018. Perforated N-doped monoclinic ZnWO 4 nanorods for efficient photocatalytic hydrogen generation and RhB degradation under natural sunlight. *Catalysis Science & Technology*, *8*(11), pp.2909-2919.

Shah, A.H. and Rather, M.A., 2021. Pharmaceutical residues: new emerging contaminants and their mitigation by nano-photocatalysis. *Adv Nano Res*, *10*(4), pp.397-414.

Shaojun, J.I.A.O., Zheng, S., Daqiang, Y.I.N., Lianhong, W.A.N.G. and Liangyan, C.H.E.N., 2008. Aqueous oxytetracycline degradation and the toxicity change of degradation compounds in photoirradiation process. *Journal of Environmental Sciences*, *20*(7), pp.806-813.

Shi, H., Zhang, C. and Zhou, C., 2015. gC 3 N 4 hybridized with AgVO 3 nanowires: preparation and its enhanced visible-light-induced photocatalytic activity. *RSC Advances*, *5*(62), pp.50146-50154.

Shi, L., Wang, T., Zhang, H., Chang, K., Meng, X., Liu, H. and Ye, J., 2015. An amine-functionalized iron (III) metal–organic framework as efficient visible-light photocatalyst for Cr (VI) reduction. *Advanced science*, *2*(3), p.1500006.

Sinar Mashuri, S.I., Ibrahim, M.L., Kasim, M.F., Mastuli, M.S., Rashid, U., Abdullah, A.H., Islam, A., Asikin Mijan, N., Tan, Y.H., Mansir, N. and Mohd Kaus, N.H., 2020. Photocatalysis for organic wastewater treatment: From the basis to current challenges for society. *Catalysts*, *10*(11), p.1260.

Sindhu, R., Binod, P. and Pandey, A., 2015. Microbial poly-3-hydroxybutyrate and related copolymers. In *Industrial Biorefineries & White Biotechnology* (pp. 575-605). Elsevier.

Singh, D.P., Polychronopoulou, K., Rebholz, C. and Aouadi, S.M., 2010. Room temperature synthesis and high temperature frictional study of silver vanadate nanorods. *Nanotechnology*, *21*(32), p.325601.

Sivakumar, V., Suresh, R., Giribabu, K. and Narayanan, V., 2015. AgVO3 nanorods: Synthesis, characterization and visible light photocatalytic activity. *Solid State Sciences*, *39*, pp.34-39.

Sivakumar, V., Suresh, R., Giribabu, K., Manigandan, R., Munusamy, S., Praveen Kumar, S., Muthamizh, S. and Narayanan, V., 2014. Copper vanadate nanoparticles: synthesis, characterization and its electrochemical sensing property. *Journal of Materials Science: Materials in Electronics*, *25*(3), pp.1485-1491.

Soltani, T., Tayyebi, A. and Lee, B.K., 2019. Photolysis and photocatalysis of tetracycline by sonochemically heterojunctioned BiVO4/reduced graphene oxide under visible-light irradiation. *Journal of environmental management*, *232*, pp.713-721.

Sonawane, G.H., Patil, S.P. and Sonawane, S.H., 2018. Nanocomposites and its applications. In *Applications of nanomaterials* (pp. 1-22). Woodhead Publishing.

Song, J.M., Lin, Y.Z., Yao, H.B., Fan, F.J., Li, X.G. and Yu, S.H., 2009. Superlong β-AgVO3 nanoribbons: high-yield synthesis by a pyridine-assisted solution approach, their stability, electrical and electrochemical properties. *ACS nano*, *3*(3), pp.653-660.

Sun, M., Li, S., Yan, T., Ji, P., Zhao, X., Yuan, K., Wei, D. and Du, B., 2017. Fabrication of heterostructured Bi2O2CO3/Bi2O4 photocatalyst and efficient photodegradation of organic contaminants under visible-light. *Journal of hazardous materials*, *333*, pp.169-178.

Szekeres, E., Chiriac, C.M., Baricz, A., Szőke-Nagy, T., Lung, I., Soran, M.L., Rudi, K., Dragos, N. and Coman, C., 2018. Investigating antibiotics, antibiotic resistance genes, and microbial contaminants in groundwater in relation to the proximity of urban areas. *Environmental Pollution*, *236*, pp.734-744.

Takeuchi, K.J., Marschilok, A.C., Davis, S.M., Leising, R.A. and Takeuchi, E.S., 2001. Silver vanadium oxides and related battery applications. *Coordination Chemistry Reviews*, *219*, pp.283-310.

Thalluri, S.M., Hernandez, S., Bensaid, S., Saracco, G. and Russo, N., 2016. Green-synthesized W-and Mo-doped BiVO4 oriented along the {0 4 0} facet with enhanced activity for the sun-driven water oxidation. *Applied Catalysis B: Environmental*, *180*, pp.630-636.

The World Bank, 2020. *Wastewater A Resource that Can Pay Dividends for People, the Environment, and Economies, Says World Bank.* Retrieved from https://www.worldbank.org/en/news/press-release/2020/03/19/wastewater-a-resource-that-can-pay-dividends-for-people-the-environment-and-economies-says-world-bank

Thongam, D.D. and Chaturvedi, H., 2021. Advances in nanomaterials for heterogeneous photocatalysis. *Nano Express*, *2*(1), p.012005.

Tungler, A., Szabados, E. and Hosseini, A.M., 2015. Wet air oxidation of aqueous wastes. *Wastewater Treatment Engineering*, p.153.

ul Haq, A., Saeed, M., Khan, S.G. and Ibrahim, M., 2021. Photocatalytic Applications of Titanium Dioxide (TiO 2). In *Titanium Dioxide-Advances and Applications*. IntechOpen.

Umar, M. and Aziz, H.A., 2013. Photocatalytic degradation of organic pollutants in water. *Organic pollutants-monitoring, risk and treatment*, *8*, pp.196-197.

Vali, A., Sarker, H.P., Jee, H.W., Kormányos, A., Firouzan, F., Myung, N., Paeng, K.J., Huda, M.N., Janáky, C. and Rajeshwar, K., 2019. Electrodeposition of Silver Vanadate Films: A Tale of Two Polymorphs. *ChemPhysChem*, *20*(20), pp.2635-2646.

Van Boeckel, T.P., Brower, C., Gilbert, M., Grenfell, B.T., Levin, S.A., Robinson, T.P., Teillant, A. and Laxminarayan, R., 2015. Global trends in antimicrobial use in food animals. *Proceedings of the National Academy of Sciences*, *112*(18), pp.5649-5654.

Van Der Grinten, E., Pikkemaat, M.G., Van Den Brandhof, E.J., Stroomberg, G.J. and Kraak, M.H., 2010. Comparing the sensitivity of algal, cyanobacterial and bacterial bioassays to different groups of antibiotics. *Chemosphere*, *80*(1), pp.1-6.

Vu, T.A., Dao, C.D., Hoang, T.T., Dang, P.T., Tran, H.T., Nguyen, K.T., Le, G.H., Nguyen, T.V. and Lee, G.D., 2014. Synthesis of novel silver vanadates with high photocatalytic and antibacterial activities. *Materials Letters*, *123*, pp.176-180.

Wammer, K.H., Slattery, M.T., Stemig, A.M. and Ditty, J.L., 2011. Tetracycline photolysis in natural waters: loss of antibacterial activity. *Chemosphere*, *85*(9), pp.1505-1510.

Wang, C., Lin, H., Xu, Z., Cheng, H. and Zhang, C., 2015. One-step hydrothermal synthesis of flowerlike MoS 2/CdS heterostructures for enhanced visible-light photocatalytic activities. *RSC Advances*, *5*(20), pp.15621-15626.

Wang, G.C., 2016. *The utilization of slag in civil infrastructure construction*. Woodhead Publishing.

Wang, J. and Bai, Z., 2017. Fe-based catalysts for heterogeneous catalytic ozonation of emerging contaminants in water and wastewater. *Chemical Engineering Journal*, *312*, pp.79-98.

Wang, J. and Zhuan, R., 2020. Degradation of antibiotics by advanced oxidation processes: An overview. *Science of the Total Environment*, *701*, p.135023.

Wang, J., Chu, L., Wojnárovits, L. and Takács, E., 2020. Occurrence and fate of antibiotics, antibiotic resistant genes (ARGs) and antibiotic resistant bacteria (ARB) in municipal wastewater treatment plant: An overview. *Science of the Total Environment*, *744*, p.140997.

Wang, J.L. and Xu, L.J., 2012. Advanced oxidation processes for wastewater treatment: formation of hydroxyl radical and application. *Critical reviews in environmental science and technology*, *42*(3), pp.251-325.

Wang, W., Gu, W., Li, G., Xie, H., Wong, P.K. and An, T., 2020. Few-layered tungsten selenide as a co-catalyst for visible-light-driven photocatalytic production of hydrogen peroxide for bacterial inactivation. *Environmental Science: Nano*, *7*(12), pp.3877-3887.

Wang, Y., Ma, X., Li, H., Liu, B., Li, H., Yin, S. and Sato, T., 2016. Recent Advances in Visible-Light Driven Photocatalysis. *Advanced Catalytic materials*, *12*, p.337.

Wang, Z., Huang, X. and Wang, X., 2019. Recent progresses in the design of BiVO4-based photocatalysts for efficient solar water splitting. *Catalysis Today*, *335*, pp.31-38.

Water Science School (2019). *How Much Water is There on Earth? | U.S. Geological Survey*. [online] www.usgs.gov. Available at: https://www.usgs.gov/special-topics/water-science-school/science/how-much-water-there-earth.

Watson, R.R. and Preedy, V.R. eds., 2012. *Bioactive food as dietary interventions for liver and gastrointestinal disease: bioactive foods in chronic disease states*. Academic press.

Wen, J., Xie, J., Chen, X. and Li, X., 2017. A review on g-C3N4-based photocatalysts. *Applied surface science*, *391*, pp.72-123.

World Health Organization, 2014. *Antimicrobial resistance: global report on surveillance*. World Health Organization.

World Health Organization, 2018. WHO report on surveillance of antibiotic consumption: 2016-2018 early implementation.

Wu, S.Z., Li, K. and Zhang, W.D., 2015. On the heterostructured photocatalysts Ag3VO4/g-C3N4 with enhanced visible light photocatalytic activity. *Applied Surface Science*, *324*, pp.324-331.

Wu, Y., Wang, H., Tu, W., Liu, Y., Tan, Y.Z., Yuan, X. and Chew, J.W., 2018. Quasi-polymeric construction of stable perovskite-type LaFeO3/g-C3N4 heterostructured photocatalyst for improved Z-scheme photocatalytic activity via solid pn heterojunction interfacial effect. *Journal of hazardous materials*, *347*, pp.412-422.

Xiang, Z., Wang, Y., Ju, P. and Zhang, D., 2016. Optical determination of hydrogen peroxide by exploiting the peroxidase-like activity of AgVO 3 nanobelts. *Microchimica Acta*, *183*, pp.457-463.

Xu, J., Brenner, T.J., Chabanne, L., Neher, D., Antonietti, M. and Shalom, M., 2014. Liquid-based growth of polymeric carbon nitride layers and their use in a mesostructured polymer solar cell with V oc exceeding 1 V. *Journal of the American Chemical Society*, *136*(39), pp.13486-13489.

Xu, J., Hu, C., Xi, Y., Wan, B., Zhang, C. and Zhang, Y., 2012. Synthesis and visible light photocatalytic activity of β-AgVO3 nanowires. *Solid state sciences*, *14*(4), pp.535-539.

Xu, J., Wang, G., Fan, J., Liu, B., Cao, S. and Yu, J., 2015. g-C3N4 modified TiO2 nanosheets with enhanced photoelectric conversion efficiency in dye-sensitized solar cells. *Journal of Power Sources*, *274*, pp.77-84.

Xu, L., Zhang, H., Xiong, P., Zhu, Q., Liao, C. and Jiang, G., 2021. Occurrence, fate, and risk assessment of typical tetracycline antibiotics in the aquatic environment: A review. *Science of the Total Environment*, *753*, p.141975.

Xu, M., Han, L. and Dong, S., 2013. Facile fabrication of highly efficient g-C3N4/Ag2O heterostructured photocatalysts with enhanced visible-light photocatalytic activity. *ACS applied materials & interfaces*, *5*(23), pp.12533-12540.

Xue, X., Chen, X. and Gong, X., 2021. Fast electron transfer and enhanced visible light photocatalytic activity of silver and Ag2O co-doped titanium dioxide with the doping of electron mediator for removing gaseous toluene. *Materials Science in Semiconductor Processing*, *132*, p.105901.

Yan, H., 2012. Soft-templating synthesis of mesoporous graphitic carbon nitride with enhanced photocatalytic H 2 evolution under visible light. *Chemical Communications*, *48*(28), pp.3430-3432.

Yan, H., Chen, W., Liao, G., Li, X., Ma, S. and Li, L., 2016. Activity assessment of direct synthesized Fe-SBA-15 for catalytic ozonation of oxalic acid. *Separation and Purification Technology*, *159*, pp.1-6.

Yang, S., Cha, J. and Carlson, K., 2005. Simultaneous extraction and analysis of 11 tetracycline and sulfonamide antibiotics in influent and effluent domestic wastewater by solid-phase extraction and liquid chromatography-electrospray ionization tandem mass spectrometry. *Journal of Chromatography A*, *1097*(1-2), pp.40-53.

Yang, W., Jia, L., Wu, P., Zhai, H., He, J., Liu, C. and Jiang, W., 2021. Effect of thermal program on structure–activity relationship of g-C3N4 prepared by urea pyrolysis and its application for controllable production of g-C3N4. *Journal of Solid State Chemistry*, *304*, p.122545.

Ye, M.Y., Zhao, Z.H., Hu, Z.F., Liu, L.Q., Ji, H.M., Shen, Z.R. and Ma, T.Y., 2017. 0D/2D heterojunctions of vanadate quantum dots/graphitic carbon nitride nanosheets for enhanced visible-light-driven photocatalysis. *Angewandte Chemie International Edition*, *56*(29), pp.8407-8411.

Yi, X., Yuan, J., Tang, H., Du, Y., Hassan, B., Yin, K., Chen, Y. and Liu, X., 2020. Embedding few-layer Ti3C2Tx into alkalized g-C3N4 nanosheets for efficient photocatalytic degradation. *Journal of colloid and interface science*, *571*, pp.297-306.

Yin, S., Han, J., Zhou, T. and Xu, R., 2015. Recent progress in gC 3 N 4 based low cost photocatalytic system: activity enhancement and emerging applications. *Catalysis science & technology*, *5*(12), pp.5048-5061.

Zang, Y., Li, L., Li, X., Lin, R. and Li, G., 2014. Synergistic collaboration of g-C3N4/SnO2 composites for enhanced visible-light photocatalytic activity. *Chemical Engineering Journal*, *246*, pp.277-286.

Zhang, C., Li, Y., Shuai, D., Shen, Y., Xiong, W. and Wang, L., 2019. Graphitic carbon nitride (g-C3N4)-based photocatalysts for water disinfection and microbial control: A review. *Chemosphere*, *214*, pp.462-479.

Zhang, F., Wang, X., Liu, H., Liu, C., Wan, Y., Long, Y. and Cai, Z., 2019. Recent advances and applications of semiconductor photocatalytic technology. *Applied Sciences*, *9*(12), p.2489.

Zhang, J., Sun, J., Maeda, K., Domen, K., Liu, P., Antonietti, M., Fu, X. and Wang, X., 2011. Sulfur-mediated synthesis of carbon nitride: band-gap engineering and improved functions for photocatalysis. *Energy & Environmental Science*, *4*(3), pp.675-678.

Zhang, J., Tian, B., Wang, L., Xing, M. and Lei, J., 2018. *Photocatalysis: fundamentals, materials and applications* (Vol. 100). Springer.

Zhang, J., Wang, Y. and Hu, S., 2015. Simulated solar light responsive carbon nitride/TiO2 nanofiber heterojunction photocatalyst: synthesis, characterization, and photocatalytic performance. *Bulletin of the Korean Chemical Society*, *36*(1), pp.333-339.

Zhang, J., Yuan, X., Jiang, L., Wu, Z., Chen, X., Wang, H., Wang, H. and Zeng, G., 2018. Highly efficient photocatalysis toward tetracycline of nitrogen doped carbon quantum dots sensitized bismuth tungstate based on interfacial charge transfer. *Journal of colloid and interface science*, *511*, pp.296-306.

Zhang, S., Zhao, S., Huang, S., Hu, B., Wang, M., Zhang, Z., He, L. and Du, M., 2021. Photocatalytic degradation of oxytetracycline under visible light by nanohybrids of CoFe alloy nanoparticles and nitrogen-/sulfur-codoped mesoporous carbon. *Chemical Engineering Journal*, *420*, p.130516.

Zhang, T., Shao, X., Zhang, D., Pu, X., Tang, Y., Yin, J., Ge, B. and Li, W., 2018. Synthesis of direct Z-scheme g-C3N4/Ag2VO2PO4 photocatalysts with enhanced visible light photocatalytic activity. *Separation and Purification Technology*, *195*, pp.332-338.

Zhang, Y., Chen, H., Jing, L. and Teng, Y., 2020. Ecotoxicological risk assessment and source apportionment of antibiotics in the waters and sediments of a peri-urban river. *Science of the Total Environment*, *731*, p.139128.

Zhang, Y., Shaad, K., Vollmer, D. and Ma, C., 2021. Treatment of Textile Wastewater Using Advanced Oxidation Processes—A Critical Review. *Water*, *13*(24), p.3515.

Zhang, Z., Wang, W. and Gao, E., 2014. Polypyrrole/Bi2WO6 composite with high charge separation efficiency and enhanced photocatalytic activity. *Journal of Materials Science*, *49*(20), pp.7325-7332.

Zhao, J., Ma, L., Wang, H., Zhao, Y., Zhang, J. and Hu, S., 2015. Novel band gap-tunable K–Na co-doped graphitic carbon nitride prepared by molten salt method. *Applied Surface Science*, *332*, pp.625-630.

Zhao, W., Adeel, M., Zhang, P., Zhou, P., Huang, L., Zhao, Y., Noman, S., Ahmad, M.A., Lou, B., Jiang, Y. and Lynch, I., 2022. A critical review on surface modified nano-catalysts application for photocatalytic degradation of volatile organic compounds. *Environmental Science: Nano*.

Zhao, Z., Ma, Y., Fan, J., Xue, Y., Chang, H., Masubuchi, Y. and Yin, S., 2018. Synthesis of graphitic carbon nitride from different precursors by fractional thermal polymerization method and their visible light induced photocatalytic activities. *Journal of Alloys and Compounds*, *735*, pp.1297-1305.

Zhi, D., Yang, D., Zheng, Y., Yang, Y., He, Y., Luo, L. and Zhou, Y., 2019. Current progress in the adsorption, transport and biodegradation of antibiotics in soil. *Journal of environmental management*, *251*, p.109598.

Zhou, Y., Yu, M., Liang, H., Chen, J., Xu, L. and Niu, J., 2021. Novel dual-effective Z-scheme heterojunction with g-C3N4, Ti3C2 MXene and black phosphorus for improving visible light-induced degradation of ciprofloxacin. *Applied Catalysis B: Environmental*, *291*, p.120105.

Zhou, Z., Zhang, Z., Feng, L., Zhang, J., Li, Y., Lu, T. and Qian, H., 2020. Adverse effects of levofloxacin and oxytetracycline on aquatic microbial communities. *Science of the Total Environment*, *734*, p.139499.

Zhu, J., Xiao, P., Li, H. and Carabineiro, S.A., 2014. Graphitic carbon nitride: synthesis, properties, and applications in catalysis. *ACS applied materials & interfaces*, *6*(19), pp.16449-16465.

Zimmerman, J.L., Williams, R., Khabashesku, V.N. and Margrave, J.L., 2001. Preparation of sphere-shaped nanoscale carbon nitride polymer. *Russian chemical bulletin*, *50*(11), pp.2020-2027.

APPENDICES

Appendix A: EDX Reports

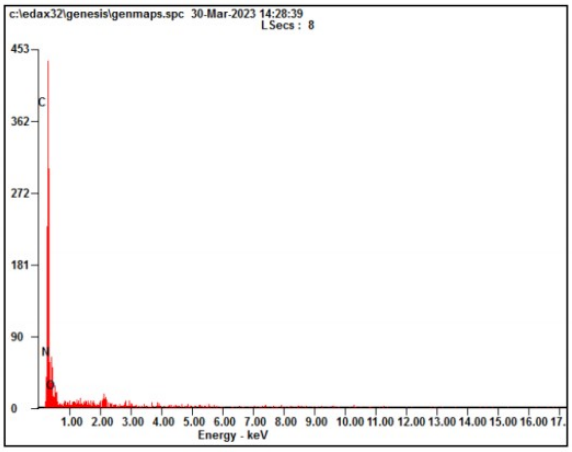

Element	Wt%	At%
CK	47.57	52.01
NK	42.41	39.76
OK	10.02	08.23
Matrix	Correction	ZAF

Figure A-1: Elemental Composition of Pure g-C_3N_4.

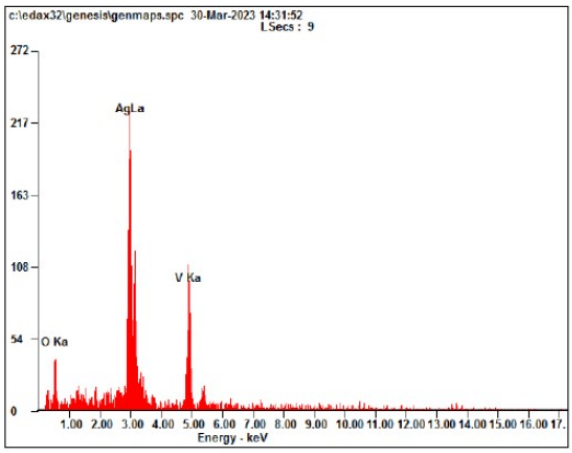

Element	Wt%	At%
OK	16.77	50.41
AgL	58.19	25.95
VK	25.04	23.64
Matrix	Correction	ZAF

Figure A-2: Elemental Composition of Pure AgVA.

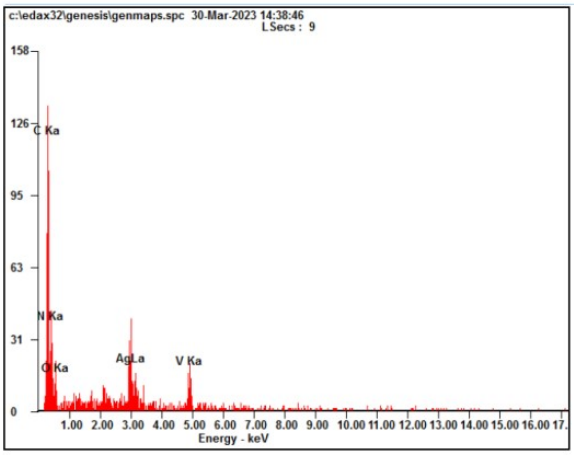

Element	Wt%	At%
CK	34.17	46.11
NK	32.88	38.05
OK	11.22	11.37
AgL	14.56	02.19
VK	07.17	02.28
Matrix	Correction	ZAF

Figure A-3: Elemental Composition of A10.

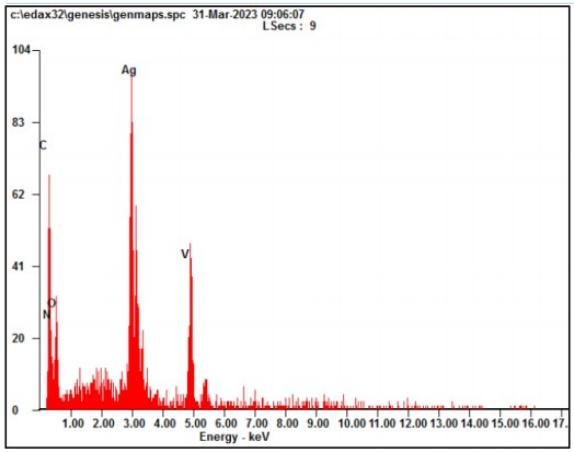

Element	Wt%	At%
CK	18.38	39.06
NK	09.32	16.98
OK	16.38	26.13
AgL	38.55	09.12
VK	17.38	08.71
Matrix	Correction	ZAF

Figure A-4: Elemental Composition of A30.

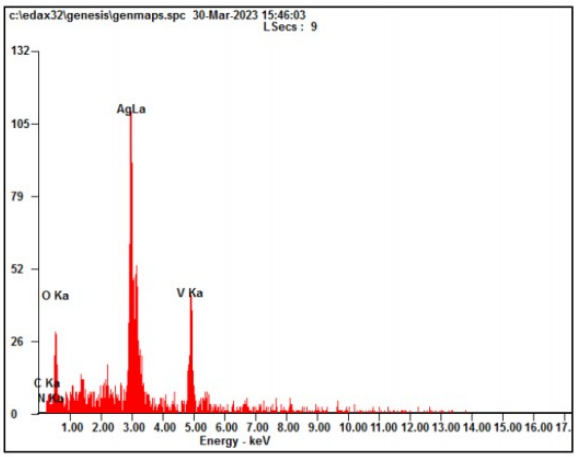

Element	Wt%	At%
CK	01.31	05.22
NK	00.83	02.84
OK	14.27	42.82
AgL	59.66	26.56
VK	23.94	22.57
Matrix	Correction	ZAF

Figure A-5: Elemental Composition of A50.

Appendix B: FTIR Reports

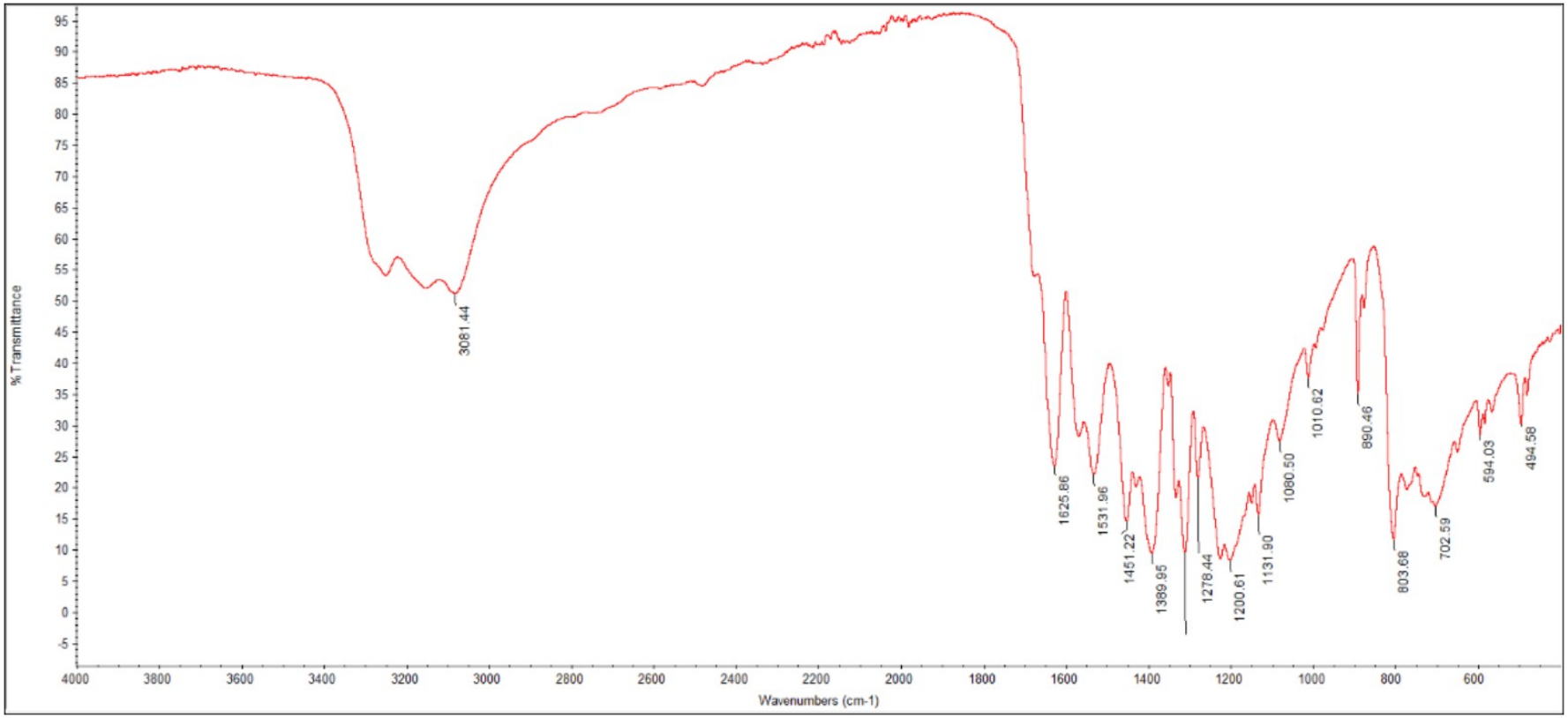

Figure B-1: FTIR Spectrum of Pure g-C_3N_4.

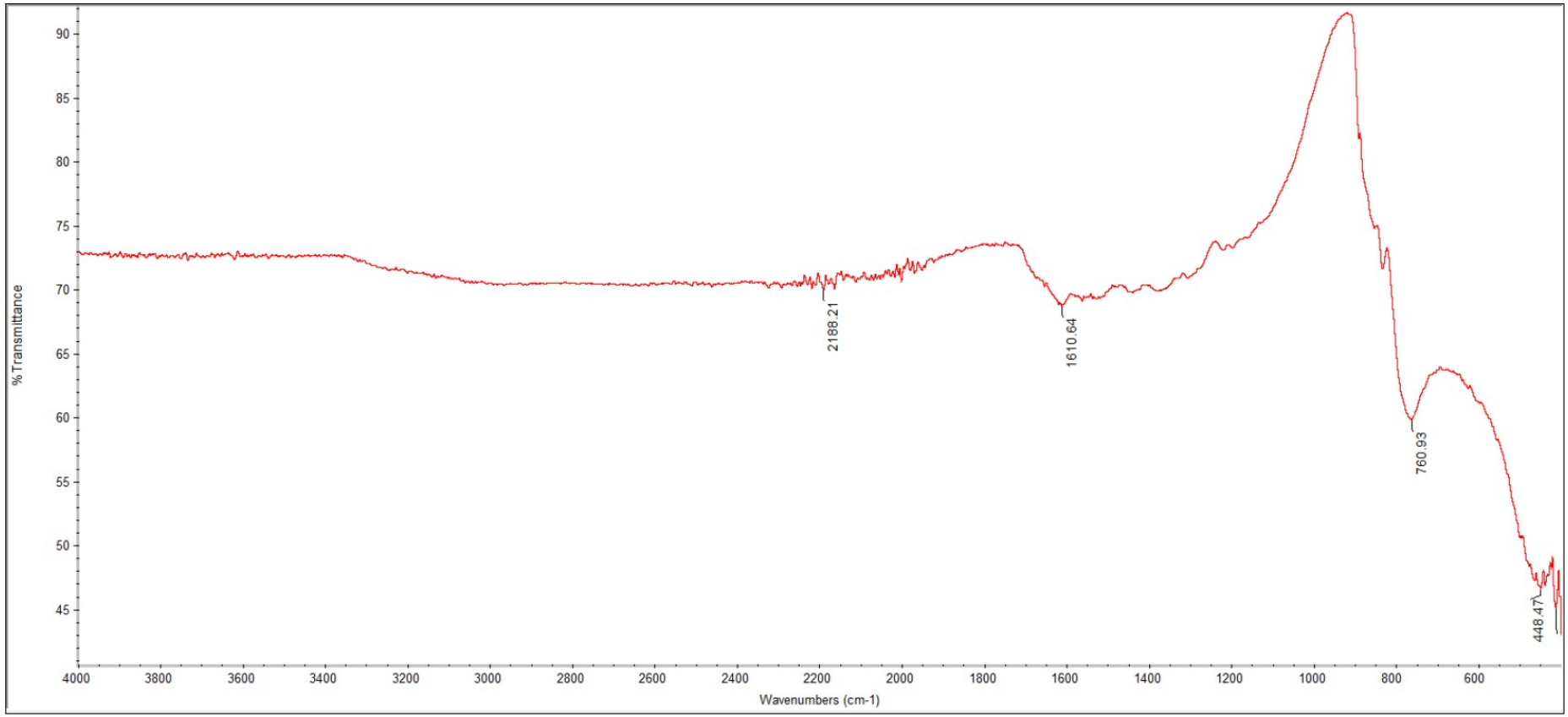

Figure B-2: FTIR Spectrum of Pure AgVA.

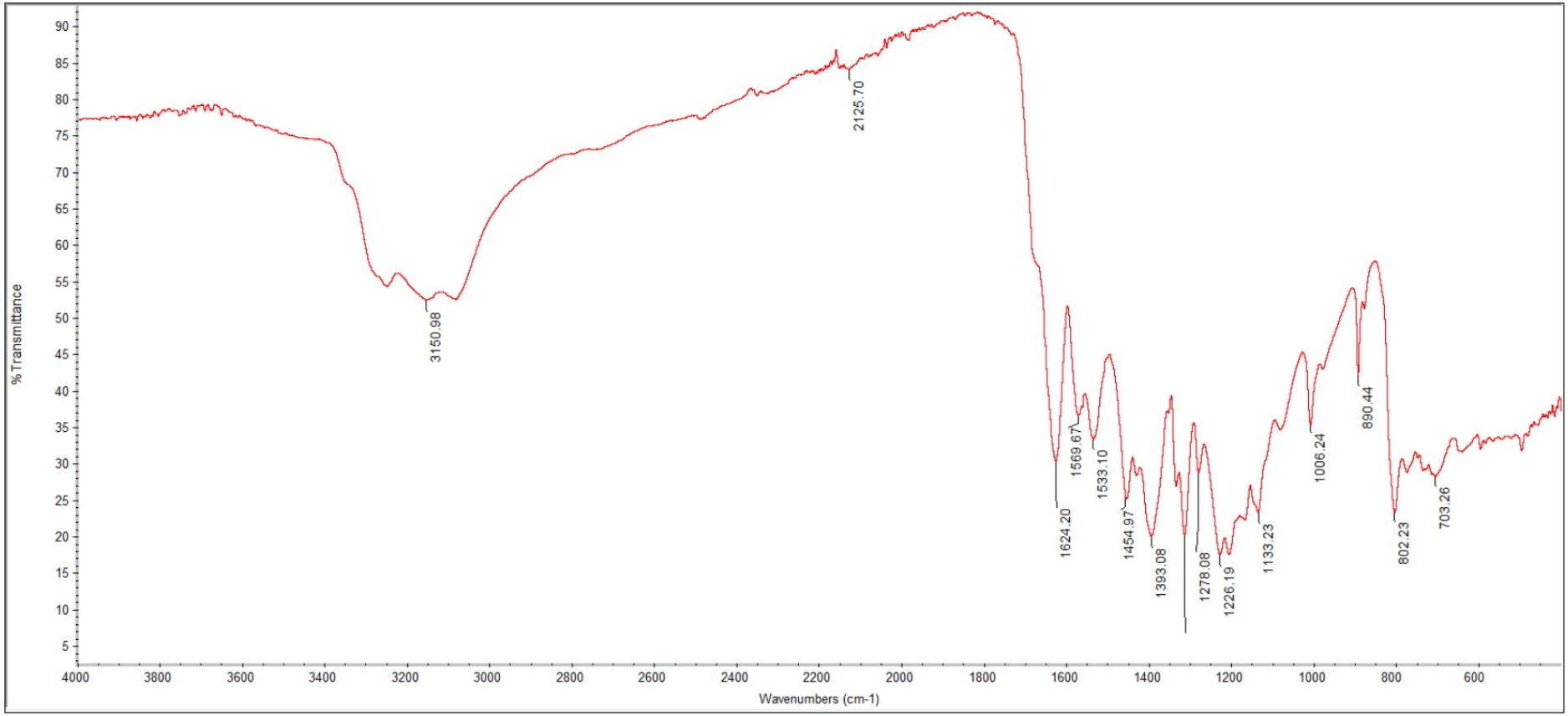

Figure B-3: FTIR Spectrum of A10.

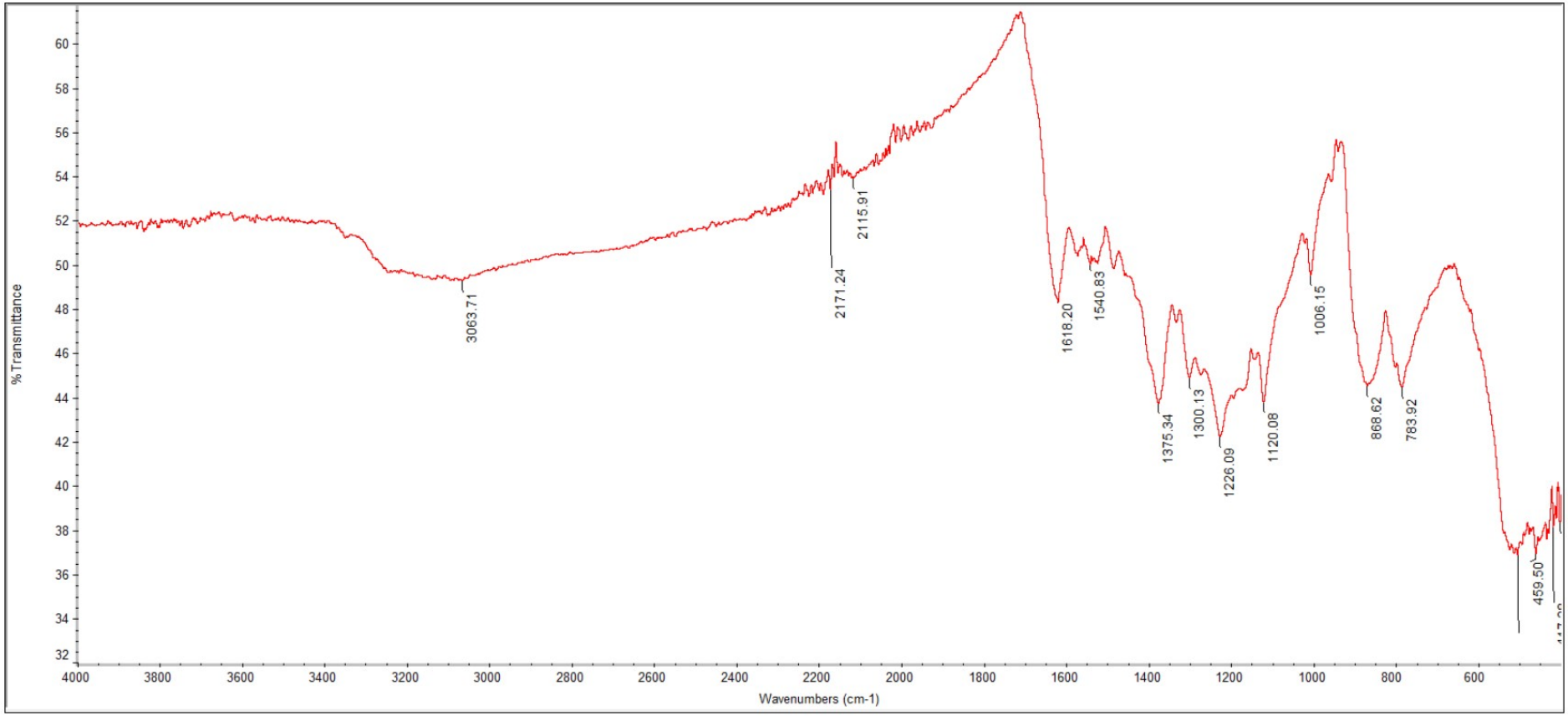

Figure B-4: FTIR Spectrum of A30.

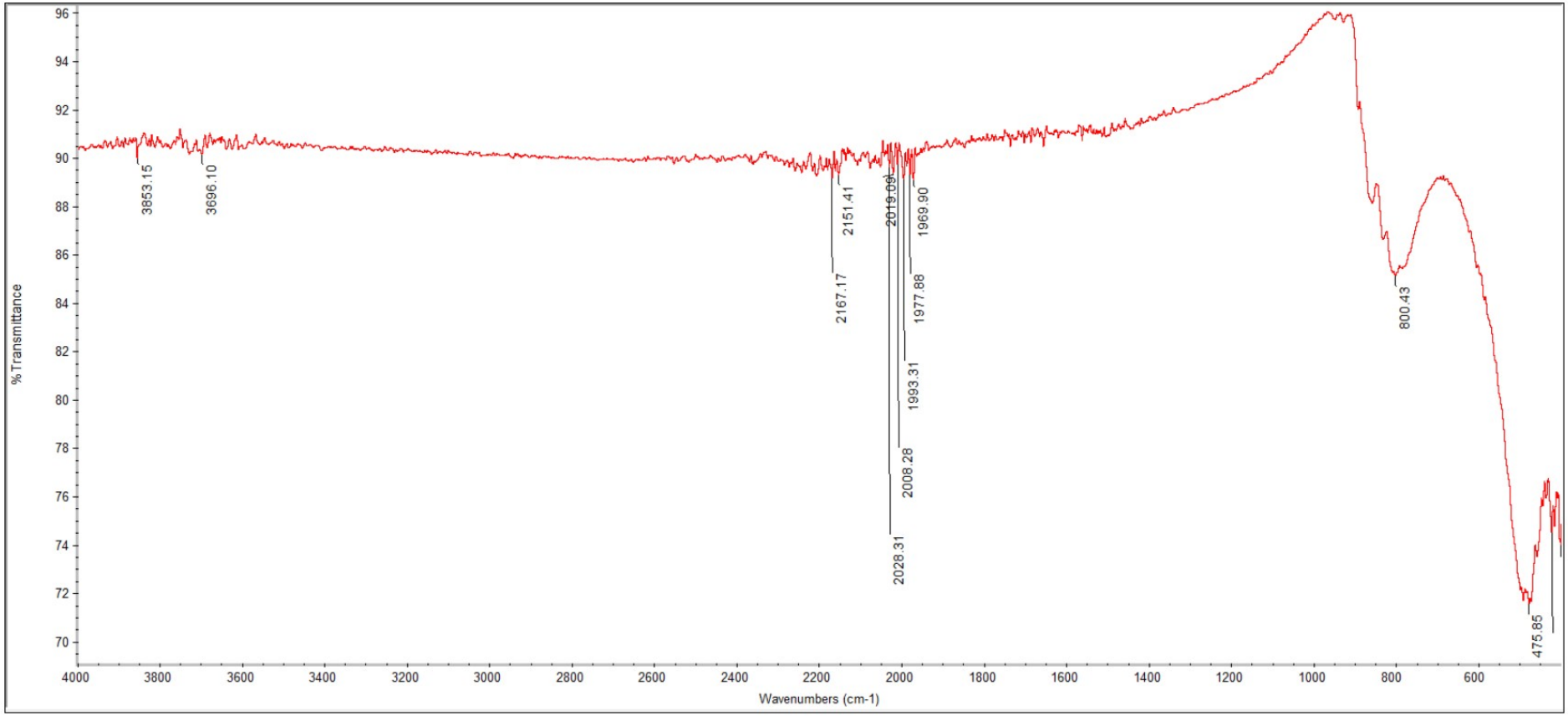

Figure B-5: FTIR Spectrum of A50.